Electronic Thesis and Dissertation Repository

8-6-2019 1:00 PM

# Mapping and functional characterization of proteolytic cleavage of murine kidney injury molecule-1

Saranga Sriranganathan, *The University of Western Ontario*

# Abstract

Kidney injury molecule-1 (KIM-1) is a transmembrane glycoprotein expressed apically on proximal tubule epithelia during acute kidney injury (AKI). KIM-1, as a phagocytic receptor, facilitates clearance of apoptotic cells (efferocytosis) from tubular lumen, thereby reducing inflammation and promoting repair. Human KIM-1 undergoes spontaneous and accelerated ectodomain shedding into urine and blood via metalloproteases; tumour necrosis factor-$\alpha$ converting enzyme (TACE/ADAM17) and a disintegrin and metalloprotease 10 (ADAM10). Blood and urine KIM-1 are clinical AKI biomarkers, however, biological significance of KIM-1 shedding is unknown. To study this *in vivo* in mice, I first aimed to identify murine KIM-1 cleavage site and study its functional relevance *in vitro*.

I202 was mapped out as the potential cleavage site and mutated to Q or A. Mutants showed significantly reduced ability to accelerate KIM-1 shedding and efferocytosis. ADAM10 mediated both baseline and accelerated shedding of murine KIM-1. Surprisingly, ADAM10-mediated KIM-1 shedding was required for efficient efferocytosis.

## Keywords

# Lay Summary

**Background**

Acute kidney injury (AKI) affects about 5-20% of hospitalized patients and is associated with increased mortality and risk of future chronic kidney disease. Severe AKI results in massive death of kidney epithelial cells. Rapid removal of dead cells occurs via "phagocytosis" which is vital for preventing further inflammation and hastening tissue repair. Recently, we discovered that injured kidney epithelial cells express KIM-1, a gene product not normally found in healthy kidney, which transforms surviving kidney epithelial cells into phagocytes that clear dead or dying cells and protect from AKI. KIM-1 is expressed on the cell membrane and "cut" by an enzyme and shed into urine and blood from kidney cells. In humans, KIM-1 is known to be primarily shed by tumour necrosis factor-a converting enzyme (TACE/ADAM17) and a disintegrin and metalloprotease 10 (ADAM10). Blood and urinary KIM-1 are used in clinics to identify kidney injury, but the importance of this shedding mechanism in biology is yet to be understood. We therefore attempted to identify and alter the cut site on mouse KIM-1 (mKIM-1) to study any changes in its shedding and phagocytic function, in hopes of eventually generating a KIM-1 shedding defective mutant mouse. This will be an invaluable tool to study the importance of shedding in the context of the animal as a whole.

**Hypothesis**

The cleavage site of mKIM-1 is in a region near the cell membrane outside the cell (T194 to I202) and altering nearby amino acids will render it shedding defective but maintain phagocytic function.

**Methods**

Mapped out potential cut site based on patterns observed on other proteins cut by TACE and/or ADAM10. Alter relevant amino acids at the predicted cut site of mKIM-1 to make mutants for testing effect on shedding and phagocytosis.

**Results**

Interestingly, it was observed that ADAM10 is the major enzyme cutting mKIM-1. Position I202 was determined to be a potential cut site. Reducing mKIM-1 shedding unexpectedly resulted in reduced phagocytosis levels.

# Co-Authorship statement

Dr. Lakshman Gunaratnam supervised this entire project, contributed to planning and designing all experiments, procurement of all required reagents and equipment, and editing thesis.

# Acknowledgments

First, I would like to extend my sincerest gratitude to Dr. Lakshman Gunaratnam, the best thesis supervisor I could have ever asked for. Words cannot describe how fortunate I am to have had the opportunity to work for someone who genuinely cares for the well-being of each and every one of his students. His constant high energy, fun-loving personality, undying optimism, and indestructible passion for research and medicine are just some of the many astonishing qualities I admire in him. As a mentor, I have looked up to him many times for advice and he has never failed to keep my best interests in mind, and for that I will be forever grateful. I have learned so much just by observing him work on a day to day basis as a very successful clinician scientist. There have been many times when I have looked up to him in awe of his accomplishments and he has continuously inspired me to step out of my comfort zone and reach beyond what I had initially thought I was capable of achieving. His continuous words of encouragement have also been invaluable during my times of uncertainty. Thank you Dr. Gunaratnam for all that you have done and for the wonderful experience I have had completing my MSc under your guidance.

Next, I would like to thank the other pivotal members of my lab family. Dr. Xizhong Zhang, Dr. Elena Tutunea-Fatan, and Brad Shrum have been guiding and teaching me many of the lab techniques that I have learned during my time at the LG lab. They have been so patient with me from day 1 and have continued to support and mentor me throughout my grad school journey. Alina Abbasi, thank you for being patient with all my questions when I initially took on this project from you. Your guidance was critical, and I appreciate all your help. Ji Yun Lee, thank you for being such a sweet colleague, but more importantly a very close friend who I could always rely on. Your magical hands always solved my experimental setbacks and you always looked out for me in every scenario. Jasper Lee, thank you for teaching me to never be afraid of asking questions. Your empathy for others is truly inspiring and you have been such a great friend. Demitra Yotis, where do I even start with you. Thank you for being so chirpy and always bringing a smile to my face when I needed it most. I have laughed so hard at and with you which has made working in SDRI that much more fun. Ingrid Hon, thank you for being so co-operative as a fellow graduate student and making our work space comfortable. Zhengzuo Li (Leo), we both started our work in lab together, and I was so fortunate to have you there during the initial training process. I look forward to collaborating with you in the

# Table of Contents

# Abbreviations

| | |
|---|---|
| ADAM10 | A Disintegrin and Metalloprotease 10 |
| ADAM17 | A Disintegrin and Metalloprotease 17 |
| AIM | Apoptosis Inhibitor of Macrophage |
| AKI | Acute Kidney Injury |
| ATN | Acute Tubular Necrosis |
| ATP | Adenosine Triphosphate |
| CKD | Chronic Kidney Disease |
| DMEM | Dulbecco's Modified Eagle Medium |
| DMSO | Dimethyl sulfoxide |
| DYNLT-1 | Dynein Light Chain Tctex Type-1 |
| ECM | Extracellular Matrix |
| ESI-MS | Electrospray Ionization Mass Spectrometry |
| ESRD | End Stage Renal Disease |
| G$\alpha$12 | Alpha subunit of heterotrimeric G protein 12 |
| HEK293 | Human Embryonic Kidney-293 |
| IgV | Immunoglobulin V |
| IL-6R | Interleukin-6 Receptor |
| IRI | Ischemia Reperfusion Injury |
| KIM-1 | Kidney Injury Molecule-1 |
| mKIM-1 | Murine Kidney Injury Molecule-1 |
| hKIM-1 | Human Kidney Injury Molecule-1 |
| NF-$\kappa$B | Nuclear Factor kappa-light-chain-enhancer of activated B cells |
| PBS | Phosphate Buffered Saline |
| PI3K | Phosphoinositide 3-kinase |
| PMA | Phorbol 12-Myristate 13-Acetate |
| P/S | Penicillin/Streptomycin |
| PTEC | Proximal Tubular Epithelial Cell |
| RENCA | Renal Cell Carcinoma |
| rmADAM10 | Recombinant murine ADAM10 |
| rmTACE | Recombinant murine TACE |
| ROS | Reactive Oxygen Species |
| SDS | Sodium Dodecyl Sulphate |
| SDM | Site-Directed Mutagenesis |
| TACE | Tumour Necrosis Factor-$\alpha$ Converting Enzyme |
| TCTEX-1 | T-complex testis specific protein-1 |
| TFMS | Trifluoromethanesulfonic Acid |
| TLR4 | Toll-like receptor 4 |

# List of Tables

# List of Figures

Chapter 1

# 1 Introduction

## 1.1 Kidney Disease

Kidneys are highly vascularized vital organs receiving approximately 20% of cardiac output to perform its primary function in blood filtration and processing urinary filtrate. In addition to regulating excretion of waste products, the kidneys are also involved in tightly regulating plasma osmolarity, electrolyte balance, blood pH, blood pressure, hormone production, and gluconeogenesis (Gerich 2010, Lote 2012).

### 1.1.1 Renal Physiology

The kidney is encased in a fibrous capsule and has an outer cortex layer and inner medulla layer. The basic structural and functional unit is the nephron, surrounded by peritubular capillaries in this highly vascularized organ. Nephrons are made up of two components; renal corpuscle and the tubule. Renal corpuscles are found in the outer cortex layer, while portions of the renal tubule extend into the renal medulla. On average, each human kidney is comprised of about 1 million nephrons, in comparison to mice which possess about 12,000 nephrons per kidney (Bonvalet, Champion et al. 1977, Nyengaard and Bendtsen 1992, Wang and Garrett 2017).

Renal corpuscles consist of the glomerulus and the glomerular capsule known as the Bowman's capsule. The glomerulus is a leaky capillary bed, surrounded by the Bowman's capsule composed of a single layer of epithelial cells. The glomerulus acts as a sieve allowing small molecules such as water, ions, glucose, amino acids, urea, creatinine and other waste products to filter through, enter the Bowman's space and eventually move into the tubular lumen. Larger substances like proteins and erythrocytes are retained in circulation. The filtered component flowing through the tubular lumen is referred to as filtrate. The tubule is responsible for further processing the filtrate before it collects in the bladder as fully processed urine ready to be excreted. This processing occurs via secretion, or the movement of substances from the surrounding peritubular capillaries into the filtrate, or reabsorption which involves the movement of substances from the filtrate back into

peritubular capillary circulation. The entire renal tubule is lined with a single layer of epithelial cells held together by tight junctions and adhesion junctions. The apical membrane of these epithelial cells faces the tubular lumen and is distinct from the basolateral membrane positioned towards the peritubular capillaries giving the cells a polarized phenotype. There are numerous transporters and channels found distinctively on these membranes to regulate filtrate processing. The tubule can be further divided into different sections starting from the proximal tubule (PT), down the descending limb of the Loop of Henle, up the ascending limb of the Loop of Henle, the distal convoluted tubule and finally the collecting duct which eventually drains into the ureter. Each section processes the filtrate differently. The PT is where majority of reabsorption, about 65% of the filtrate volume, first occurs. Then mostly water reabsorption occurs in the descending limb of the Loop of Henle, followed by ion reabsorption in the ascending limb and distal convoluted tubule. The collecting duct acts as a fine tuner and can be regulated by hormones such as antidiuretic hormone and aldosterone to regulate water and $Na^+/K^+$ reabsorption, respectively.

## 1.1.2    Renal Pathophysiology

There are various forms of kidney disease ranging from acute kidney injury (AKI), chronic kidney disease (CKD) and end stage renal disease (ESRD).

## 1.1.2.1    Acute Kidney Injury

AKI is defined as a sudden and rapid decline in renal function in response to ischemic (Ichimura, Bonventre et al. 1998) or toxic insults (Thadhani, Pascual et al. 1996, Ichimura, Hung et al. 2004) most often in response to conditions such as acute interstitial nephritis and acute tubular necrosis (Wilson, Turner et al. 1976, Perazella 2014). With an incidence rate of 5-20% in all hospitalized patients, the prognosis is very poor with high morbidity and mortality rates (Waikar, Liu et al. 2008, Coca, Yusuf et al. 2009, Susantitaphong, Cruz et al. 2013). AKI is most often caused by ischemia-reperfusion injury (IRI) to the kidneys which frequently occurs in patients suffering from septic shock (Rangel-Frausto, Pittet et al. 1995), or undergoing cardiac bypass surgery (Bhat, Gluck et al. 1976).

The lack of blood flow (ischemia) resulting in hypoxic conditions, followed by restoration of blood flow (reperfusion) leads to the generation of reactive oxygen species which can cause tissue damage (Thadhani, Pascual et al. 1996). The PT is especially susceptible to hypoxic conditions. It is a highly metabolic region responsible for most filtrate reabsorption and relies on oxidative phosphorylation for adenosine triphosphate (ATP) production, unlike other portions of the nephron which continue to produce ATP via anaerobic glycolysis during prolonged periods of ischemia (Bagnasco, Good et al. 1985). It has been demonstrated that epithelial cells in the S3 segment, latter portion of the PT, are most susceptible to IRI *in vivo*. (Venkatachalam, Bernard et al. 1978, Lieberthal and Nigam 1998). This is likely the result of hemodynamic factors which result in disproportionately prolonged blood flow reduction to the outer portion of the medulla during ischemic events (Olof, Hellberg et al. 1991, Bonventre and Yang 2011).

ATP depletion and oxidative stress resulting from IRI leads to various structural and functional changes in these epithelial cells. Firstly, lack of ATP causes actin cytoskeleton and microtubule structures to dissociate such that transmembrane proteins like $Na^+/K^+$ ATPase and integrins, normally observed on the basolateral membrane redistribute to the apical membrane, leading to inefficient salt reabsorption and cell detachment from the extracellular matrix, respectively (Molitoris, Dahl et al. 1992, Goligorsky and DiBona 1993, Abbate, Bonventre et al. 1994). In response to ischemic injury, renal tubular epithelial cells can become necrotic via two major forms of regulated cell death, necroptosis or ferroptosis. Ferroptosis is an iron-dependent form of necrosis that results from lipid peroxide accumulation under conditions of oxidative stress (Linkermann, Skouta et al. 2014). Although, intracellular iron levels is key in regulating ferroptosis, the exact mechanism is still unknown (Lei, Bai et al. 2019). These processes can result in acute tubular necrosis (ATN), the standard diagnosis for patients with AKI. Necrotic and apoptotic cells, along with live cells that have now detached from the extracellular matrix and neighbouring epithelial cells due to loss of tight junctions and adhesion junctions, slough off into the tubular lumen (Figure 1.) (Racusen, Fivush et al. 1991, Thadhani, Pascual et al. 1996, Racusen 1998). Tubular obstruction of dead cells is believed to be a major contributor to decreased kidney function or glomerular filtration (Wahlberg, Karlberg et al. 1984).

In addition, injured tubular cells can induce inflammation by generating pro-inflammatory cytokines and chemokines to recruit inflammatory cells to the injured site and further amplify these responses via their Toll-like receptors and T-cell costimulatory molecules (Bonventre and Yang 2011). Neutrophils, macrophages, natural killer T cells and dendritic cells all contribute to the immune response and can aggravate kidney injury (Bonventre and Yang 2011). Necrotic cells are especially known to initiate a more robust inflammatory response, when compared to apoptotic cells because of their distinctive loss of cell membrane integrity, expulsion of intracellular contents, and activation of innate immune responses to exacerbate tissue injury (Kaushal, Basnakian et al. 2004). During renal IRI, necrotic cells release endogenous molecules termed damage-associated molecular patterns (DAMPs) that activate cell surface receptors (e.g. Toll-like receptors), triggering inflammatory and cytotoxic responses (Wu, Chen et al. 2007, Andrassy, Volz et al. 2008). Ultimately, induced inflammation by these injured and dying epithelial cells plays an important pathophysiological role in mediating AKI by propagating further tissue damage (i.e. secondary tissue damage).
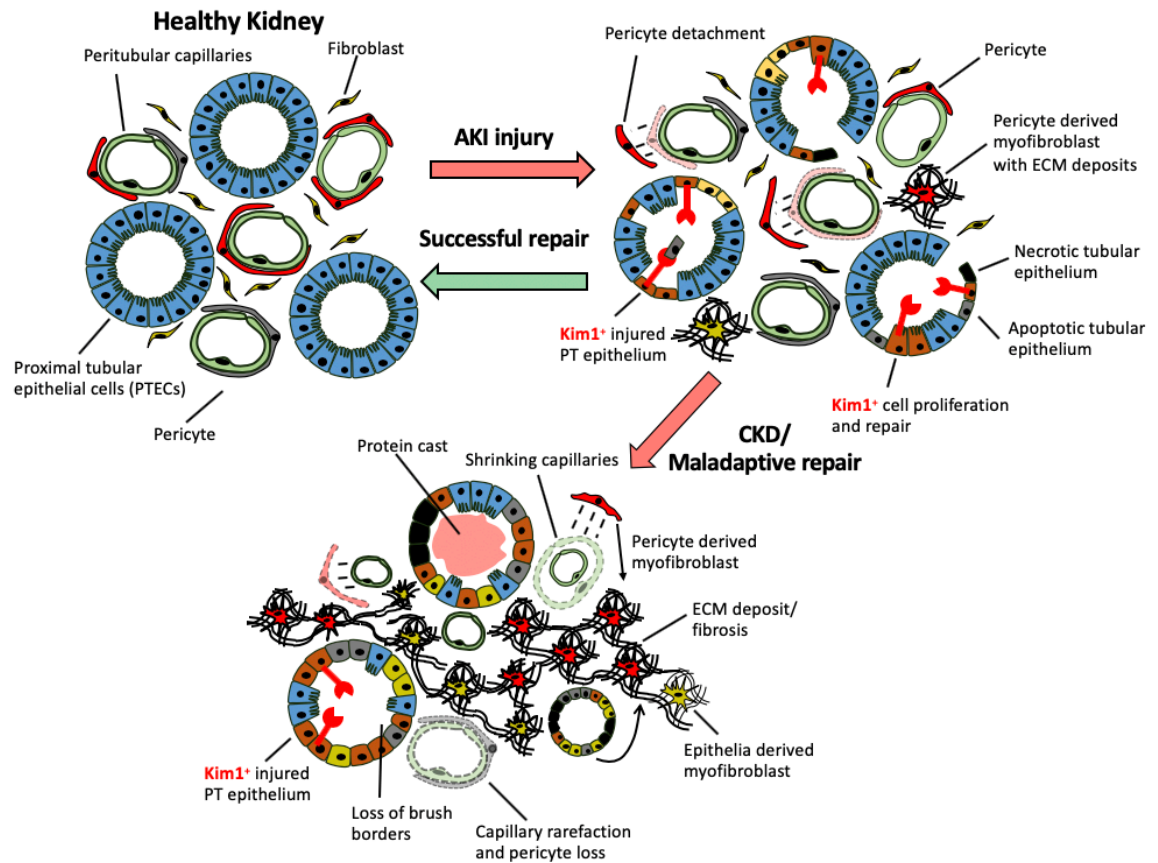
**Figure 1 Renal cellular pathophysiology.**

Modified schematic from (E and Humphreys 2017), depicting cellular level pathophysiological changes in renal tissue during various stages of kidney disease transitioning from healthy kidney to AKI and CKD.

## 1.1.2.2    Chronic Kidney Disease and End Stage Renal Disease

AKI also increases the risk for progressing to a more severe, irreversible stage of kidney injury known as CKD (Coca, Yusuf et al. 2009, Wald, Quinn et al. 2009). Other more common causes of CKD include diabetes and hypertension (Ghaderian and Beladi-Mousavi 2014).

CKD patients develop fibrosis or scarring in their renal tissue leading to a further decline in renal function (Zhang, Humphreys et al. 2007). Myofibroblasts secrete extracellular matrix (ECM) proteins such as collagen and fibronectin and are essential for wound repair, however excess ECM deposit can lead to pathological fibrosis. The origin of these myofibroblasts during kidney fibrosis was somewhat controversial with some earlier suggestions that most originate from epithelial precursors (Okada, Danoff et al. 1997), whereas more recent studies suggest that pericytes, fibroblasts wrapped around blood vessels, are primarily responsible for transforming into myofibroblasts (Humphreys, Lin et al. 2010). Pericytes normally help to stabilize blood vessels and their increased detachment can lead to capillary rarefaction (Figure 1.) (E and Humphreys 2017, Kramann, Wongboonsin et al. 2017). Reduced blood flow in this otherwise highly vascularized organ can further compound hypoxic conditions.

Cells which have sloughed off into the tubular lumen after AKI and not been cleared can then adhere to each other and other proteins in the tubular lumen such as Tamm-Horsfall protein (Patel, McKenzie et al. 1964) or fibronectin (Zuk, Bonventre et al. 2001) to form intraluminal casts often observed in patients with ATN (Figure 1.). These casts result in tubular obstruction and increased intratubular pressure to further exacerbate tissue damage (Goligorsky and DiBona 1993). Moreover, the disrupted barrier of epithelial cells from the absence of tight junctions along the tubule allows for backleak of filtrate contents into the interstitial space (Donohoe, Venkatachalam et al. 1978). As filtered solutes re-enter circulation, the glomerular filtration rate (GFR) is effectively reduced leading to post-ischemic renal failure (Donohoe, Venkatachalam et al. 1978).

The progression of CKD ultimately can result in ESRD at which point there is only one of two treatment options: either dialysis or renal transplantation (Wald, Quinn et al. 2009).

Kidney disease, being a worldwide phenomenon, is highly underdiagnosed with no effective treatment for AKI, which at a severe and recurring level can further progress to CKD and ESRD (Yang, Xing et al. 2015).

## 1.2 Kidney Injury Molecule-1

### 1.2.1 Structure and expression

Kidney injury molecule -1 (KIM-1) is a type I transmembrane glycoprotein found on the apical surface of proximal tubule epithelial cells (PTEC) of the nephron (Ichimura, Bonventre et al. 1998, van Timmeren, van den Heuvel et al. 2007). While KIM-1 is not normally expressed in healthy kidneys, it is transiently upregulated during periods of AKI (Ichimura, Bonventre et al. 1998) or other conditions when PTECs dedifferentiate such as renal cell carcinoma (Han, Alinani et al. 2005), tubulointerstitial disease (van Timmeren, Bakker et al. 2006), polycystic kidney disease (Kuehn, Park et al. 2002) or drug-induced nephrotoxicity (Perez-Rojas, Blanco et al. 2007). More recently, KIM-1 has been shown to be upregulated in CKD (Sabbisetti, Waikar et al. 2014) and potentially a marker of recurrent tubular injury that may be driving disease progression (Nowak, Skupien et al. 2016).

KIM-1 is also known as T cell immunoglobulin and mucin domain-1 (TIM-1) as it is expressed on various immune cells such as $CD4^+$ T cells, $CD8^+$ T cells, natural killer cells, macrophages, dendritic cells, B regulatory cells and mast cells (Freeman, Casasnovas et al. 2010, Ding, Yeung et al. 2011). It can also be referred to as hepatitis A virus cellular receptor-1 (HAVCR-1) when expressed on hepatocytes (Govorkova, Murti et al. 1996). However, TIM-1 expression levels on immune cells has been shown to be orders of magnitudes less than that of KIM-1 on injured PTECs (Ichimura, Asseldonk et al. 2008, Nozaki, Nikolic-Paterson et al. 2012, Brooks, Yeung et al. 2015) In humans, the TIM-1 family has three members (TIM-1, TIM-2 and TIM-4) located on chromosome region 5q33, whereas in mouse there are eight members (TIM-1-8) on chromosome 11. Both human and mouse TIM-1 family genes are highly homologous (Kuchroo, Umetsu et al. 2003).

KIM-1 has five major structural domains (Figure 2). The outermost portion is the N-terminal immunoglobulin variable (IgV) domain containing six cysteine residues important for its metal-ion dependent binding to ligands like phosphatidylserine expressing apoptotic cells (Ichimura, Bonventre et al. 1998, Santiago, Ballesteros et al. 2007, Bonventre 2009). The mucin domain, a threonine, serine, proline (TSP)-rich region, is commonly known to be heavily glycosylated with O-linked, and to a lesser extent, N-linked glycans. Mouse KIM-1 (mKIM-1) specifically has 37 potential sites for O-linked glycosylations in this region. The stalk-region is the membrane proximal region of the ectodomain with potential sites for 3 N-linked glycans. There is a single transmembrane domain and a short C-terminal cytoplasmic domain which contains a conserved tyrosine phosphorylation motif (QAEDNIY).

In addition, human KIM-1 has two isoforms that can result from alternative splicing; KIM-1a predominantly expressed in the liver and KIM-1b in the kidneys (Bailly, Zhang et al. 2002). KIM-1a and KIM-1b are identical except that the cytoplasmic tail is shorter for KIM-1a and therefore lacks the tyrosine phosphorylation site. Human KIM-1 (hKIM-1) has 3 cytoplasmic tyrosine residues (Y314, Y350 and Y356) of which two are conserved in mouse and rat (Y314 and Y350).

## 1.2.2    Function

KIM-1 acts as a receptor for phosphatidylserine, an 'eat me' signal, expressed on the outer leaflet of apoptotic cells (Ichimura, Asseldonk et al. 2008). Oxidized phospholipids can also be found to accumulate on the outer leaflet of dying cells and allow them to bind KIM-1 (Ichimura, Asseldonk et al. 2008). This binding induces a semi-phagocytic phenotype on surviving KIM-1 expressing epithelial cells to facilitate clearing of apoptotic cells from the tubular luminal area in a process known as efferocytosis (Ichimura, Asseldonk et al. 2008, Ismail, Zhang et al. 2015, Yang, Brooks et al. 2015). Necrotic debris can also be cleared by KIM-1 after being opsonized with Apoptosis Inhibitor of Macrophage (AIM) (Arai, Kitada et al. 2016) which is also filtered through the glomerulus and excreted in urine during AKI (Yamazaki, Sugisawa et al. 2016). This clearance of dead and dying cells dissipates obstruction in the tubular lumen, thereby reducing inflammation and permitting repair. Failure to clear these cells can lead to the production of autoantibodies to induce

detrimental inflammatory responses (Savill, Dransfield et al. 2002, Umetsu, Lee et al. 2005, Nakayama, Akiba et al. 2009). In the setting of kidney transplantation, where IRI is inevitable, genetic ablation of KIM-1 in the donor kidneys has been shown to lead to severe graft dysfunction and systemic inflammation in the recipients in a mouse model of kidney transplantation (Lee, Ismail et al. 2018).

Only a few studies have looked at the downstream signaling mechanisms of KIM-1 and potential interacting proteins during efferocytosis and tissue repair after injury. Therefore, the complete signaling cascade is not well understood. As a phagocytic receptor, it is expected that KIM-1 will have downstream effects on cytoskeletal remodeling. Our group has shown that Dynein Light Chain Tctex Type-1 (DYNLT-1) also known as T-complex testis specific protein-1 (Tctex-1), acts as a cytosolic interaction partner for KIM-1, playing a crucial role in mediating the early phases of KIM-1 dependent efferocytosis in a cytoskeleton dependent manner via actin and microtubule associations (Ismail, Sriranganathan et al. 2018). Our group has also reported the alpha subunit of heterotrimeric G protein 12 (Gα12) as a negative regulator of KIM-1 mediated efferocytosis (Ismail, Zhang et al. 2016). In response to renal IRI, Gα12 becomes activated by inflammatory stimuli such as reactive oxygen species (ROS) and inhibits efferocytosis (Ismail, Zhang et al. 2015). This inhibitory process is mediated by downstream activation of a small GTPase, RhoA, which induces actin cytoskeletal remodeling to inhibit efferocytosis (Ismail, Zhang et al. 2016). Gα12 can also stimulate Src-dependent injury pathways that further exacerbate tissue damage by disrupting tight junctions which normally seal adjacent PTECs lining the renal tubule (Ismail, Zhang et al. 2015). Like all GTPases, both Gα12 and RhoA, are inactive when GDP-bound and become active when GTP bound (Ridley 2001, Kozasa, Hajicek et al. 2011). KIM-1, when expressed, can bind directly to Gα12 to block GTP binding and prevent its activation thereby protecting against the damaging downstream effects of renal IRI.

Others have reported the anti-inflammatory effect of KIM-1 expression via a signaling cascade which involves direct binding of phosphorylated KIM-1 to p85 and subsequent PI3K mediated downmodulation of NF-κB signaling (de Souza, Oak et al. 2008, Yang, Brooks et al. 2015). This pathway leads to reduced toll-like receptor 4 (TLR4) expression

which normally amplifies innate immune responses, reduced proinflammatory cytokine production, and reduced ability to activate macrophages (Yang, Brooks et al. 2015). Importantly, apoptotic cell ligand binding to KIM-1 is the initial trigger for phosphorylation of its cytosolic tyrosine residue and subsequent interaction with p85 (de Souza, Oak et al. 2008, Brooks, Yeung et al. 2015). KIM-1 association with p85 has also been linked with promoting phagosome maturation via the autophagy 'self-eating' pathway (Brooks, Yeung et al. 2015). This results in apoptotic cell self-antigen presentation by these phagocytic epithelial cells that leads to an anti-inflammatory response by suppressing T cell proliferation.

KIM-1 can also induce dedifferentiation, proliferation and migration of renal epithelial cells via the extracellular signal-regulated kinase (ERK) mitogen-activated protein kinase (MAPK) signaling cascade pathway (Zhang and Cai 2016). All these processes are crucially important for surviving KIM-1 expressing PTECs to repair and replace damaged tubular epithelium (Figure 1). During renal injury, the basement membrane becomes exposed as PTECs slough off into the tubular lumen, leading to loss of nephron functional integrity (Bonventre 2003). The loss of this barrier results in backleak of filtrate contents into the interstitital space and peritubular capillaries as well as the appearance of plasma proteins, like fibronectin, in the tubule which can further exacerbate tubular obstruction (Zuk, Bonventre et al. 1998). The high proliferative capacity of dedifferentiated KIM-1 expressing PTECs and their ability to migrate are both important to replace irreversibly damaged epithelial cells.

On the other hand, it is interesting to note that KIM-1 was discovered to be an endogenous ligand for leukocyte mono-Ig like receptor 5 (LMIR5) expressed on myeloid immune cells and this binding interaction leads to neutrophil recruitment to the kidney and tubular damage in response to IRI (Yamanishi, Kitaura et al. 2010). Overall, it is clear that KIM-1 signaling is quite complex and likely a multitude of different interacting proteins are at play in terms of mediating renal response to IRI.

## 1.2.3 KIM-1 Shedding

Human KIM-1 undergoes constitutive and accelerated ectodomain shedding by metalloprotease-mediated membrane proximal proteolytic cleavage to release soluble KIM-1 (sKIM-1) (Bailly, Zhang et al. 2002, Zhang, Humphreys et al. 2007, Gandhi, Yi et al. 2014) (Figure 2.). Human sKIM-1 has a molecular weight of ~90-kDa with a 14-kDa cleaved portion remaining in the membrane (Bailly, Zhang et al. 2002), whereas mouse sKIM-1 has a molecular weight of ~60-kDa as previously reported (Ichimura, Bonventre et al. 1998, Gandhi, Yi et al. 2014). Human KIM-1 is also shed into the urine of patients afflicted with AKI and can be readily detected using western blotting or enzyme linked immunosorbent assay (ELISA). Urine sKIM-1 is a sensitive and specific biomarker for AKI in humans and rodent models (Han, Bailly et al. 2002, Vaidya, Ozer et al. 2010, Coca, Garg et al. 2014).

Constitutive and accelerated hKIM-1 shedding has been shown to be differentially regulated by ERK MAPK and p38 MAPK signaling, respectively, suggesting different downstream signaling mechanisms can be at play under various shedding conditions. Studies using broad spectrum hydroxamate-based matrix metalloprotease (MMP) and ADAM enzyme inhibitors, such as batismastat (BB-94) and ilomastat (GM6001), showed efficient inhibition of baseline and accelerated KIM-1 shedding indicating cleavage is likely mediated by a metalloprotease enzyme (Bailly, Zhang et al. 2002, Zhang, Humphreys et al. 2007). Tumour necrosis factor-$\alpha$ converting enzyme, also known as a disintegrin and metalloprotease protein 17 (TACE or ADAM17), is a zinc-dependent membrane anchored metalloprotease. TACE has been previously shown to be involved in constitutive as well as accelerated cleavage of hKIM-1 in its ectodomain region (Gandhi, Yi et al. 2014). Accelerated shedding of transmembrane proteins is often induced with phorbol esters such as phorbol 12-myristate 13-acetate (PMA), a chemical activator of protein kinase C which can stimulate downstream TACE activity and potentially other metalloproteases (Bazzi and Nelsestuen 1989, Hahn, Pischitzis et al. 2003). PMA is used to induce accelerated KIM-1 shedding along with other stimulators such as $H_2O_2$, apoptotic cells, or pervanadate (PV), a potent inhibitor of protein tyrosine phosphatases (Bazzi and Nelsestuen 1989, Hahn, Pischitzis et al. 2003, Gandhi, Yi et al. 2014). A disintegrin and

metalloprotease protein 10 (ADAM10) has also been reported as a sheddase that mediates hKIM-1 shedding (Schweigert, Dewitz et al. 2014). Membrane-type MMP-1 (MT-MMP1), when co-expressed with KIM-1, is also capable of moderating baseline shedding (Guo, Takino et al. 2012). Thus far, MMP3 is the only matrix metalloprotease implicated to play a role not only in hKIM-1 but also mKIM-1 shedding (Lim, Chan et al. 2012).

KIM-1 expressed on the apical surface of PTECs can release sKIM-1 into urine, but it has also been demonstrated that sKIM-1 can be found in blood and used as a useful blood biomarker for AKI, CKD and progression to ESRD (Sabbisetti, Waikar et al. 2014). In response to renal injury, loss of tubular cell polarity can result in KIM-1 expression on the basolateral membrane of PTECS to allow direct entry into the interstitial space (Zuk, Bonventre et al. 1998, Sabbisetti, Waikar et al. 2014). Increased transepithelial permeability after injury will also allow for tubular content backleak (Myers, Chui et al. 1979). Additionally, increased microvascular permeability after injury will allow sKIM-1 to enter blood circulation more efficiently (Sutton 2009, Sabbisetti, Waikar et al. 2014).

An increase in urinary and plasma sKIM-1 can be detected in mice subjected to bilateral IRI as early as 3 hours after reperfusion (Sabbisetti, Waikar et al. 2014). In humans, KIM-1 can be detected in urine within 12 hours post-ischemic injury, and elevated at much higher levels in plasma for patients who develop AKI or CKD compared to healthy controls (Han, Bailly et al. 2002, Sabbisetti, Waikar et al. 2014). KIM-1 is a highly specific and sensitive blood and urinary biomarker for injury specific to the proximal tubule in response to ischemic or nephrotoxic insults (Ichimura, Hung et al. 2004, Sabbisetti, Waikar et al. 2014).

Most studies have been focused on elucidating the shedding mechanism of hKIM-1, whereas mKIM-1 shedding has been largely unexplored.
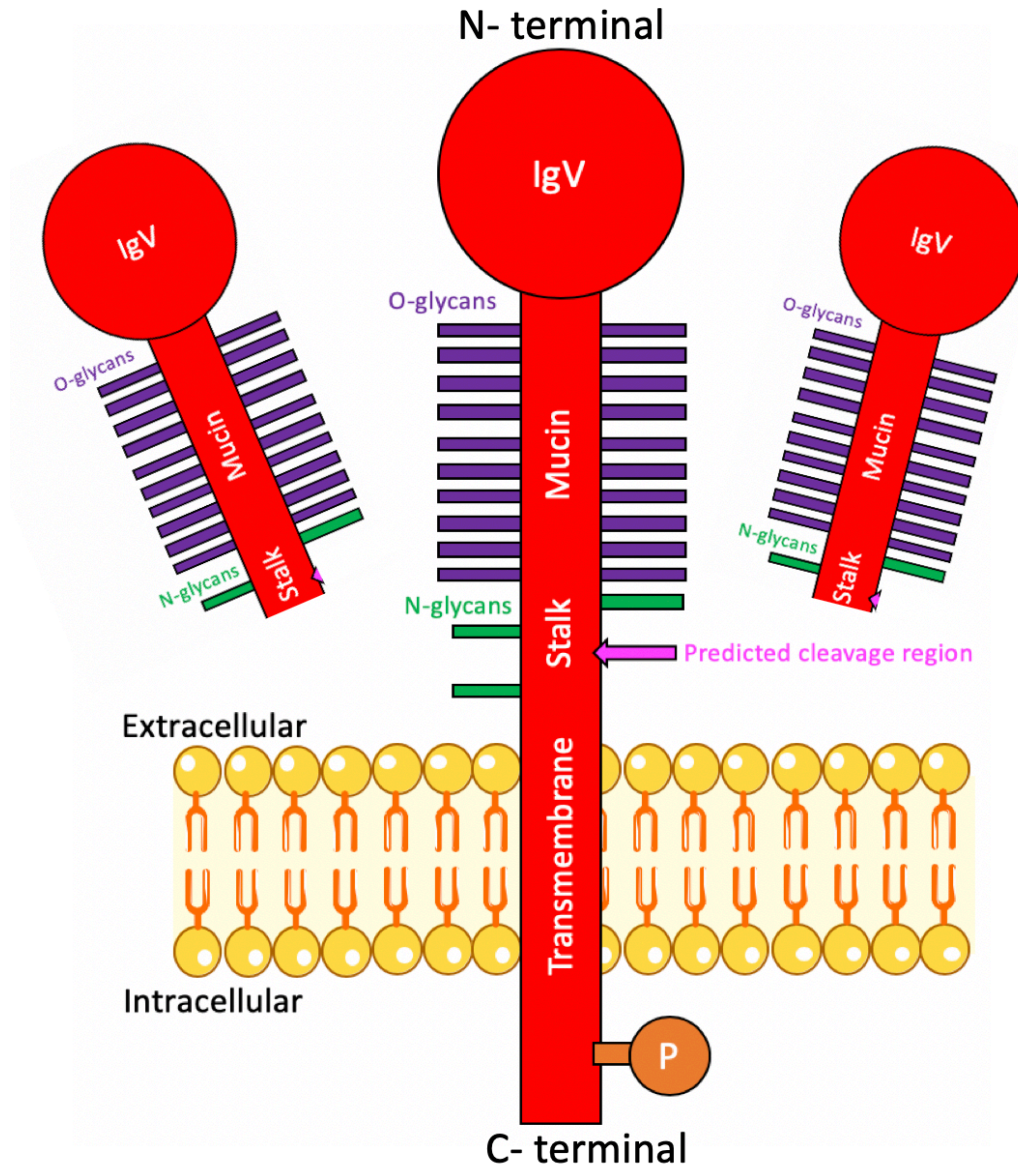
**Figure 2 Murine KIM-1 structural domains.**

Type I transmembrane glycoprotein KIM-1 (282 amino acids) structural domains consisting of IgV domain (P16 to T122), mucin domain and stalk region (T133 to K213), transmembrane domain (G214 to T236) and cytoplasmic domain (R237 to P282). O-linked and N-linked glycosylations on extracellular domains. Membrane proximal cleavage releases sKIM-1. Tyrosine phosphorylation site (Y276) on cytoplasmic domain.

## 1.3 TACE-/ADAM10-mediated proteolytic cleavage

TACE/ADAM17 and ADAM10 are both expressed in the kidney and are the two major sheddases in the *ADAM* gene family responsible for ectodomain proteolytic cleavage of over 100 substrates including various growth factors, cytokines, receptors and adhesion molecules (Edwards, Handsley et al. 2008, Kato, Hagiyama et al. 2018). TACE is the principal sheddase for substrates such as tumour necrosis factor (TNF)-alpha, transforming growth factor (TGF)-alpha, amphiregulin, L-selectin, heparin-binding epidermal growth factor, and interleukin 6 receptor (IL-6R) (Black, Rauch et al. 1997, Peschon, Slack et al. 1998, Sahin, Weskamp et al. 2004, Schumacher, Meyer et al. 2015). ADAM10 is involved with shedding substrates such as Notch, Fas ligand, N-cadherin, and E-cadherin (Pan and Rubin 1997, Kirkin, Cahuzac et al. 2007, Edwards, Handsley et al. 2008). Many of these substrates can be cleaved by either TACE and/or ADAM10 depending on the substrate, cell type or the stimulus used to induce shedding.

Chemical stimulators such as PMA and ionomycin, as well as physiological stimulators such as ATP, G protein coupled receptor ligands, insulin (Chen, Podvin et al. 2007), serum albumin (Lim, Chan et al. 2012), and apoptosis induction (Edwards, Handsley et al. 2008), can be used to activate various ADAM proteases and induce shedding of transmembrane substrates. Many studies use PMA as a PKC activator to induce TACE-mediated accelerated shedding of substrates, whereas ionomycin is generally used as an ionophore to allow the rapid influx of calcium to stimulate ADAM10- mediated shedding (Horiuchi, Le Gall et al. 2007).

Interestingly, TACE and ADAM10 are closely related and have been previously shown to differentially regulate shedding of the same substrate (Scheller, Chalaris et al. 2011). In the case of the transmembrane protein IL-6R, TACE is responsible for PMA-induced accelerated shedding whereas ADAM10 mediates constitutive baseline shedding in both humans and mice (Schumacher, Meyer et al. 2015). The CX3C chemokine fractalkine (CX3CL1) transmembrane protein also undergoes baseline cleavage via ADAM10 and PMA-induced cleavage via TACE (Hundhausen, Misztela et al. 2003).

## 1.4   Rationale, Objective, Hypothesis

### 1.4.1     Rationale

AKI has an incidence rate of 5-20% in all hospitalized patients, with high morbidity and mortality rates (Waikar, Liu et al. 2008, Coca, Yusuf et al. 2009, Susantitaphong, Cruz et al. 2013). Despite advances in technology over the past few decades, mortality rates for critically ill AKI patients remain high and unchanged at about 50% (Ympa, Sakr et al. 2005), highlighting the need for effective treatments. It is important that we focus on treatments for early stages of AKI to prevent the progression to more severe and irreversible renal damage associated with CKD or ESRD (Coca, Yusuf et al. 2009, Wald, Quinn et al. 2009, Yang, Xing et al. 2015). In light of this, KIM-1, which is used as an early biomarker for AKI, has tremendous potential to be targeted for therapy.

IRI is a model often used to study AKI in mice which involves clamping and releasing the renal pedicle to regulate blood flow to the kidney (Zhang, Shek et al. 2010, Ismail, Zhang et al. 2015). Using this model, we have shown that during moderate (warm) IRI with 35 minutes of ischemia, KIM-1 is protective in AKI (Ismail, Zhang et al. 2015). In addition, KIM-1 upregulation in the donor kidneys during transplantation was found to be protective against tissue damage and graft dysfunction from transplant-related (cold) IRI. However, unpublished data from our lab suggests that during severe IRI with 45 minutes of ischeima, this protective ability is lost and KIM-1 paradoxically promotes renal fibrosis, a phenotype observed in CKD. We show that KIM-1-deficient mice, in comparison to wild type mice, are protected from renal fibrosis when subjected to severe AKI. Also, genetic overexpression of KIM-1 in renal tubular cells in the absence of injury has been shown to spontaneously trigger renal fibrosis (Humphreys, Xu et al. 2013, Humphreys, Xu et al. 2013). Therefore, KIM-1 may play a key role in mediating the transition from AKI to CKD by triggering profibrotic pathways.

Importantly, the mechanism of KIM-1 shedding into urine and blood needs to be further explored. Although the clinical significance is apparent in its use as sensitive and specific biomarker for AKI, the biological significance of KIM-1 shedding is not so well understood. Previous *in vitro* studies have shown that accelerated shedding of human KIM-

1 via TACE activity induction, inhibits clearance of apoptotic cells, as sKIM-1 acts as a decoy receptor to competitively inhibit binding of phagocytic KIM-1 expressing epithelial cells (Gandhi, Yi et al. 2014). This was, however, a sKIM-1 concentration dependent effect, and not reflective of *in vivo* conditions. <u>The biological significance of KIM-1 shedding in AKI *in vivo* is yet to be determined.</u>

In order to conduct *in vivo* studies, the specific shedding enzymes and cleavage site on mKIM-1 needed to be elucidated. TACE, believed to be the major sheddase for hKIM-1, is responsible for shedding a wide range of susceptible growth factor substrates and lacks any particular sequence specificity around the cleavage site (Caescu, Jeschke et al. 2009, Thorp, Vaisar et al. 2011), therefore the exact cleavage site on KIM-1 cannot be easily deduced.

## 1.4.2    Objective and Aims

The overall aim was to identify the cleavage site for mKIM-1 and ultimately alter the relevant amino acid(s) to generate a shedding defective mutant. This information would be necessary for generating transgenic mice expressing shedding defective KIM-1. These mice will then be instrumental for studying the biological significance of KIM-1 shedding in an *in vivo* model, including the possible effect of KIM-1 shedding on AKI to CKD and ESRD transition as well as the functional relevance of sKIM-1 in blood and urine. Studies characterizing the functional differences between wild type KIM-1 and the shedding defective mutant KIM-1 will be critical for deepening our understanding of the shedding mechanism and any further considerations that should be made when using the shedding defective mouse model for further studies.

The specific aims of the work outlined in this thesis were 1) to identify the cleavage site of mKIM-1, 2) generate shedding defective mutant mKIM-1 *in vitro*, and 3) study the functional relevance of a shedding defect *in vitro*.

### 1.4.3 Hypothesis

I hypothesized that the mKIM-1 cleavage site is situated between T194 and I202, based on basic local alignment search tool (BLAST) sequence alignment with the predicted cleavage region on hKIM-1 and that altering relevant amino acids around the cleavage site will result in a shedding defective mutant that will remain functionally intact in terms of its phagocytic capacity. Based on previous studies, I predicted that the spontaneous shedding of KIM-1 has biological significance in protecting against kidney fibrosis and transition from AKI to CKD.

# Chapter 2

## 2   Materials & Methods

## 2.1   Cell culture

Human Embryonic Kidney 293 (HEK293) cells were cultured at 37°C in 5% (v/v) $CO_2$ in Dulbecco's Modified Eagle Medium (DMEM; Lonza, Walkersville, MD) containing 10% (v/v) fetal bovine serum (FBS; GIBCO Cat No. 10437028) and 5% (v/v) penicillin/streptomycin solution (P/S; Invitrogen, Carlsbad, CA). HEK293 cells made to stably express the expression plasmid for Flag (DYKDDDDK)-tagged mKIM-1 (Addgene plasmid # 49205) were maintained in DMEM at 37°C in 5% (v/v) $CO_2$ supplemented 400 μg/mL Geneticin (G418) Sulfate (Santa Cruz Biotechnology, CA) in addition to 10% (v/v) FBS, and 5% (v/v) P/S. All HEK293 cell lines were maintained in plates coated with poly-DL-lysine hydrobromide (Sigma-Aldrich, St. Louis, MO) for better cell attachment.

Renal epithelial cell carcinoma cells (RENCA) transduced with lenti ORF particles containing a vector with murine KIM-1 (RENCA KIM-1; MR203831L3V; Origene, Rockville, MD) or control vector (RENCA Control; MR203831L3V; Origene, Rockville, MD) were cultured at 37°C in 5% (v/v) $CO_2$ in RPMI-1640 medium containing 10% FBS, 5% P/S, 0.1 mM non-essential amino acids (ThermoFisherScientific, Waltham, MA), 1 mM sodium pyruvate (ThermoFisher Scientific), and 2 mM L-glutamine (ThermoFisher Scientific).

Primary PTECs were obtained from 3-6 week old C57Bl/6 wild-type mice (WT PTECs) and IRI-injured mice (IRI PTECs) and maintained in serum-free DMEM supplemented with 5% Insulin-Transferrin-Selenium (Invitrogen), 5% P/S, 0.5 μg/mL of mouse epidermal growth factor (Peprotech, Rocky Hill, NJ), and 50 ng/mL hydrocortisone (Thermo Fisher Scientific, Rockford, IL) for 6 days at 37°C with 5% (v/v) $CO_2$. After 6 days, media was supplemented with 5% (v/v) FBS.

## 2.2 Western Blots

Cell lysates were collected with 4% (w/v) sodium dodecyl sulfate (SDS; BioBasic Inc.) in $1 \times$ phosphate buffered saline (PBS; 137 mM NaCl, 2.7 mM KCl, 4.3 mM $Na_2HOP_4$, 1.47 mM $KH_2PO_4$, pH 7.4), and conditioned media were collected from cell monolayers following the appropriate treatments. Media samples were centrifuged at 16,000 g for 15 mins to pellet any cell remnants, supernatant was collected and EDTA-free mini protease inhibitor tablets (Sigma Aldrich Cat No. 4693159001) were added. Equal volumes of the supernatant (70 µL) was combined with 10 µL of 6× loading dye containing ß-mercaptoethanol as a reducing reagent. Protein concentrations of cell lysates were determined using the Pierce BCA Protein Assay Kit (Thermo Fisher Scientific) and lysate samples were prepared to contain 50 µg for loading. All samples were boiled for 5 minutes at 95°C to denature. Samples were separated by SDS-PAGE, and transferred to polyvinylidene difluoride membranes (Millipore, Billerica, MA) for 50 minutes at 90 V. Membranes were blocked with 3% (w/v) BSA (bovine serum albumin; BioBasic Cat No. AD0023) in TBST (Tris-buffered saline, 0.2% Tween-20) for 30 minutes and then incubated overnight at 4°C with anti-KIM-1 goat primary antibody (dilution 1:2000; Cat No. AF1817, R&D Systems, Minneapolis, MN) against the extracellular domain of KIM-1, anti-GAPDH (6C5) mouse antibody (dilution 1:1500; Santa Cruz Biotechnology) or anti-ADAM10 rabbit antibody (dilution 1:500, Cat # AB19026, Millipore) . Membranes were subsequently washed with TBST four times for 7 minutes each and then incubated with the appropriate horseradish peroxidase-conjugated secondary antibody (dilution 1:20000; Jackson ImmunoResearch Laboratories, West Grove, PA) for 1 hour at room temperature in blocking buffer in the dark, and then washed again four times for 7 minutes each. Proteins were visualized using chemiluminescent HRP substrate (Millipore) on Licor C-digit imaging device. Results were quantified by analyzing densitometric values from western blot images using Image Studio Lite.

## 2.3   Endogenous cleavage of KIM-1 method

### 2.3.1   Accelerated KIM-1 shedding into media

HEK293 cells stably expressing flag (DYKDDDDK)-tagged murine KIM-1 were plated on twenty 15cm plates and grown to about 90% confluency. Cells were washed with PBS, then treated with 1 µM phorbol 12-myristate 13-acetate (PMA) (Sigma-Aldrich, St. Louis, MO) in serum-free DMEM for 1 hour at 37°C with 5% (v/v) $CO_2$ to induce accelerated shedding of KIM-1 ectodomain into condition media. Media samples were collected and centrifuged at 500 g for 5 mins to remove any cellular remnants leaving behind the cleaved ectodomain portion of KIM-1 in the supernatant. Mini-protease inhibitor tablets (Sigma Aldrich) were added to prevent any further unwanted degradation of protein.

### 2.3.2   Immunoprecipitation, Deglycosylation, Dialysis

Media samples were incubated with Anti-DYKDDDDK Tag (L5) affinity gel (BioLegend) at 4°C overnight to immunoprecipitate cleaved KIM-1. Gel was then washed and centrifuged at 500 g for 5 mins three times with PBS. Immunoprecipitated KIM-1 was released from the gel by boiling at 95°C for 5 mins in 1% (w/v) SDS. This was repeated three times and kept in separate aliquots to ensure complete release of KIM-1 from gel. Samples were lyophilized before undergoing chemical deglycosylation (Sigma Glycoprofile IV Deglycosylation Kit). To remove N- and O- linked glycans trifluoromethanesulfonic (TFMS) acid, anisole was used as a free-radical scavenger to increase yield of reaction product. Enzyme-mediated deglycosylation method was also tried with PNGase F (Promega) to remove only N-linked glycans. This deglycosylation step is critically important for efficient protein sequencing during the subsequent analysis stages. Samples are then either desalted using Amicon Ultra-0.5 centrifugal filters (Millipore Sigma) to remove any impurities and concentrate or dialyzed using a 3,500 Da molecular weight cut-off dialysis membrane (BioDesign Inc.) in acetonitrile (ACN)/50 mM ammonium bicarbonate (ABC) buffer solution to remove any impurities. Dialysis was performed with 3 exchanges against 1L buffer with a minimum of 8 h between exchanges.

### 2.3.3    Coomassie gel stain, in-gel digest and mass spectrometry

The protein samples were concentrated with a Speedvac vacuum concentrator (ThermoFisher Scientific) before being run on SDS-PAGE to resolve deglycosylated soluble KIM-1. The polyacrylamide gels are then stained with Coomassie Brilliant Blue R-250 (Bio Basic Canada Inc.) to better visualize KIM-1 bands. Gels were first fixed for 30 minutes in fixing solution (50:10:40 (v/v); 100% methanol: glacial acetic acid: $H_2O$), then stained in Coomassie solution for 30 minutes. Gels were then destained until no background remained using destaining solution (45:10:45 (v/v); 100% methanol: glacial acetic acid: $H_2O$). Gels were stored in 5% glacial acetic acid until bands were excised. Bands of interest are cut using Ettan^TM Spot Picker robotic system as 1 mm rounds and in-gel digestion performed with thermolysin (Promega) and/or ArgC (Promega) at the Functional Proteomics Facility at Western University using the Waters MassPREP Station for Automated In-gel Digestion (Appendix A6). Digested samples were analyzed by protein identification services at the UWO Biological Mass Spectrometry Laboratory / Dr. Don Rix Protein Identification Facility using Ultra High Pressure Liquid Chromatography Electrospray Ionization Mass Spectrometry (ESI-MS/MS) (Appendix A7) and Peaks 7.5 (Bioinformatics Solutions Inc., Waterloo, ON) for data analysis. Figure legend for post-translational modifications marked on ESI-MS/MS results can be found in Appendix A5.

## 2.4    Synthetic KIM-1 peptide cleavage method

As a second strategy, a twenty amino acid long KIM-1 custom synthetic peptide (Genscript) was made to contain the predicted cleavage region (T194 to I202 SSGDTWSNHTEAIPPGKPQK, Figure 2.) devoid of any N- and O- linked glycans which are normally observed on the endogenous protein. This prevents the need to perform any deglycosylation or desalting steps, as required in the first strategy, which is where most of the sample is likely to become lost. The synthesized peptides were first analyzed by size exclusion chromatography to assess purity. The AKTA Pure 25L Fast Protein Liquid chromatography (FPLC) (GE Healthcare) system housed at ~6°C was used with size-exclusion Superdex Peptide 10/300 column for gel filtration. KIM-1 peptide (200ug) elution was monitored using UV absorbance at 214 nm. The flow rate was set to 0.5 mL/min and the running buffer was 50 mM Tris-HCl (pH=9.0) solution.

The KIM-1 synthetic peptide (10 µM) was incubated with and without (negative control) recombinant mouse TACE (rmTACE, 0.01 µg, R&D systems) in TACE assay buffer (50 mM Tris, pH 9.0) or recombinant mouse ADAM10 (rmADAM10, 0.1 µg, Cat # 946-AD, 2978-AD, R&D systems) in ADAM10 assay buffer (25mM Tris, 2.5µM $ZnCl_2$, 0.005% (w/v) Brij-35, pH 9.0) for 1 h shaking at 37°C then another 15 h without shaking at 37°C with 5% (v/v) $CO_2$. Samples incubated with detergent (ie. Brij-35) had to be purified using Zip Tips $C_{18}$ (EMD Millipore, Cat no. ZTC18S096) before being sent for analysis by protein identification services at the UWO Biological Mass Spectrometry Laboratory / Dr. Don Rix Protein Identification Facility by ESI-MS/MS. Enzymatic activity was confirmed for both rmTACE and rmADAM10 using the positive control fluorescent substrate MCA-P-L-A-Q-A-V-DPA-R-S-S-S-R-NH2 (Cat# ES003, R&D) and MCA-P-L-OH (Bachem, Catalog # M-1975) as the calibration standard as described by the R&D enzyme activity assay manufacturer protocol.

## 2.5 Generation of KIM-1 mutants

### 2.5.1 Site-directed mutagenesis and stable transfections

Site-directed mutagenesis (SDM) (Stratagene Protocol) was performed with Quikchange Lightning mutagenesis kit (Agilent Technologies, Cat No. 210518), expression plasmid for Flag (DYKDDDDK)-tagged mKIM-1 (Addgene plasmid # 49205) and forward and reverse primers (IDT) designed with the mutated sequence I202Q or I202A, as shown in Table 1. According to the stratagene protocol mutated plasmids were transformed into XL10 Gold ultracompetent DH5α bacteria and plated on lysogeny broth (LB) agar plates with 100 µg/mL ampicillin (Fisher Bioreagents, Cat No. BP17605) for selection. Single colonies were picked and inoculated in LB broth with ampicillin (100 µg/mL) for 12-16 h before plasmids were extracted using Monarch Plasmid Mini-prep kits (NEB, Cat No. T1010). Extracted plasmids were sequenced at Robarts Research Institute DNA sequencing facility with Ef1α and/or PrimerBlast designed primer KIM-1 Sequence 1 (Table 1.) to ensure successful mutation. Correctly mutated plasmids were transfected into parental HEK293 cells (Lipofectamine® 2000 Thermo Fisher Scientific) in 6-well dishes (2000 ng/well) for 48 h. Cells from a single well were then transferred to a 15 cm plate to

select stably transfected cells by culturing in complete selection media containing 800 µg/mL of G418 antibiotic for 10 consecutive days until non-transfected cells were completely killed. Individual G418-resistant colonies were picked by aspirating medium, washing cells with 1x PBS, and incubating cells with filter paper soaked in 0.25% trypsin-EDTA (Invitrogen) for 5 minutes in a 37°C, 5% (v/v) CO2 incubator. Filter paper with attached cells were picked and grown in 24-well plates in full medium containing 400 µg/ml G418 until cells reached confluency. Individual colonies were then expanded and colonies with highest expression of KIM-1 according to western blot analysis were maintained for further studies.

**Table 1. Primer Sequences**

Sequence details of forward (FW) and reverse (RV) primers designed for site-directed mutagenesis (Quikchange primer design – Agilent Technologies) or DNA sequencing (PrimerBlast) of pCDEF3-CD8SS Flag mKIM-1. (nucleotide, nt.; melting temperature, Tm)

| *Primer Name* | *Primer Sequence 5' → 3'* | *Length (nt)* | *Tm (°C)* |
|---|---|---|---|
| *KIM-1 I202Q* | FW: gcggcttccctggaggttgtgcttcagtgtgattactccag | 41 | 79.72 |
| | RV: ctggagtaatcacactgaagcacaacctccagggaagccgc | 41 | 79.72 |
| *KIM-1 I202A* | FW: ttccctggaggggctgcttcagtgtgattactccagg | 37 | 78.91 |
| | RV: cctggagtaatcacactgaagcagcccctccagggaa | 37 | 78.91 |
| *Ef1α* | FW: tcaagcctcagacagtggtt | 21 | 57 |
| *KIM-1 Sequence 1* | FW: ccacagctacaggaagaccc | 20 | 60 |

## 2.5.2  Cell Surface KIM-1 Expression

Experimental cells from culture were detached using 0.25% trypsin-EDTA (Invitrogen) and incubated for 5 mins at 37°C. DMEM media with 10% FBS was then added to stop trypsin activity and for single cell resuspension. Cells were counted using a hemocytometer to allocate $1 \times 10^6$ cells of each cell type for experimentation. Negative control sample had a mixture of all cell types tested. Samples were centrifuged at 500 g for 5 mins and

resuspended in 100 µL of staining buffer (PBS + 0.2% BSA) before being transferred to flow tubes on ice. Then 5 µL of KIM-1 antibody (AF1817; R&D Systems, Minneapolis, MN) was added to each tube, except the negative control, vortexed and incubated on ice for 30 – 60 minutes. Samples were vortexed again half-way through incubation period. After incubation, samples were washed with 1 mL – 2 mL of staining buffer, centrifuged at 500 g for 5 minutes and resuspended in 100 µL of staining buffer. Then 5 µL of secondary antibody rabbit anti-goat IgG (H+L) Dylight 488 (Invitrogen, SAS-10078) was added to each tube including the negative control, vortexed and incubated on ice for another 30 – 60 minutes. Wash step was then repeated, and stained cells were resuspended in 300 µL of staining buffer to be transferred to a 96-well plate. Samples were analyzed by flow cytometry on cytoFLEX cytometer as a single colour experiment with FITC and analyzed using FlowJo X software.

## 2.6   KIM-1 shedding assay

I compared KIM-1 ectodomain shedding between HEK293 cells stably transfected with wild type (WT) or the mutated KIM-1 constructs. Cells were cultured in 6-well plates until >80% confluency. I then treated cells with either DMSO, PMA (Calbiochem, Cat No. 524400) (1 µM), ionomycin (Peprotech, Cat No. 5608212 ) (500 nM), and/or ADAM10 selective inhibitor GI254023X (Sigma Aldrich, Cat No. SML0789) (4 µM) to study differences in accelerated and spontaneous KIM-1 shedding and the possible role of ADAM10 and/or ADAM17 in mediating this shedding mechanism. Condition media was collected, centrifuged at 16,000 g for 15 minutes to remove any cellular debris. Equal volumes of the supernatant (70 µL) was combined with 10 µL of 6X loading dye containing ß-mercaptoethanol as a reducing reagent. Samples were boiled for 5 minutes at 95°C to denature. Cell lysates were collected and quantified as previously described. Results were quantified by analyzing densitometric values from western blot.

## 2.7   Phagocytosis assay

### 2.7.1   Collection and staining of apoptotic thymocytes

Thymuses were dissected from sacrificed C57BL/6 mice and placed in DMEM media + 1% P/S. All animal work was conducted under an animal protocol (2018-36), approved by

the Animal Use Subcommittee at Western University. Generally, the thymus from one mouse results in about 10 million apoptotic thymocytes for staining. Cells were strained through a 40 μm cell strainer (Fisherbrand, Cat No. 22363547) into a 50 mL tube using the plunger of a syringe to break up the thymus. PBS (1x) was added 5 mL at a time three times during the straining process to help break up the tissue. Strained thymocytes were centrifuged at 500 g for 5 mins and supernatant was aspirated. Ammonium chloride potassium (ACK) lysis buffer (ThermoFisher Scientific) was then used to lyse any remnant red blood cells in the mixture by adding 1 mL directly to tube and resuspending cells immediately. The solution was incubated with cap open for 3 mins at room temperature. Subsequently, 1 x PBS was added to stop lysis buffer activity by diluting the solution. Tubes were centrifuged at 500 g for 5 mins and supernatant was aspirated. DMEM media with low serum (2% FBS) + 1% P/S was used to resuspend cells and break up any visible clumps. Cells were transferred to a Petri dish and placed under UV light for 7 mins with the lid off to induce apoptosis. Cells were then moved to the 37°C incubator with 5% (v/v) $CO_2$ to incubate overnight. This method results in over 90% of cells becoming early apoptotic cells based on positive staining with FITC-conjugated annexin V (Biolegend) and exclusion of propidium iodide which stains necrotic cells, as previously reported (Ichimura, Asseldonk et al. 2008).

The next day, apoptotic cells were washed with 1 x PBS, centrifuged at 500 g for 5 mins, and resuspended in 20 mL of 1 x PBS. Thymocytes were counted using a hemocytometer and 30 million cells were centrifuged at 500 g for 5 mins and resuspended in 1 mL of 1 x PBS. Next, 1.5 μL of 1 mg/μL pHrodo™ Red, SE (ThermoFisher Scientific, Cat No. P36600) was added to 1 mL PBS per 30 million thymocytes in the dark. Cells were stained at room temperature for 30 mins in the dark. Then, 5 mL of 1 x PBS was used to wash the cells, the mixture was centrifuged at 500 g for 5 mins and the supernatant was aspirated. This wash procedure was repeated a second time to ensure removal of excess dye.

## 2.7.2    Phagocytosis and Flow Cytometry

Experimental HEK293 cells were plated in 6-well plates and cultured to be 70% confluent on day of phagocytosis experiment. Cells were washed with 1 x PBS, then replaced with 1 mL antibiotic-free DMEM + 10% (v/v) FBS per well. pHrodo™ Red stained thymocytes

were added directly to the media (3 million cells per well) and plates were briefly rocked back and forth before 90 mins incubation at 37°C with 5% (v/v) $CO_2$. Cells were then placed on ice for 30 minutes to reduce non-specific binding of apoptotic cells. Media was then aspirated from wells and cells were washed three times with cold 1 x PBS. Cells were detached with 0.25% EDTA-trypsin (Invitrogen) and incubated for 5 mins at 37°C. DMEM media with 10% (v/v) FBS was then added to stop trypsin activity and for cell resuspension. Cells were transferred to labelled flow tubes and centrifuged at 500 g for 5 mins. The supernatant was decanted, and cells were resuspended in 300 µL of 1 x PBS and vortexed prior to transfer to a 96-well flat bottom plate. Samples were analyzed by cytoFLEX flow cytometry as a single colour experiment. HEK293 cells not incubated with apoptotic thymocytes were used as a negative control for gating ($<10^3$ fluorescence intensity). Percentage phagocytosis was determined as the fraction of HEK293 cells that have internalized apoptotic thymocytes as indicated by higher fluorescence ($10^4 - 10^5$ logarithmic scale) out of all HEK293 cells.

## 2.8 siRNA transfection for ADAM10 silencing

On the day before transfection, $5 \times 10^5$ HEK293 cells stably expressing WT KIM-1 were seeded per well in a 12-well plate with DMEM + 10% (v/v) FBS culture media free of antibiotics. The next day, cells were 90-95% confluent and ready for transfection with Endofectin™ Max Transfection reagent (Cat. EF103, GeneCopoeia™ Inc.). ADAM10 siRNA (sc-41410-h, Santa Cruz) was used as a pool of 3 target specific 19-25 nucleotides long siRNAs. Control siRNA-A (Santa Cruz) was used alongside as a negative control for transfections. siRNA was reconstituted to 10 µM of which 4 µL was diluted with 46 µL of Opti-MEM I Reduced Serum media (Cat. 31985-088, Life Technologies) per well and incubated at room temperature for 5 mins. Endofectin™ Max Transfection reagent (2 µL) was diluted with 48 µL of Opti-MEM per well. Diluted DNA and diluted transfection reagent were combined and incubated at room temperature for another 15 minutes to allow DNA-transfection reagent complexes to form. Cells were washed three times with 1 x PBS and 900 µL of antibiotic-free DMEM with 10% FBS was added to each well. Then 100 µL of the combined DNA-transfection reagent mixture were added to the cells in a dropwise manner and rocked back and forth to mix before incubation at 37°C in 5% (v/v) $CO_2$ for

24 h. Control cells were washed three times with 1 x PBS, then replaced with 1 mL of antibiotic-free DMEM with 10% FBS per well. After 24 h, all cells were washed three times with 1 x PBS to remove any remaining transfection reagents, then replaced with 350 μL of serum-free antibiotic-free DMEM per well to start the shedding assay. Samples were incubated at 37°C in 5% (v/v) $CO_2$ for 1 h to allow for KIM-1 shedding into media. Media and lysate samples were collected and run on SDS-PAGE for western blot as described above.

## 2.9   Data and Statistical Analysis

ESI-MS/MS sequencing results for KIM-1 were analyzed by determining the percentage of full-length KIM-1 construct sequence coverage and the number of supporting peptides analyzed.  Western blot results were quantified by analyzing densitometric values from images using Image Studio Lite. KIM-1 in lysates was normalized using densitometric values for GAPDH in the respective lanes. Differences in KIM-1 shedding after control siRNA and ADAM10 siRNA transfections was compared using Student's unpaired parametric $t$-test. Differences in KIM-1 shedding between WT and mutants in response to drug treatments was compared using two-way analysis of variance (ANOVA) and Tukey's post-hoc multiple comparisons test to compare individual means. Percentage of phagocytosis between treatment groups was analyzed using one-way ANOVA and Tukey's post-hoc test to compare individual means. All statistical analysis and graphing were done in GraphPad Prism 6.01 (GraphPad Software Inc.; La Jolla, CA) and all data are presented as mean ± standard error of the mean (SEM) with a p-value less than 0.05 considered to be significant.

# Chapter 3

# 3 Results

## 3.1 ESI-MS/MS sequencing to identify mKIM-1 cleavage site

The predicted cleavage region on mKIM-1 was determined to be between T194 and I202 based on BLAST sequence alignment with the predicted cleavage region on hKIM-1 (Bailly, Zhang et al. 2002) (Figure 3). T194 to I202 is situated in the stalk region with a heavily glycosylated mucin domain upstream and the transmembrane region downstream (Figure 3).

**A.**

| | 10 | 20 | 30 | 40 | 50 |
|---|---|---|---|---|---|
| | MNQIQVFISG | LILLLPGAVD | SYVEVKGVVG | HPVTLPCTYS | TYRGITTTCW |
| | 60 | 70 | 80 | 90 | 100 |
| | GRGQCPSSAC | QNTLIWTNGH | RVTYQKSSRY | NLKGHISEGD | VSLTIENSVE |
| | 110 | 120 | 130 | 140 | 150 |
| | SDSGLYCCRV | EIPGWFNDQK | VTFSLQVKPE | IPTRPPRRPT | TTRPTATGRP |
| | 160 | 170 | 180 | 190 | 200 |
| | TTISTRSTHV | PTSTRVSTST | PPTSHTWTH | KPDWNGTVTS | SGDTWSNHTE |

210 AIPPGKPQKN  220 PTKGFYVGIC  230 IAALLLLLLV  240 STVAITRYIL  250 MKRKSASLSV

260 VAFRVSKIEA  270 LQNAAVVHSR  280 AEDNIYIVED  RP

**Predicted O- and N-linked glycosylation sites**
Predicted cleavage site region
Predicted transmembrane domain
Cytoplasmic tyrosine phosphorylation motif

**B.**

| Start | | End | Organism |
|---|---|---|---|
| 1 | | 359 | Homo sapiens |
| 1 | | 282 | Mus musculus |
| 1 | | 307 | Rattus norveqicus |
| 1 | | 478 | Chlorocebus aethiops |
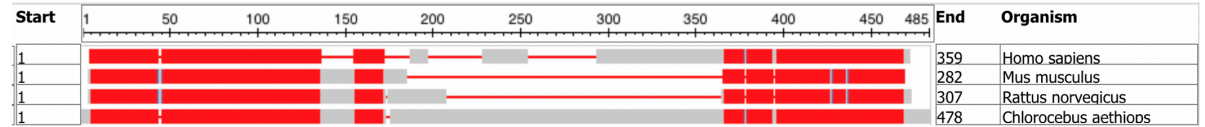
```
Homo sapiens          1    -MHPQVVILSLILHLADSVAGSVKVGGEAGPSVTLPCHYS--GAVTSMCWNRGSCSLFTCQNGIVWTNGTHVTYRKD   74
Mus musculus          1    MNQIQVFISGLILLLPGAVDSYVEVKGVVGHPVTLPCTYSTYRGITTTCWGRGQCPSSACQNTLIWTNGHRVTYQKS   77
Rattus norveqicus     1    MVQLQVFISGLLLLLPGSVDSYEVVKGVVGHPVTIPCTYSTRGGITTTCWGRGQCPYSSCQNILIWTNGYQVTYRSS   77
Chlorocebus aethiops  1    [4]IMHLQVVILSLILHLADSVADSVNVDGVAGLSITLPCRYN--GAITSMCWNRGTCSVFSCPDGIVWTNGTHVTYRKE   79

Homo sapiens          75   TRYKLLGDLSRRDVSLTIENTAVSDSGVYCCRVEHRGWFNDMKITVSLEIVPPKVT-------------------TTPIV   135
Mus musculus          78   SRYNLKGHISEGDVSLTIENSVESDSGLYCCRVEIPGWFNDQKVTFSLQVKPEIPTRPPRRPTTTRPTATGRPTTISTRS   157
Rattus norveqicus     78   GRYNIKGRISEGDVSLTIENSVDSDSGLYCCRVEIPGWFNDQKMTFSLEVKPEIPTSPPTRPTTTRPTTT-RPTTISTRS   156
Chlorocebus aethiops  80   TRYKLLGNLSRRDVSLTIANTAVSDSGIYCCRVKHSGWFNDMKITISLKIGPPRVTIPIVRTVRTSTTVPTTTTTTLPTT   159

Homo sapiens          136  TTVPTVTTVRTS---------------TTVPTTTTVP----------     TTTVPTTMSIPTTTTVLTTMTVSTTT      183
Mus musculus          158  THVPTSTRVSTSTpPTSTHTWTHKP----------------------  --------------------------       182
Rattus norveqicus     157  THVPTSTRVSTST-PTPEQTQTHKPEITTFYAHETTAEVTETPSYTP  --------------------------       202
Chlorocebus aethiops  160  TTLPTTTTLPTTM---TLPTTTTLPMTTTLPTTTTVPMTTTLPTTLP[21]TTTLPTTMTLPMTTTLPTTTTLPTTT[40]  290

Homo sapiens          184  SVPTTTSIPTTTSVPVTTTVSTFVPPMPLPRQNHEPVATSPSSPQPAETHPTTLQGAIRREPTSSPLYSYTTDGNDTVTE   263
Mus musculus          183  -------------------------------------------------------------------------DWNGTVTS   190
Rattus norveqicus     203  -------------------------------------------------------------------------ADWNGTVTS  211
Chlorocebus aethiops  291  TLPTTTTLPTTTTLPTTTMVSTFVPPTPLPMQDHEPVATSPSSAQPAETHPVTLLGATRTQPTSSPLYSYTTDGSDTVTE   370

Homo sapiens          264  SSDGLWNNNQTQLFLEHSLLTANTTKGIYAGVCISVLVLLALLGVIIAKKYFF-KKEVQQLS-VSFSSLQIKALQNAVEK   341
Mus musculus          191  SGDT-WSNHTEAIPPGKPQK--NPTKGFYVGICIAALLLLLLVSTVAITRYILMKRKSASLSVVAFRVSKIEALQNAAVV   267
Rattus norveqicus     212  SEEA-WNNHTVRIPLRKPQR--NPTKGFYVGMSVAALLLLLLASTVVVTRYIIIRKKMGSLSFVAFHVSKSRALQNAAIV   288
Chlorocebus aethiops  371  SSDGLWNNNQTQLSPEHSPQMVNTTEGIYAGVCISVLVLLAVLGVVIAKKYFF-KKEIQQLS-VSFSNHQFKTLQNAVKK   448

Homo sapiens          342  EVQAEDNIYIENSLYATD-        359
Mus musculus          268  HSRAEDNIYIVEDRP----        282
Rattus norveqicus     289  HPRAEDNIYIIEDRSRGAE        307
Chlorocebus aethiops  449  EVHAEDNIYIENNLYAMNQ[11]    478
```

```
264   SSDGLWNNNQTQLFLEHSLLTAN
191   SGDT-WSNHTEAIPPGKPQK--N
212   SEEA-WNNHTVRIPLRKPQR--N
371   SSDGLWNNNQTQLSPEHSPQMVN
```
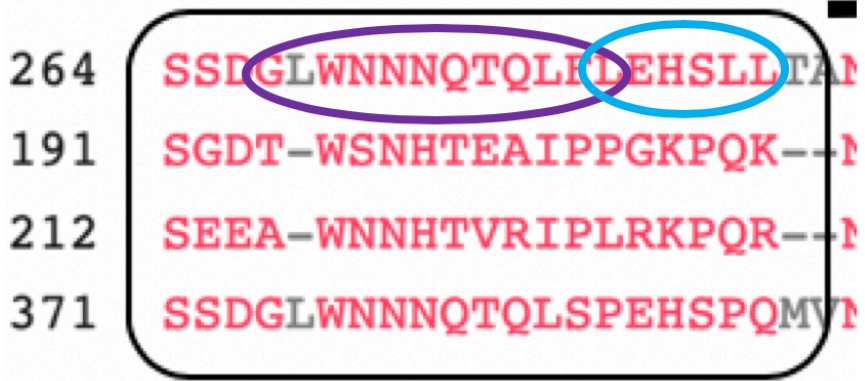
**Figure 3 Murine KIM-1 sequence and BLAST alignment**

**(A)** mKIM-1 sequence (NCBI accession sequence ID Q3V033) with 282 amino acids. O- and N-linked glycosylation sites in mucin domain were predicted using NetOGlyc 4.0 (Steentoft, Vakhrushev et al. 2013) and NetNGlyc 1.0 servers (Gupta 2004), respectively. Transmembrane region predicted using TMHMM v.2.0 server (Krogh, Larsson et al. 2001). Predicted cleavage region determined from (B) BLAST sequence alignment. **(B)** BLAST sequence alignment of KIM-1 from different species. Homo sapiens - sequence ID Q96D42, Mus musculus - sequence ID Q3V033, Rattus norveqicus sequence ID - O54947 and Chlorocebus aethiops sequence ID - O46598. Predicted cleavage region on hKIM-1 (Bailly, Zhang et al. 2002), G267 to L278, outlined in purple and aligns with T194 to I202 on mKIM-1. Deletion mutant Δ278-283 outlined in blue on hKIM-1 results in shedding defective mutant (Zhang, Humphreys et al. 2007, Gandhi, Yi et al. 2014).

### 3.1.1    Endogenous enzyme cleavage method

To find the exact cleavage site within mKIM-1, transfected HEK293 cells stably expressing FLAG-tagged WT mKIM-1 were stimulated with PMA, a known potent inducer of TACE (Lorenzen, Lokau et al. 2016). mKIM-1 was cleaved and a portion of the extracellular domain was shed into media via enzymes endogenously expressed by these cells. Media samples were immunoprecipitated for FLAG-KIM-1 and run on SDS-PAGE gels for western blot or spot-picking for ESI-MS/MS sequence analysis.

Sequence coverage for cleaved mKIM-1 covered the N-terminus region from FLAG to phenylalanine (F113) as observed on Figure 4. Predicted glycosylation sites (Figure 3.) start downstream of this position and is likely interfering with digesting, ionizing, fragmenting, and sequencing peptides in this region. Therefore, I then performed deglycosylation of shed mKIM-1 to allow for efficient protein digestion and sequencing.

**Figure 4. ESI-MS/MS analysis of sKIM-1.**

FLAG mKIM-1 HEK293 cells were treated with PMA for 1 hour. sKIM-1 (55 kDa) was immunoprecipitated from media and run on SDS-PAGE and Coomassie brilliant blue stained. Samples were spot-picked near 55 kDa mark and digested in-gel with trypsin and chymotrypsin. Protein coverage was 37% of full-sized KIM-1, or approximately 51% of sKIM-1, supported by 51 peptides. Blue lines indicate successfully massed peptides.

Chemical deglycosylation with TFMS acid would be the most efficient for removing complex O-linked glycans commonly observed in mucin domains as well as N-linked glycans in the stalk region. A major issue with running samples that were deglycosylated with a harsh acid like TFMS on SDS-PAGE is the aberrant migration and distortion of bands (Figure 5A and 5B.). This made it difficult to pinpoint where deglycosylated sKIM-1 was situated on the Coomassie brilliant blue stained gel (Figure 5C) for further spot-picking and downstream ESI-MS/MS sequencing analysis. I therefore used enzyme-mediated deglycosylation method as an alternate strategy to overcome this problem.
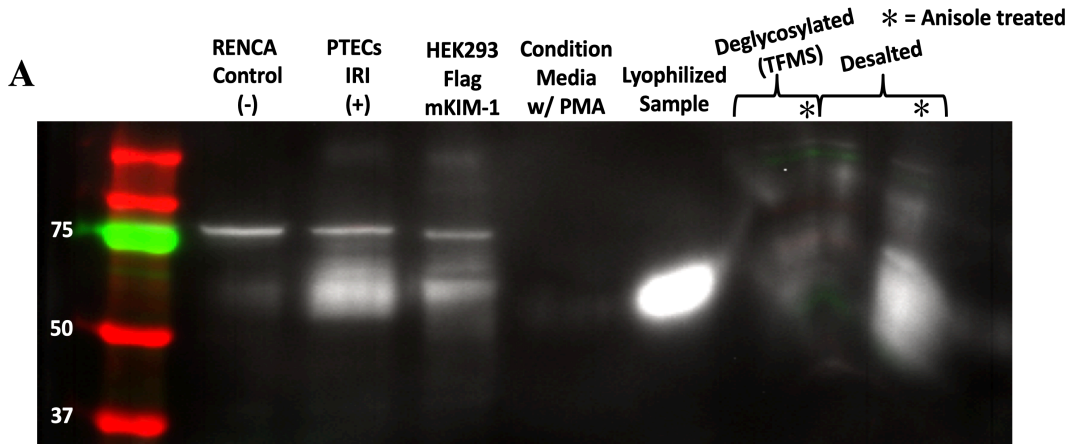
**Figure 5. Endogenous enzyme cleavage of mKIM-1 and deglycosylation with TFMS**

(A) Western blot with goat anti-mKIM-1 antibody (Ab) (AF1817, 1:2000). Samples collected at various stages of endogenous enzyme cleavage method using TFMS acid for deglycosylation and Amicon centrifugal filter tubes for desalting. Samples from left to right include lysates of RENCA control cells (negative control), primary PTEC lysates from IRI C57Bl/6 mice (positive control), HEK293 FLAG mKIM-1 cell lysates, condition media with sKIM-1 after PMA treatment, lyophilized sample of immunoprecipitated sKIM-1, two lanes of TFMS deglycosylated sKIM-1 (with and without anisole treatment), two lanes of TFMS deglycosylated and desalted sKIM-1 (with and without anisole treatment). (B) SDS-PAGE gel corresponding to the blot shown in (A). Samples in last four lanes running in distorted fashion. (C) Coomassie brilliant blue stained gel with deglycosylated and desalted samples also ran in distorted fashion.

PNGase F is a specific deglycosylation enzyme which only removes N-linked glycans. An equivalent enzyme capable of removing mucin domain linked heterogenous complex of O-linked glycans was not available. Next, I tested if removal of N-linked glycans surrounding the predicted cleavage region (T194-I202) was sufficient for sequencing near the potential cleavage site. As observed in Figure 6A, PNGase treatment of sKIM-1 collected from HEK293 FLAG mKIM-1 samples resulted in a slight downward smear likely because each N-glycan has a predicted weight of about 2.5 kDa which will be removed upon deglycosylation. No bands were observed on the corresponding Coomassie stained gel (Figure 6B), however samples were still picked at 50 kDa for in-gel digestion with thermolysin and sequence analysis. No KIM-1 was detected. Therefore, more cleaved KIM-1 samples were collected in a second trial (six 15 cm plates vs ten 15 cm plates) and incubated with PNGase F for a longer period of time (1 h vs. 3 h) in an effort to increase yield of deglycosylated cleaved mKIM-1. When compared to non-deglycosylated samples (Figure 4), sequence coverage in PNGase treated samples (Figure 7) did not improve, and the same region predicted to be rich in O- and N-linked glycosylations remained unsequenced.
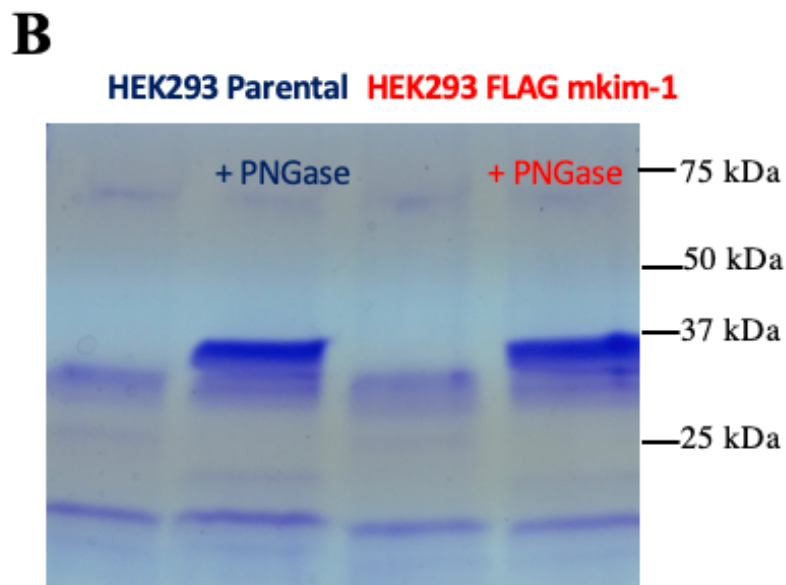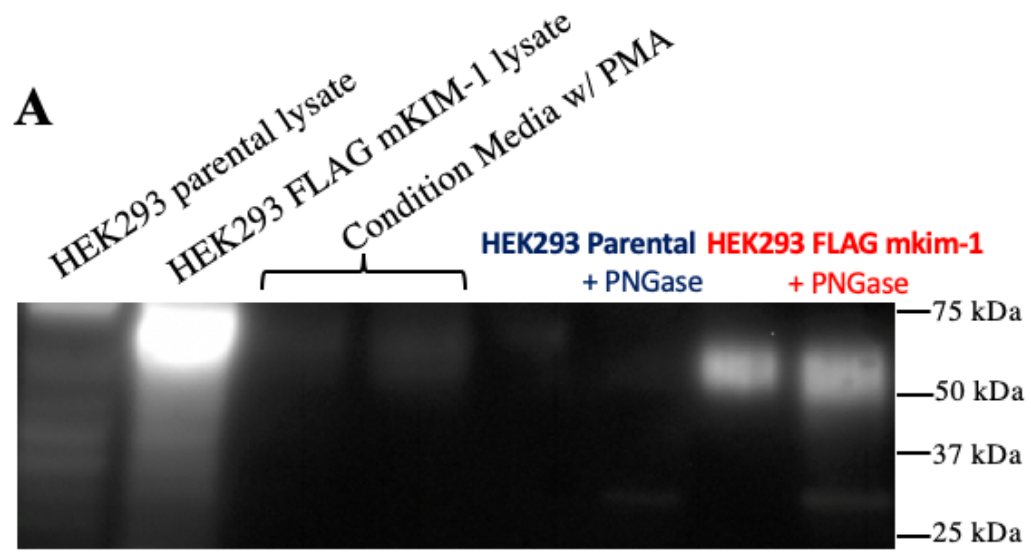
**Figure 6. Endogenous enzyme cleavage of mKIM-1 and deglycosylation with PNGase F enzyme (First Trial)**

(A) Western blot with goat anti-mKIM-1 Ab (AF1817, 1:2000). Samples collected at various stages of endogenous enzyme cleavage method using PNGase F for deglycosylation. Samples from left to right include lysates of HEK293 parental cells (negative control), HEK293 FLAG mKIM-1 cell lysates, conditioned media from HEK293 FLAG mKIM-1 cells after 1 h PMA treatment, and the last four lanes are immunoprecipitated sKIM-1 samples (10 µL) from HEK293 parental or HEK293 FLAG mKIM-1 cultured on six 15 cm plates treated with or without 4 µg PNGase F for 1 h at 37°C. (B) Coomassie brilliant blue stained gel with aliquots (40 µL) of immunoprecipitated sKIM-1 samples from (A).

**C**

```
  1  MNQIQVFISG LILLLPGAVD SYVEVKGVVG HPVTLPCTYS TYRGITTTCW GRGQCPSSAC QNTLIWTNGH RVTYQKSSRY

 81  NLKGHISEGD VSLTIENSVE SDSGLYCCRV EIPGWFNDQK VTFSLQVKPE IPTRPPTRPT TTRPTATGRP TTISTRSTHV

161  PTSIRVSTST PPTSTHTWTH KPEPTTFCPH ETTAEVTGIP SHTPTDWNGT VTSSGDTWSN HTEAIPPGKP QKNPTKGFYV
241  GICIAALLLL LLVSTVAITR YILMKRKSAS LSVVAFRVSK IEALQNAAVV HSRAEDNIYI VEDRP
```

```
  1  MNQIQVFISG LILLLPGAVD SYVEVKGVVG HPVTLPCTYS TYRGITTTCW GRGQCPSSAC QNTLIWTNGH RVTYQKSSRY

 81  NLKGHISEGD VSLTIENSVE SDSGLYCCRV EIPGWFNDQK VTFSLQVKPE IPTRPPTRPT TTRPTATGRP TTISTRSTHV
161  PTSIRVSTST PPTSTHTWTH KPEPTTFCPH ETTAEVTGIP SHTPTDWNGT VTSSGDTWSN HTEAIPPGKP QKNPTKGFYV
241  GICIAALLLL LLVSTVAITR YILMKRKSAS LSVVAFRVSK IEALQNAAVV HSRAEDNIYI VEDRP
```

**Figure 7. Endogenous enzyme cleavage of mKIM-1 and deglycosylation with PNGase F enzyme with higher KIM-1 sample concentration and longer incubation time (Second Trial)**

(A) Western blot with goat anti-mKIM-1 Ab (AF1817, 1:2000). Immunoprecipitated shed mKIM-1 samples (8 µL) from HEK293 parental cells (negative control) and HEK293 FLAG mKIM-1 cells cultured from ten 15 cm plates treated with 4 µg PNGase F for 3 h at 37°C. Green arrow indicates band observed in FLAG mKIM-1 lane but not parental HEK293. (B) Coomassie brilliant blue stained gel with larger aliquots (80 µL) of immunoprecipitated sKIM-1 samples from (A). Red arrow indicates band observed in FLAG mKIM-1 lane but not parental HEK293. (C) ESI-MS/MS sequencing for mKIM-1 samples spot-picked at 55 kDa (top panel with 28% KIM-1 sequence coverage with 15 supporting peptides) and 50 kDa (bottom panel 21% KIM-1 sequence coverage with 7 supporting peptides) and in gel digested with thermolysin.

Therefore, I resorted back to using chemical deglycosylation with TFMS, but this time performed dialysis (Figure 8.) to remove any impurities or residual acid that could be distorting the gel during electrophoresis. This method efficiently removed the impurities and allowed the samples to migrate more linearly. The deglycosylated and dialyzed sample showed a dramatic drop in molecular weight to 37 kDa from 60 kDa in cell lysates (Figure 8A). Samples were picked for sequencing near the 37 kDa mark on the corresponding Coomassie stained gel (Figure 8B). When compared to non-deglycosylated samples (Figure 4), and PNGase treated samples (Figure 7), TFMS treatment and dialysis also did not improve sequencing coverage even though a large shift in molecular weight was observed.
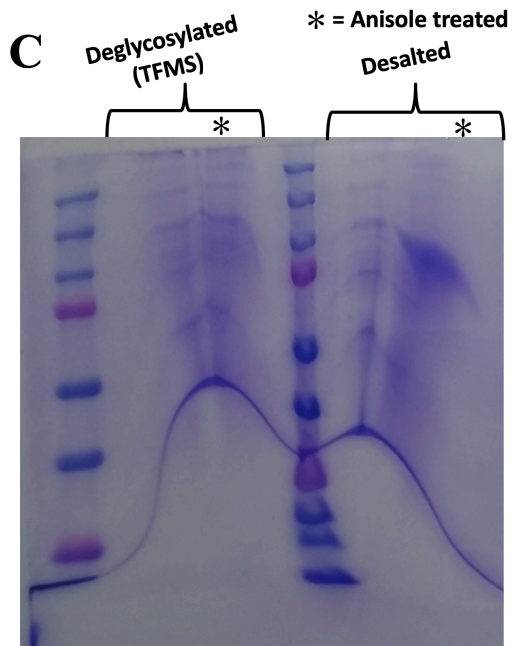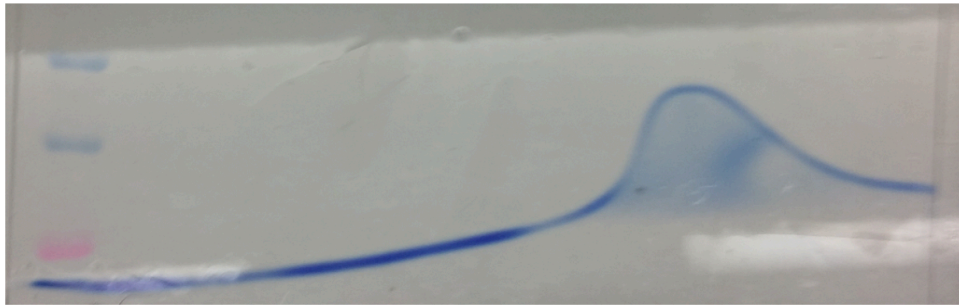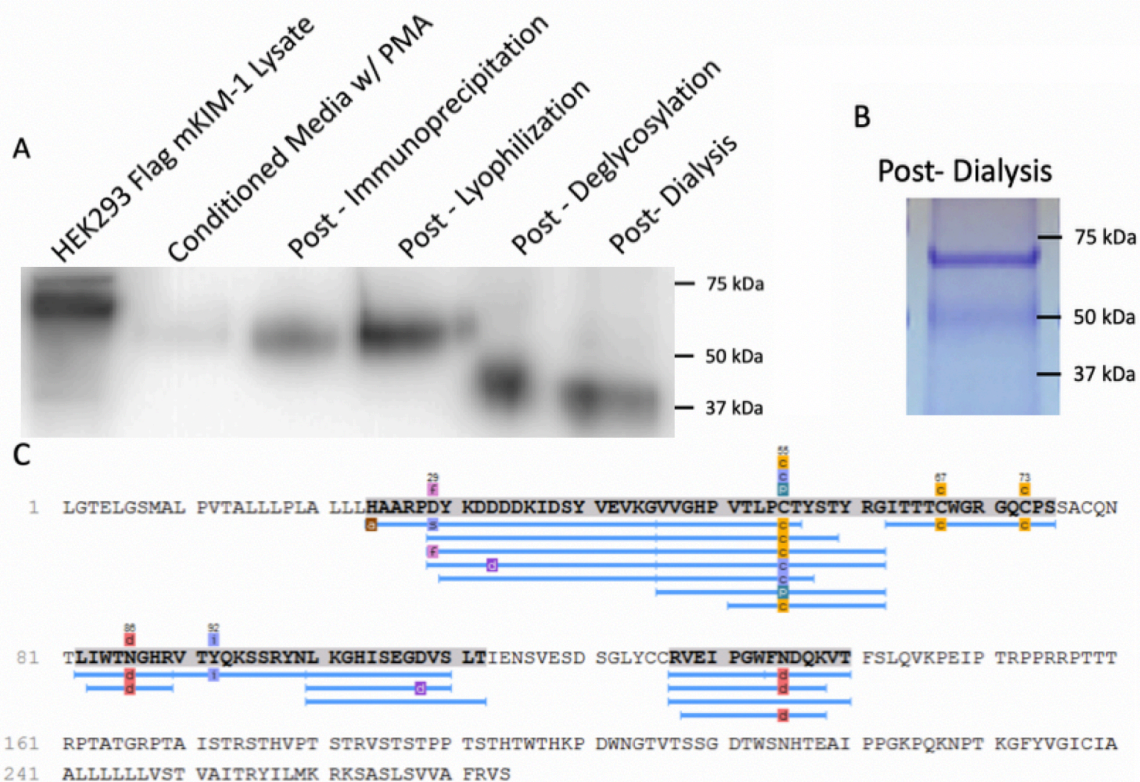
**Figure 8. Endogenous enzyme cleavage of mKIM-1, deglycosylation with TFMS and dialysis**

(A) Western blot with goat anti-mKIM-1 Ab (AF1817, 1:2000). Samples collected at various stages of endogenous enzyme cleavage method using TFMS acid for deglycosylation and dialysis with 3.5 kDa cut off membrane for desalting. (B). Coomassie brilliant blue stained gel with deglycosylated and desalted cleaved mKIM-1 sample. (C) ESI-MS/MS sequencing for mKIM-1 samples spot-picked at 37 kDa from Coomassie stained gel (B) and in -gel digested with thermolysin. 35% mKIM-1 sequence coverage with 24 supporting peptides.

Similar sequencing results with all forms of deglycosylation and purification methods suggested there could perhaps be an issue with collecting and digesting protein samples from Coomassie stained gel in preparation for ESI-MS/MS. I decided to digest the spot-picked KIM-1 sample with a different combination of enzymes that is more likely to extract the peptides near our region of interest (Figure 9A.) out of the gel in preparation for ESI-MS/MS. I used Arg-C and thermolysin, rather than just thermolysin alone as I had done previously to ensure the region of interest is being digested into small enough peptides that could be extracted from the gel.

**A**



```
                      Therm
                    Therm|
                    Therm||
            Therm     |||        Therm
         Therm  |      |         ArgC|      ArgC  Therm
            |   |      |            ||         |     |
         DYKDDDKIDSYVEVKGVVGHPVTLPCTYSTYRGITTTCWGRGQCPSSAC
       1  ---------+---------+---------+---------+---------+   50


            ArgC_Therm            Therm              Therm
         Therm   |        Therm     |      Therm     |  ArgC_Therm
         Therm|  |        ArgC  |    Therm |    Therm  |
            || |           ||   |      ||  |      ||   |
         QNTLIWTNGHRVTYQKSSRYNLKGHISEGDVSLTIENSVESDSGLYCCRV
      51  ---------+---------+---------+---------+---------+  100


                                                     ArgC
                 Therm                          Therm |
                 Therm                          Therm |
                 Therm      ArgC       ArgC     |
                 Therm      ArgC       Therm    |
         Therm   |   |      ArgC ||    ArgC |   |||   |
            |    |   |      ||   ||    |    |   ||||  |
         EIPGWFNDQKVTFSLQVKPEIPTRPPRRPTTTRPTATGRPTAISTRSTHV
      101 ---------+---------+---------+---------+---------+  150


         ArgC_Therm              Therm
            |                     |
         PTSTRVSTSTPPTSTHTWTHKPDWNGTVTSSG[TWSNHTEAI]PPGKPQKN
      151 ---------+---------+---------+---------+---------+  200


                                           ArgC_Therm
                                            Therm |
                                            Therm |
                                          Therm   |
                                          Therm   |
                                        Therm     |
                                        ArgC       |
                                      Therm        |
                                      Therm        |
                                      ArgC          |
                                    Therm           |
                                    Therm           |
                                    Therm           |
                                  Therm             |
                                  Therm             |
                                Therm               |
                                Therm               |
                              Therm                 |
                              Therm                 |
                            Therm                   |
                            Therm                   |
                          Therm |                   |
                          Therm |  |||||||||||   ||| |||| |  ||||| |
         PTKGFYVGICIAALLLLLLVSTVAITRYILMKRKSASLSVVAFRVS
      201 ---------+---------+---------+---------+------  246
```

**B**

Parental lysate   mKIM-1 lysate   Condition Media   Post-deglycosylation + dialysis

—75 kDa

—50 kDa

—37 kDa

**C**

```
            26                    39
             a                     c
  1  DYKDDDDKID SYVEVKGVVG HPVTLPCTYS TYRGITTTCW GRGQCPSSAC QNTLIWTNGH RVTYQKSSRY NLKGHISEGD
             a                    c
                                        107
                                         d
 81  VSLTIENSVE SDSGLYCCRV EIPGWFNDQK VTFSLQVKPE IPTRPPRRPT TTRPTATGRP TAISTRSTHV PTSTRVSTST
                                         d
                                         d
161  PPTSTHTWTH KPDWNGTVTS SGDTWSNHTE AIPPGKPQKN PTKGFYVGIC IAALLLLLLV STVAITRYIL MKRKSASLSV
241  VAFRVS
```

**Figure 9. Endogenous enzyme cleavage of mKIM-1, deglycosylation with TFMS, dialysis and in-gel digestion with Arg-C and thermolysin**

(A) Predicted cut sites for thermolysin and Arg-C along KIM-1 construct as determined by ExPASy peptide cutter software. Predicted cleavage region outlined with red box. (B) Western blot with goat anti-mKIM-1 Ab (AF1817, 1:2000). Samples collected at various stages of endogenous enzyme cleavage method using TFMS acid for deglycosylation and dialysis with 3.5 kDa cut off membrane for desalting. (C) Sequencing results from samples collected from HEK293 cells, deglycosylated with TFMS, and in-gel digested with Arg-C and thermolysin. 20% protein sequence coverage with 7 matching peptides.

Combined digestion with Arg-C and thermolysin also resulted in sequencing information up to the same position (F113) on the KIM-1 construct sequence (Figure 9B).

Overall, all methods used for sequencing mKIM-1 cleaved by the endogenous enzyme cleavage method resulted in sequencing information from the N-terminal FLAG tag up to the same site (F113) with no information near the predicted cleavage region (T194 to I202).

## 3.1.2    Synthetic KIM-1 peptide cleavage with rmTACE

An alternate method for identifying the cleavage site of KIM-1 was to use a synthetic peptide containing the putative cleavage site (T194-I202) flanked by additional residues to allow room for the sheddase to bind and exposing this peptide to rmTACE. We designed a peptide 20 amino acids long that contained the sequence region highlighted in Figure 3C (S190 to K219) which aligned with the predicted cleavage region on hKIM-1.

The synthesized peptides were analyzed by size exclusion chromatography to assess purity. Based on the single and symmetrical elution peak eluting at ~14 mL, it was determined that there was a highly homogeneous population of peptides (Figure 10A). The expected theoretical molecular weight of the synthetic peptide is 2137.29 Da (Protein molecular weight – Bioinformatics.org) and proteins/peptides eluted with this column between 10 to 15 mL is between ~1500 to 6000 Da (Appendix A4), so the peptide is eluting as expected when it is uncleaved.

This is important to ensure any cleaved peptides observed after incubation with enzyme are the result of enzyme-mediated cleavage and not the impurity of the synthesized sample. Although a significant amount of cleavage did not take place, there was a particular site (I202) that was being cleaved with rmTACE (Figure 10B). When repeated with and without rmTACE (Figure 10C) some cleaved peptides in this region were also observed in the negative control, resulting in inconclusive results with this experiment.
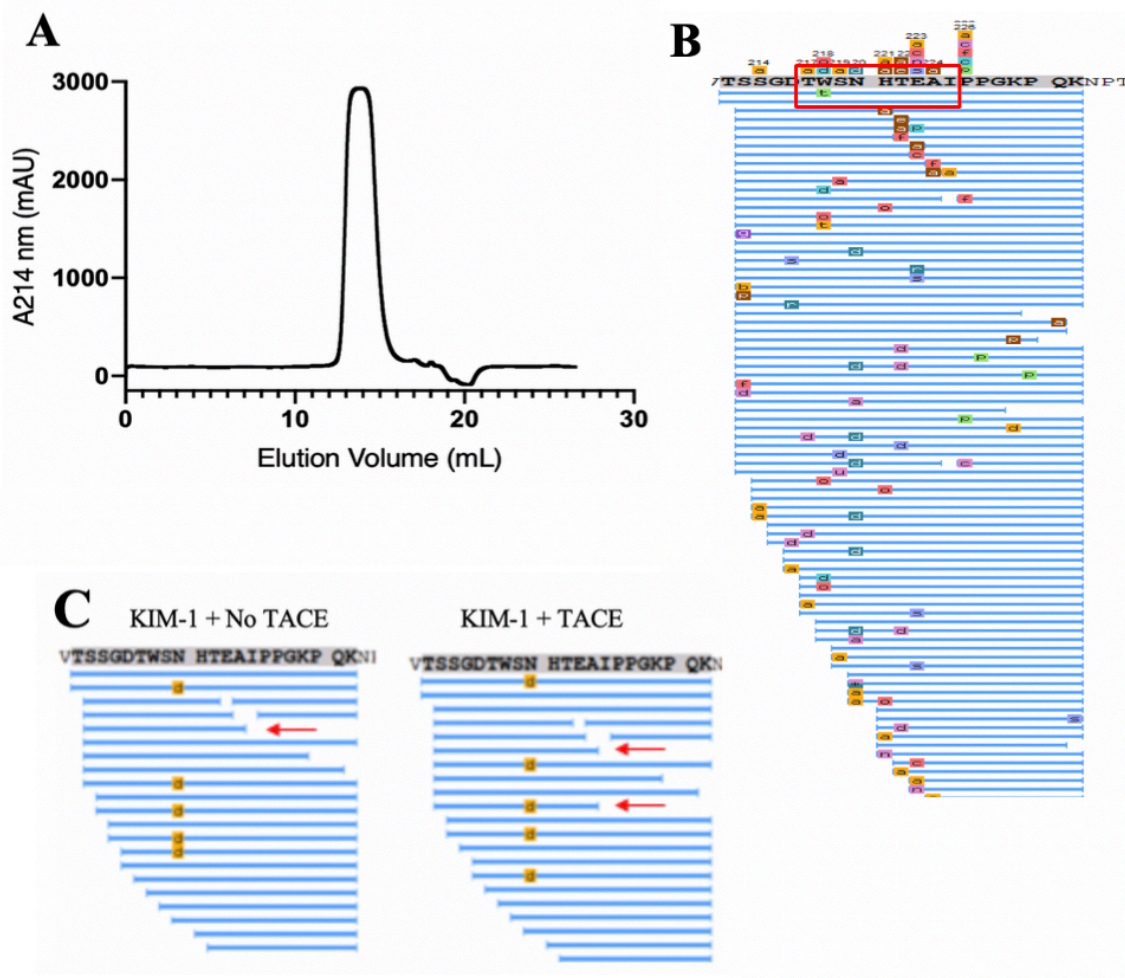
**Figure 10. Synthetic KIM-1 peptide cleavage with rmTACE**

(A) FPLC purification of KIM-1 synthetic peptide using Superdex Peptide 10/300 column gel filtration. Measured absorbance at 214 nm in milli absorbance units (mAU) plotted against elution volume of sample in 50 mM Tris-HCl solution. (B) KIM-1 peptide incubated with rmTACE for 16 h at 37°C. ESI-MS/MS sequencing showed 1359 scans for full length peptide 14 scans for cleaved peptide at I202 position. (C) KIM-1 peptide incubated with and without rmTACE (negative control). Red arrows indicate cleaved peptides at potential cleavage site (I202).

## 3.2   Mapping I202 as potential mKIM-1 cleavage site

Based on a previously published study by (Caescu, Jeschke et al. 2009), the KIM-1 synthetic peptide and potential cleavage site at I202 was mapped against common structural residue patterns observed around the cleavage site of various TACE substrates (Figure 11). I202 looked promising as a potential cleavage site for TACE.
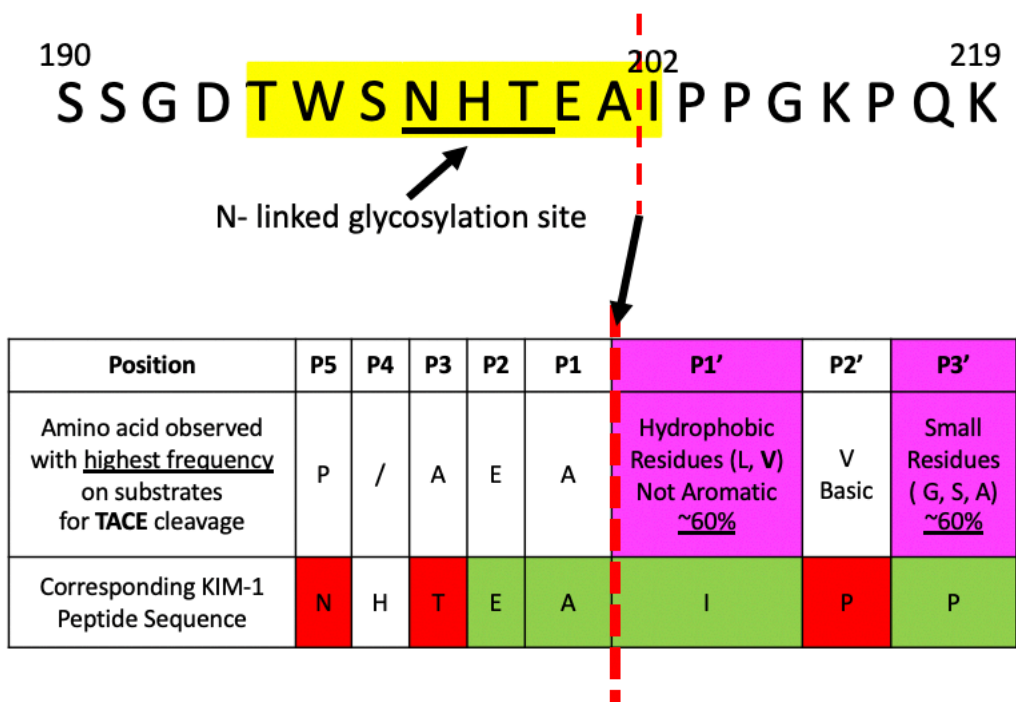
**Figure 11. Mapping I202 as potential TACE-mediated mKIM-1 cleavage site.**

KIM-1 synthetic peptide sequence mapped against common structural residue patterns observed around cleavage site of various TACE substrates. Hydrophobic residues at P1' position and small residues at P3' position appear with the highest frequency (~60%) amongst various TACE substrates (Caescu, Jeschke et al. 2009). Amino acids highlighted in green matched with observed patterns at that position, whereas those highlighted in red do not.

## 3.3 Mutant I202Q mKIM-1

To test if I202 is the putative cleavage site within mKIM-1, I performed site-directed mutagenesis to alter this position. The first mutation attempted was a base substitution mutation, producing the (I202Q) variant. I (non-polar) and Q (polar) were similar in size but differed in polarity.

### 3.3.1 Generating I202Q mutant mKIM-1

I generated HEK293 cells stably expressing pCDEF3 vector encoding the mutant KIM-1 after confirming its sequence (Figure 12A.) HEK293 cell colony #3 and #10 were stably expressing I202Q mutant KIM-1 at a high expression level comparable to cells expressing WT mKIM-1 (Figure 12B.) Colony #3 was selected and used for further testing to ensure homogenous population of cells were being used.
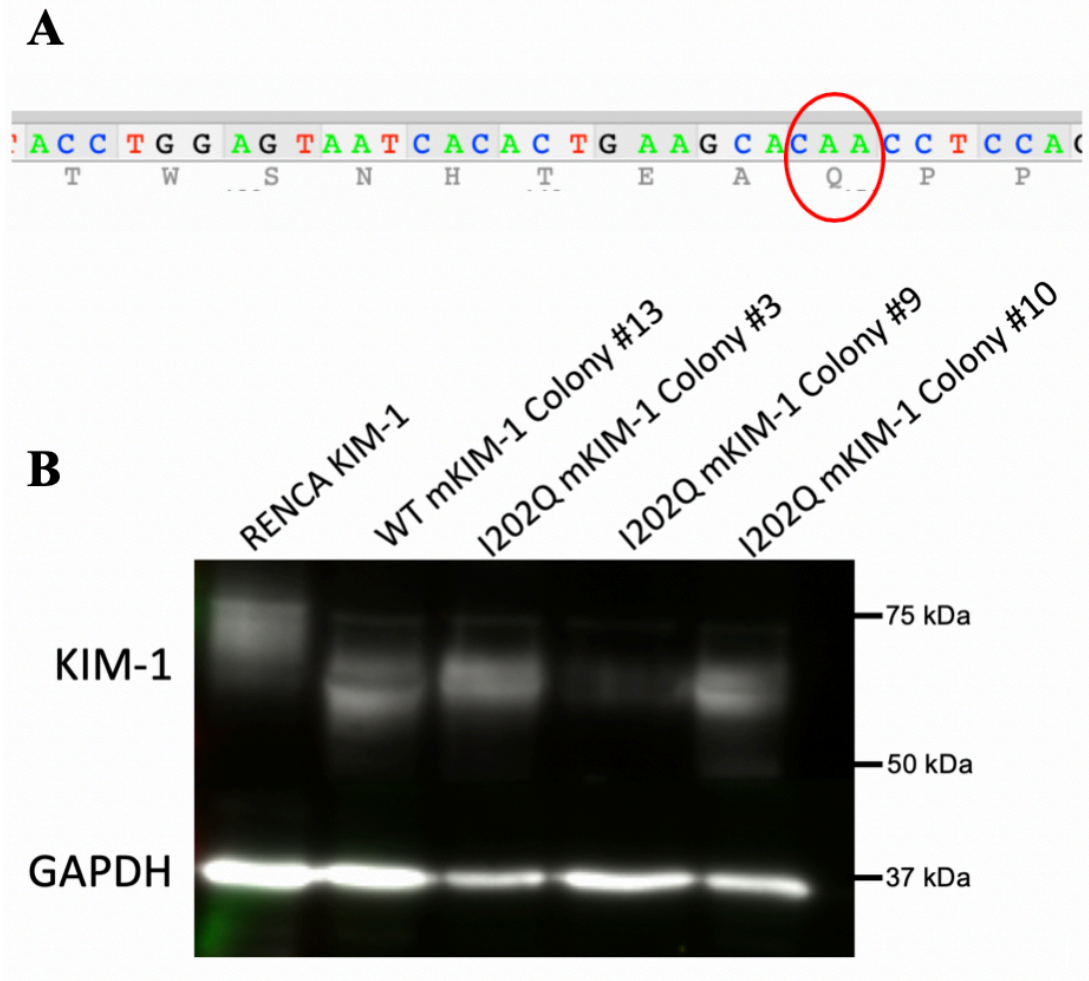
**Figure 12. Generating I202Q mutant mKIM-1 expressing HEK293 cell line**

(A) Sequencing results confirming I202Q mutation into pCDEF3 mKIM-1 plasmid after site-directed mutagenesis. (B) HEK293 cells stably expressing I202Q mKIM-1. Western blot of lysates from RENCA KIM-1 cells (positive control), HEK293 cells stably expressing WT mKIM-1, and various colonies of HEK293 cells stably expressing I202Q mutant mKIM-1. Goat anti-mKIM-1 (1:2000) and mouse anti-GAPDH (1:2000) antibodies were used.

### 3.3.2   Reduced PMA-accelerated shedding with I202Q

The I202Q mKIM-1 mutant was still capable of baseline KIM-1 shedding, however accelerated shedding with PMA was defective compared to WT mKIM-1 expressing HEK293 cells (Figure 13.). According to the densitometric values shown, PMA treatment doubled the level of sKIM-1 in media compared to no PMA treatment for WT, whereas with the mutant the sKIM-1 levels remained unchanged.

| HEK293 Cells | Parental | | WT KIM-1 | | Mut KIM-1 I220Q | |
|---|---|---|---|---|---|---|
| PMA | + | - | + | - | + | - |

Media



| 0.0 | 0.0 | 1.0 | 0.39 | 0.42 | 0.42 |

KIM-1

Lysates

KIM-1

GAPDH
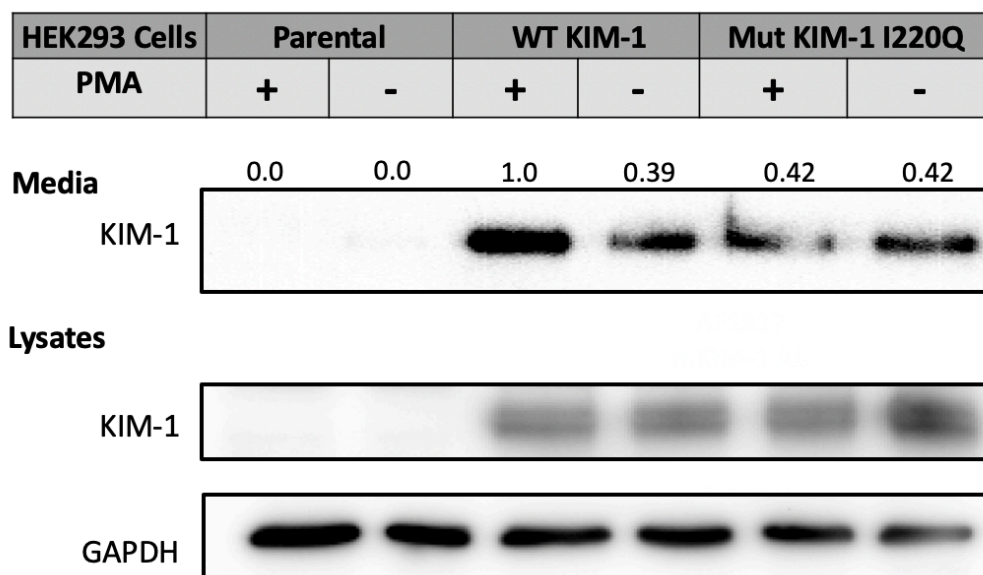
**Figure 13. Baseline and accelerated shedding assay with HEK293 cells (parental, WT KIM-1 and I202Q KIM-1).**

Western blot with media and lysates samples collected after 1 h treatment with or without 1 µM PMA in serum-free media (n=2). Goat anti-KIM-1 (1:2000) and mouse anti-GAPDH (1:2000) antibodies were used. Relative densitometric values of KIM-1 bands in media presented.

### 3.3.3 ADAM10 mediated baseline shedding of mKIM-1

PMA-accelerated TACE mediated KIM-1 shedding was defective with I202Q mutant, therefore this prompted investigation into the possibility of another closely related sheddase, ADAM10 and its involvement (Schweigert, Dewitz et al. 2014). For subsequent experiments, I introduced an ADAM10 specific inhibitor (GI253023X) to the shedding assays (Ludwig, Hundhausen et al. 2005). Surprisingly, baseline shedding of both WT mKIM-1 and I202Q mKIM-1 were drastically reduced with GI254023X compared to DMSO vehicle control (Figure 14).

| HEK293 Cells | Parental | | | WT KIM-1 | | | Mut KIM-1 I220Q | | |
|---|---|---|---|---|---|---|---|---|---|
| Treatment | DMSO Control | GI254023X ADAM10 Inhibitor | PMA | DMSO Control | GI254023X ADAM10 Inhibitor | PMA | DMSO Control | GI254023X ADAM10 Inhibitor | PMA |
| | 1.0 | 1.0 | 1.0 | 1.0 | 0.3 | 2.9 | 1.0 | 0.15 | 0.62 |

Media

KIM-1

Lysates

KIM-1

GAPDH
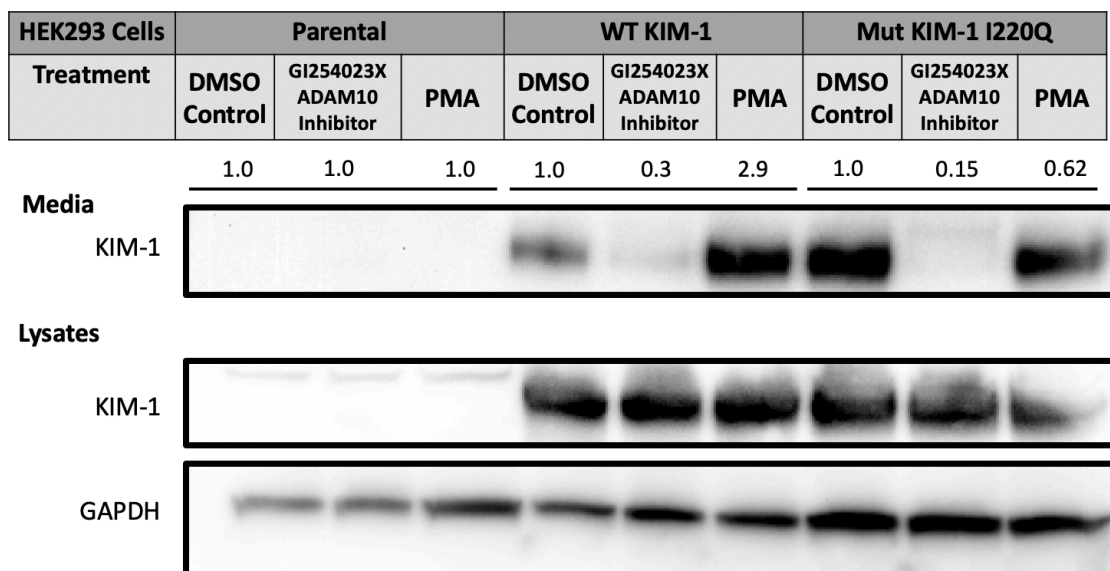
**Figure 14. Baseline and accelerated shedding assay of HEK293 cells (parental, WT KIM-1 and I202Q KIM-1) with ADAM10 specific inhibitor**

 Western blot with media and lysate samples collected after 1 h treatment with either DMSO, 4 µM GI254023X or 1 µM PMA in serum-free media (n=1). Goat anti-KIM-1 (1:2000) and mouse anti-GAPDH (1:2000) antibodies were used. Relative densitometric values of KIM-1 bands in media normalized to DMSO control within each cell type.

## 3.4   Mutant I202A mKIM-1

The second mutation attempted was a base substitution mutation, producing the (I202A) variant. I (non-polar) and Q (polar) were similar in size but differed in polarity, whereas A (non-polar) is smaller.

### 3.4.1     Generating I202A mutant mKIM-1

I generated HEK293 cells stably expressing pcDEF3 vector encoding the mutant KIM-1 after confirming its sequence (Figure 15A.) According to figure 15B., HEK293 cell colony #2 was stably expressing I202A mutant KIM-1 at a high expression level comparable to HEK293 cells expressing WT and I202Q mKIM-1 and was used for further testing to ensure homogenous population of cells were being used.
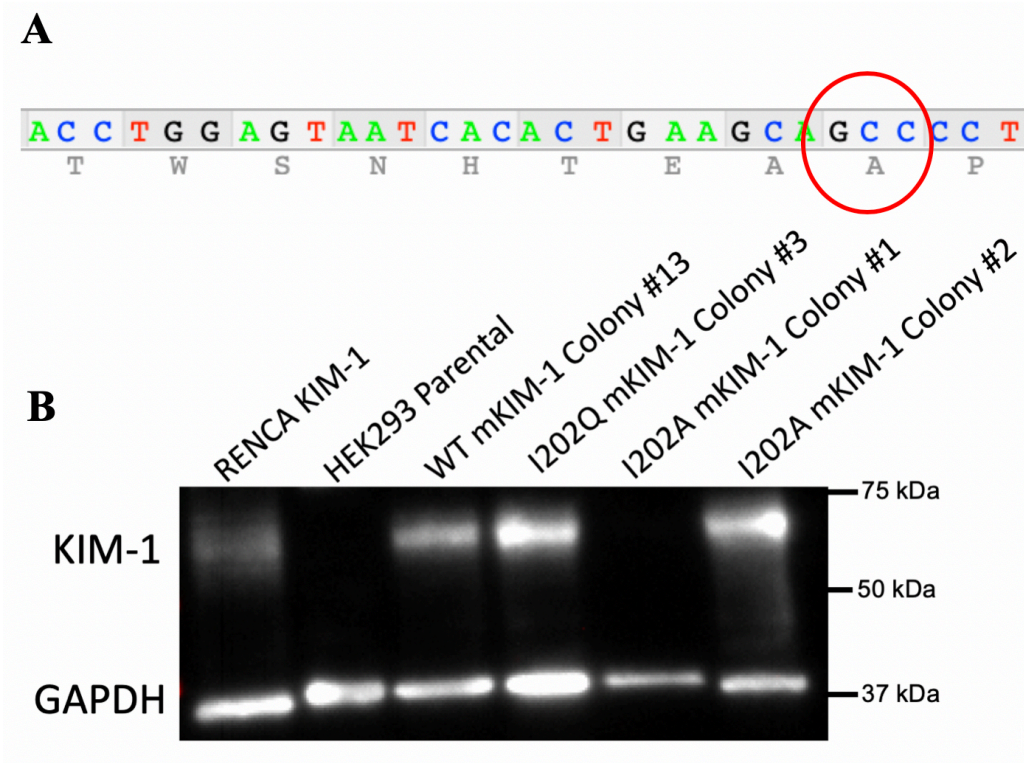
**Figure 15. Generating I202A mutant mKIM-1 expressing HEK293 cell line**

(A) Sequencing results confirming I202A mutation into pCDEF3 mKIM-1 plasmid after site-directed mutagenesis. (B) HEK293 cells stably expressing I202A mKIM-1. Western blot of lysates from RENCA KIM-1 cells (positive control), HEK293 parental cells (negative control), HEK293 cells stably expressing WT mKIM-1, I202Q mKIM-1 and various colonies of HEK293 cells stably expressing I202A mutant mKIM-1. Goat anti-mKIM-1 (1:2000) and mouse anti-GAPDH (1:2000) antibodies were used.

### 3.4.2 Comparing expression levels of WT, I202Q and I202A mKIM-1

Total protein expression from lysates showed slightly higher expression levels in I202Q and I202A compared to WT KIM-1 expressing HEK293 cells (Figure 16A.)

Given that KIM-1 is a cell-surface phagocytic receptor, I also examined surface expression of WT and the various KIM-1 mutants in the respective HEK293 cell lines. Cell surface KIM-1 expression was comparable between WT and I202A, with a homogenously high expression profile (Figure 16B). I202Q surface KIM-1 expression depicted varying levels that was generally lower than both WT and I202A (Figure 16B). Although, the total percentage of HEK293 cells expressing the various mutants or WT mKIM-1 were similar (Figure 16C), the expression profile according to flow cytometry data (Figure 16B) revealed more cells had lower KIM-1 surface expression levels in the I202Q mutants.

**A**

| HEK293 Cells | Parental | WT | I202Q | I202A |
|---|---|---|---|---|
| | 1.0 | 47.4 | 66.8 | 53.7 |

KIM-1

— 75 kDa

— 50 kDa

GAPDH — 37 kDa

**B**



SSC

FSC

Dylight 488 – KIM-1

WT
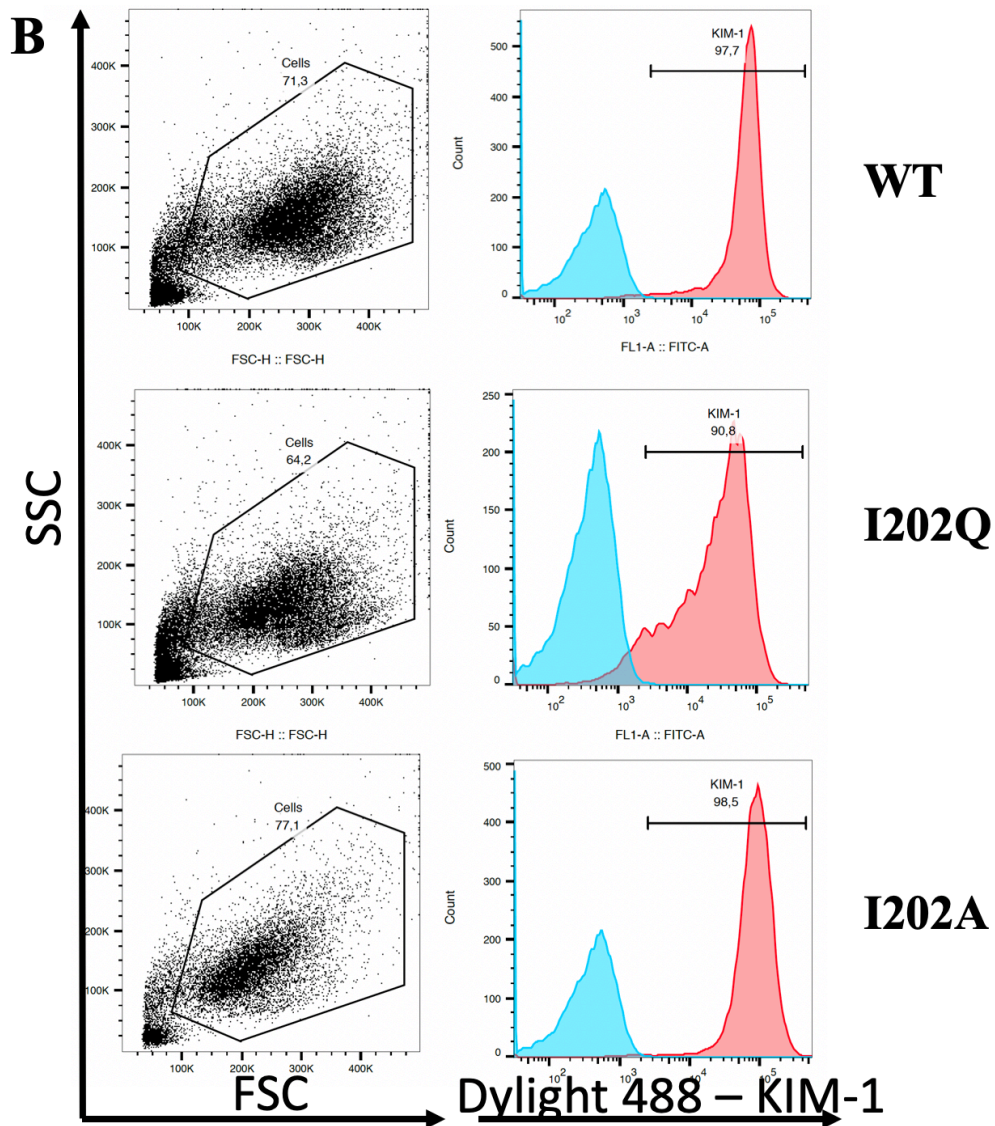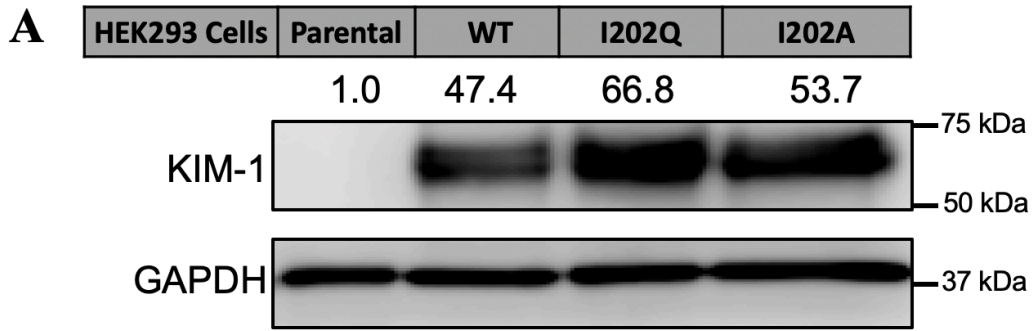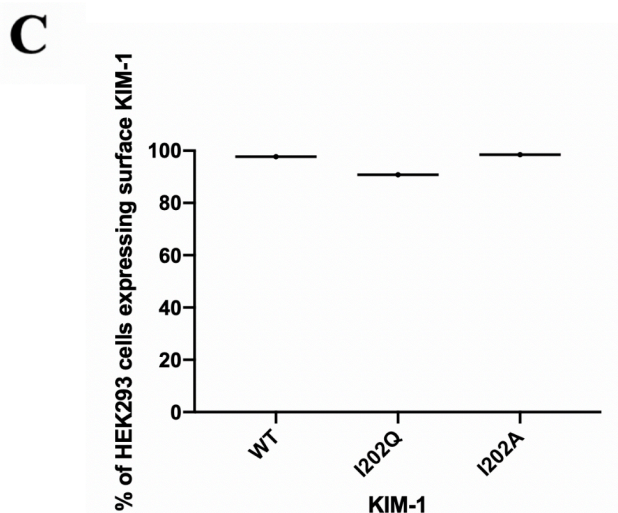
I202Q

I202A

**Figure 16. Comparing total protein and surface KIM-1 expression levels between HEK293 cells expressing WT (colony #13), I202Q (colony #3) or I202A (colony #2) mKIM-1.**

(A) Western blot of total protein lysates with relative densitometric values of KIM-1 normalized to GAPDH (n=1). Goat anti-mKIM-1 (1:2000) and mouse anti-GAPDH (1:2000) antibodies were used. (B) Cells were stained for surface KIM-1 using goat anti-mKIM-1 (AF1817) as primary and rabbit anti-goat Dylight 488 as secondary antibodies. The level of KIM-1-surface expression was determined by flow cytometry. Blue sample population is the negative control sample stained without primary antibody. (C) Comparing percentage of HEK293 cells expressing surface KIM-1 for WT and KIM-1 mutants from independent experiments (n=2).

## 3.5 KIM-1 Shedding Assays

### 3.5.1 WT, I202Q and I202A mKIM-1 expressing HEK293

Both I202Q and I202A mKIM-1 were spontaneously shed from HEK293 cells, however, the ability to accelerate shedding via PMA or ionomycin is significantly reduced compared to WT mKIM-1 (Figure 17). For WT mKIM-1 expressing cells, PMA and ionomycin treatment resulted in significant increases in the levels of shed KIM-1 in media, with $p=0.0014$ and $p<0.0001$, respectively (Two-way ANOVA, Tukey's post hoc test, Figure 17). No significant differences were observed between baseline and accelerated shedding of I202Q or I202A.

**A**
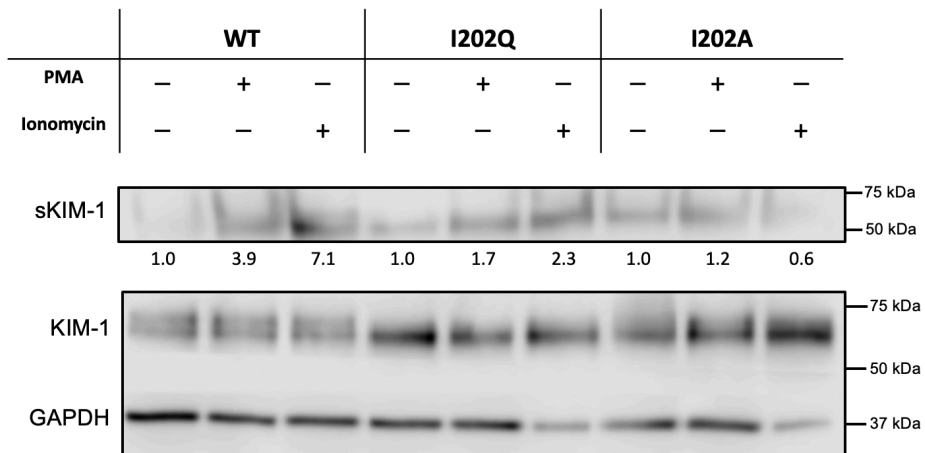


**B**
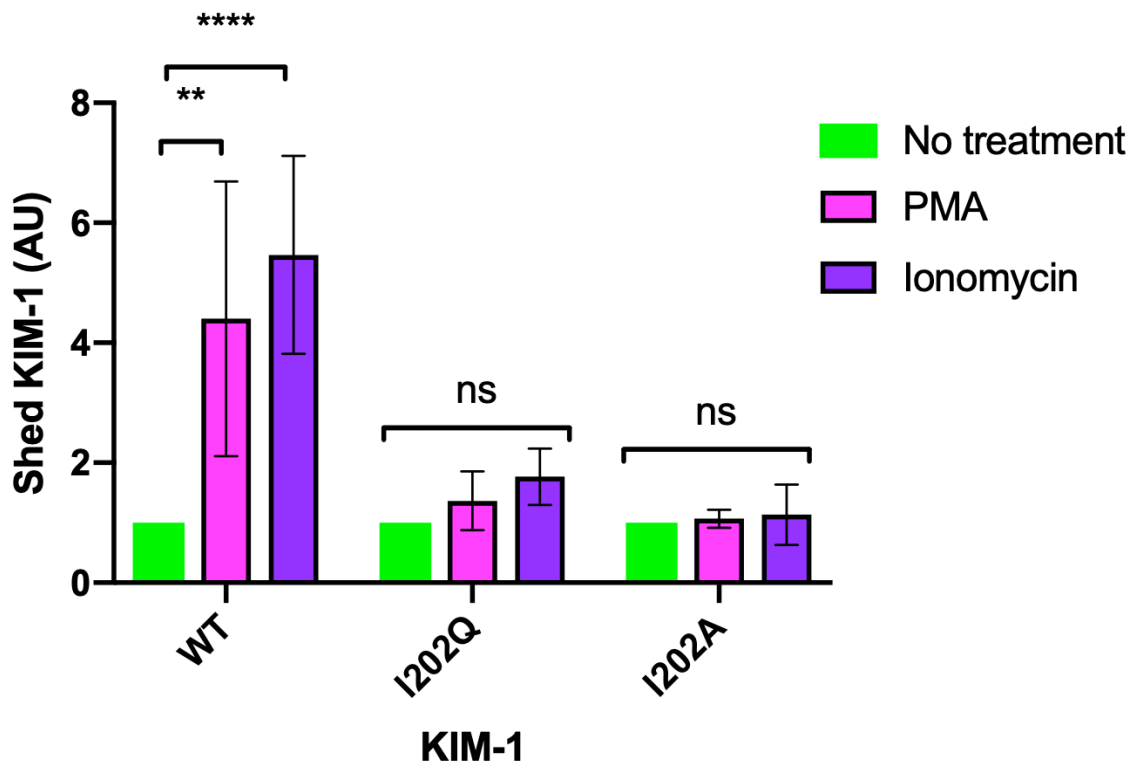
**Figure 17. Baseline and accelerated shedding assay with WT, I202Q and I202A mKIM-1 expressing HEK293 cells.**

(A) Western blot of media and lysate samples collected from HEK293 cells (WT, I202Q and I202A mKIM-1) after 1 h treatment in serum-free DMEM with or without 1 µM PMA or 500 nM ionomycin. Goat anti-KIM-1 (1:2000) and mouse anti-GAPDH (1:2000) antibodies were used. Densitometry values for sKIM-1 are relative to the no treatment group for each cell type. (B) Compiled data of relative densitometry values of sKIM-1 from independent shedding assay experiments. (n=3, ** p=0.0014 and ****p<0.0001, Two-way ANOVA, Tukey's post hoc test)

## 3.5.2    GI254023X Dose Response on HEK293 WT mKIM-1

| ADAM10 Inhibitor GI254023X (µM) | 0 | 0.1 | 1 | 10 | 100 | 1000 |
|---|---|---|---|---|---|---|
| | 1.0 | 0.6 | 0.2 | 0.1 | 0.0 | 0.0 |
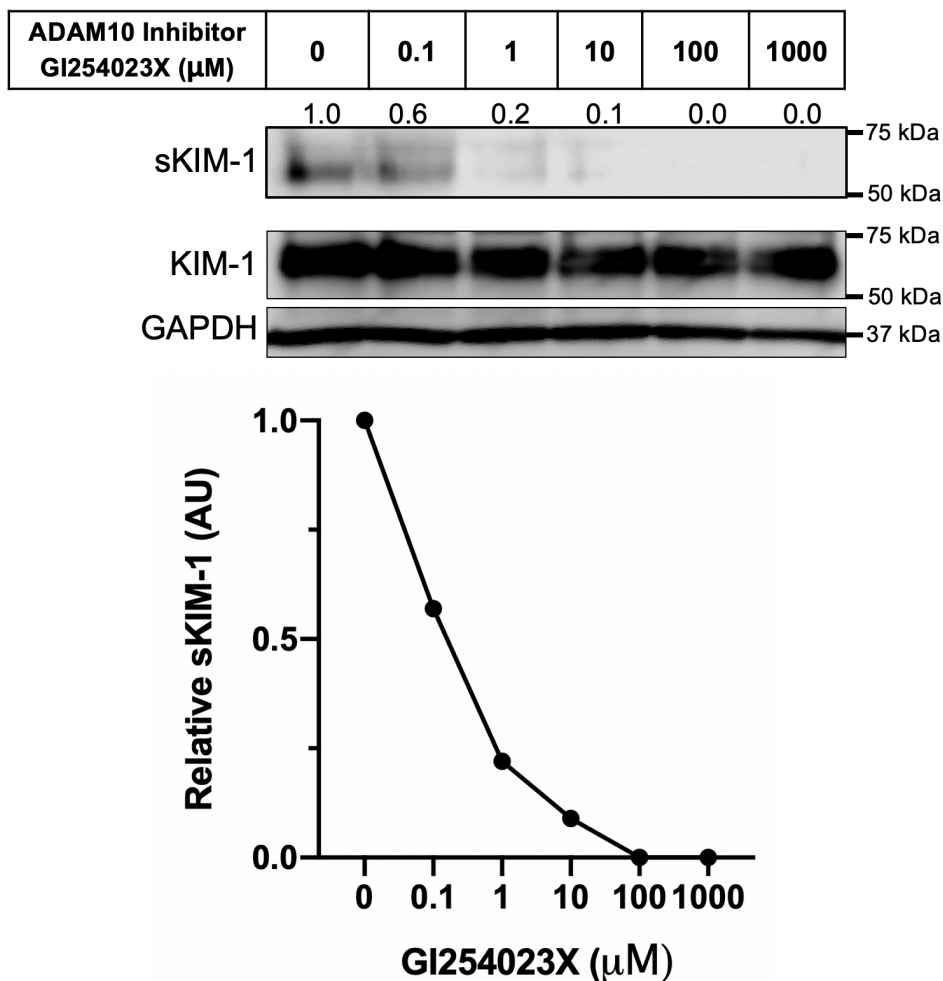


**Figure 18. ADAM10 inhibitor (GI254023X) dose response on inhibition of baseline KIM-1 shedding in HEK293 cells expressing WT mKIM-1.**

Cells were treated with various log doses of GI254023X for 1 h in serum-free DMEM before media and lysate samples were collected for Western blot analysis (n=1). Goat anti-KIM-1 (1:2000) and mouse anti-GAPDH (1:2000) antibodies were used. Densitometry values for sKIM-1 are relative to the no treatment (0 µM) control group. $IC_{50} = 0.74$ µM

### 3.5.3    Baseline and accelerated shedding inhibited by GI254023X

| Treatment | DMSO | PMA + DMSO | Ionomycin +DMSO | GI254023X | PMA + GI254023X | Ionomycin + GI254023X |
|---|---|---|---|---|---|---|



|  | 1.0 | 1.34 | 2.28 | 0.12 | 0.03 | 0.01 |
| WT | | | | | | |
|  | 1.0 | 2.24 | 2.46 | 0.02 | 0.25 | 0.37 |
| I202Q | | | | | | |
|  | 1.0 | 1.17 | 1.44 | 0.01 | 0.17 | 0.04 |
| I202A | | | | | | |
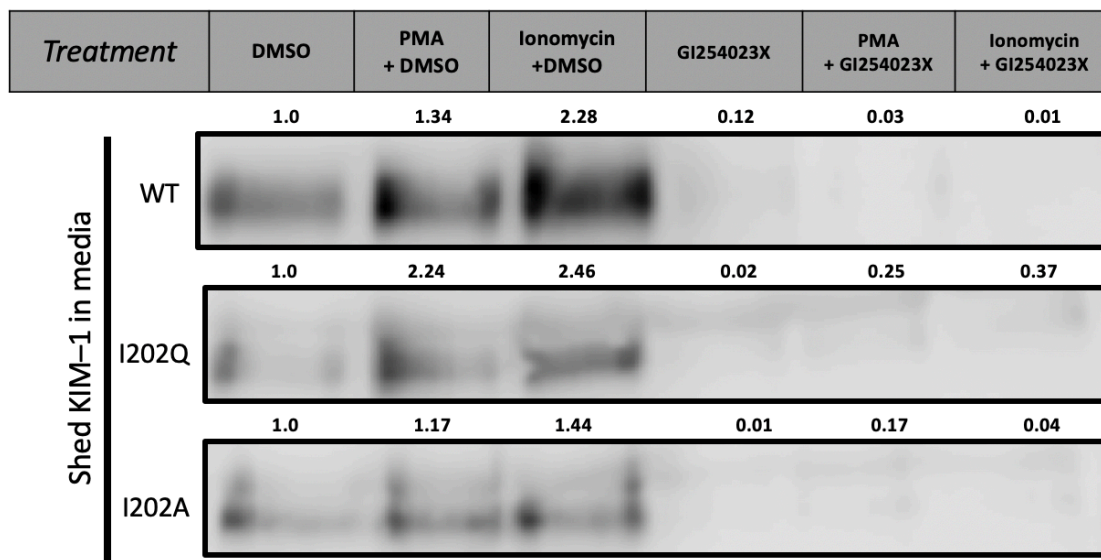
**Figure 19. Baseline and accelerated shedding assay with PMA, ionomycin, GI254023X and combination drug treatments**

(A) Western blot of media samples collected from HEK293 cells (WT, I202Q and I202A mKIM-1) after 2 h treatment in serum-free DMEM with or without 1 µM PMA, 500 nM ionomycin and 4 µM GI254023X ADAM10 inhibitor (n=2). DMSO used as a vehicle control for GI254023X. Goat anti-KIM-1 (1:2000) antibody was used. Relative densitometry values normalized to DMSO control in each cell type.

The ADAM10 specific inhibitor, GI254023X, effectively blocked both baseline and PMA/ionomycin accelerated shedding of KIM-1 from HEK293 cells (Figure 19.)

## 3.5.4   ADAM10 siRNA

siRNA-mediated ADAM10 knockdown in HEK293 cells expressing WT mKIM-1 significantly reduced shedding of KIM-1 into media (p=0.0027, Figure 20), confirming the role of ADAM10 in mediating KIM-1 shedding.

**A**
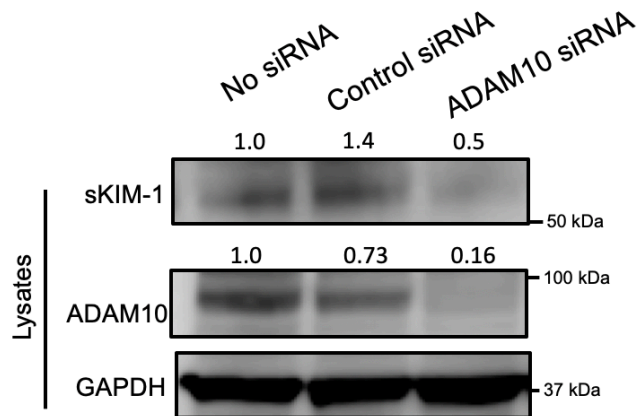


**B**
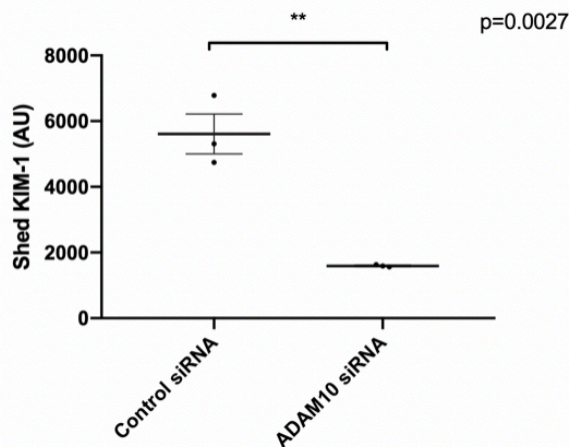


**Figure 20. Baseline shedding assay in WT mKIM-1 HEK293 cells upon silencing of ADAM10.**

(A) Western blot of media and lysate samples collected from HEK293 cells expressing WT mKIM-1 after siRNA mediated ADAM10 knockdown. Media samples collected after 1 h treatment in serum-free DMEM. Goat anti-KIM-1 (1:2000), mouse anti-GAPDH (1:2000), and rabbit anti-ADAM10 (1:500) antibodies were used. Densitometry values relative to the no siRNA group. (B) Compiled data of densitometry values of sKIM-1 from independent shedding assay experiments. (n=3, ** p=0.0027, Student's unpaired t-test)

## 3.6   Functional studies: KIM-1 Phagocytosis Assays

### 3.6.1      WT, I202Q and I202A mKIM-1

The primary function of KIM-1 in kidney epithelial cells is to mediate the phagocytic clearance of apoptotic cells following injury (Yang, Brooks et al. 2015). Compared to HEK293 cells with WT mKIM-1, cells with I202Q or I202A mKIM-1 had significantly reduced phagocytosis levels with $p < 0.0001$ and $p < 0.01$, respectively (Figure 21).
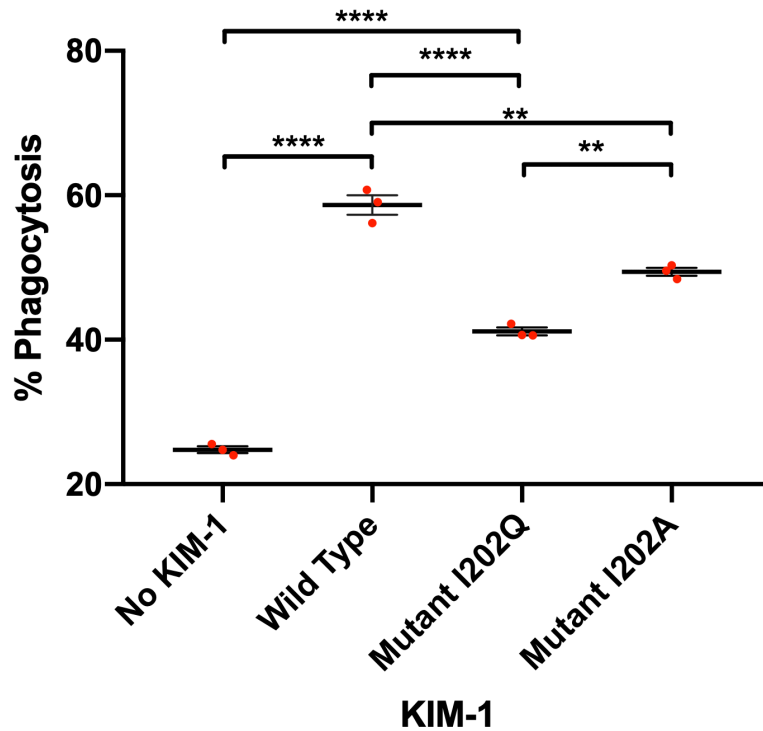
**Figure 21. Phagocytosis assay with HEK293 cells expressing WT, I202Q, or I202A mKIM-1.**

HEK293 parental cells (no KIM-1 negative control) and HEK293 cells transfected with either WT, mut I202Q or mut I202A KIM-1 were incubated with pHRodo stained apoptotic thymocytes for 90 minutes before flow cytometry analysis. Phagocytosis percentage represents percentage of HEK293 cells that have internalized stained apoptotic cells as indicated by higher fluorescence ($10^4$–$10^5$ on logarithmic scale) (One-way ANOVA, Tukey's post-hoc test, n=3, ****p<0.0001, **p<0.01).

## 3.6.2 ADAM10 inhibitor GI254023X

Treatment with ADAM10 inhibitor significantly reduced phagocytosis levels compared to no treatment controls ($p < 0.005$, Figure 22.) No significant differences were observed between DMSO and no treatment groups.
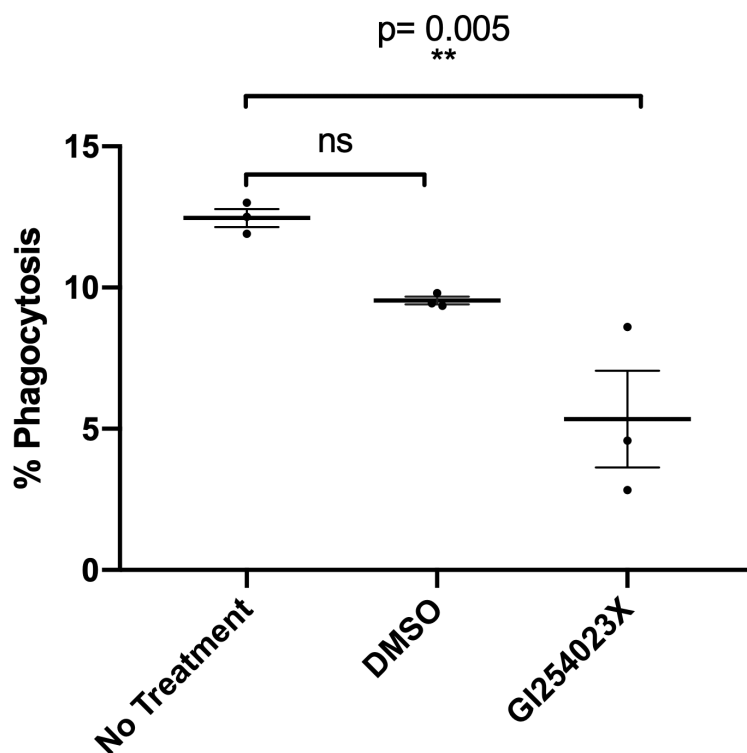
**Figure 22. Phagocytosis assay with GI254023X.**

HEK293 cells expressing WT mKIM-1 were treated with either 4μM of GI254023X, DMSO vehicle control or no treatment for 1 h. Cell were then incubated with pHRodo stained apoptotic thymocytes for 90 minutes before flow cytometry analysis. Phagocytosis percentage represents percentage of HEK293 cells that have internalized stained apoptotic cells as indicated by higher fluorescence ($10^4$–$10^5$ on logarithmic scale) (One-way ANOVA, Tukey's post-hoc test, n=3, **p<0.005).

## 3.7 Synthetic KIM-1 peptide cleavage with rmADAM10

Since I identified ADAM10 as an important enzyme involved in KIM-1 processing, the *in vitro* cleavage assay with synthetic KIM-1 peptide was repeated with recombinant mouse ADAM10 for ESI-MS/MS analysis.

First, enzymatic activity of rmADAM10 and rmADAM17 was verified for functionality. Specific activity was calculated to be 79162 pmol/min/µg for rmTACE, -2523 pmol/min/µg for an older lot of rmADAM10 (non-functional) and 11755 pmol/min/µg for a newer lot of rmADAM10 (Figure 23). The new lot rmADAM10 was used for cleavage experiment with synthetic KIM-1 peptide. No distinct cleaved peptides were observed in the treatment group (KIM-1 peptide + rmADAM10) that were absent in the negative control (KIM-1 peptide only) (Figure 24).
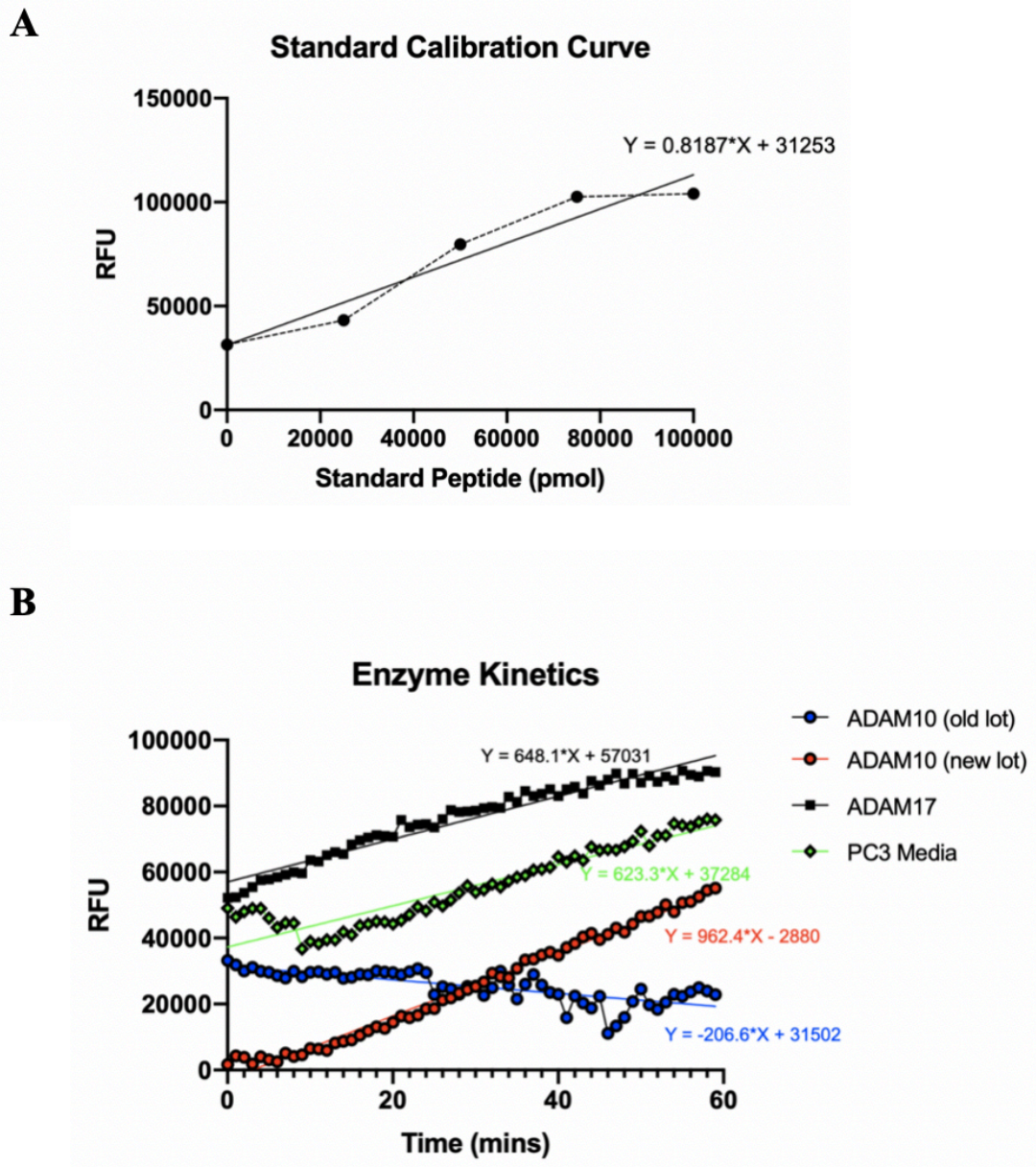
**Figure 23. rmADAM10 and rmADAM17 enzyme activity assay.**

Enzymatic activity (B) was confirmed for both rmADAM17 and rmADAM10 using the positive control fluorescent substrate MCA-P-L-A-Q-A-V-DPA-R-S-S-S-R-NH2 (Cat# ES003, R&D) and MCA-P-L-OH (Bachem, Catalog # M-1975) as the calibration standard (A) as described by the R&D enzyme activity assay protocols (Appendix A1 and A2). Human prostate cancer cell line (PC3) media contains cocktail of secreted enzymes and used as a positive control for fluorescent substrate.
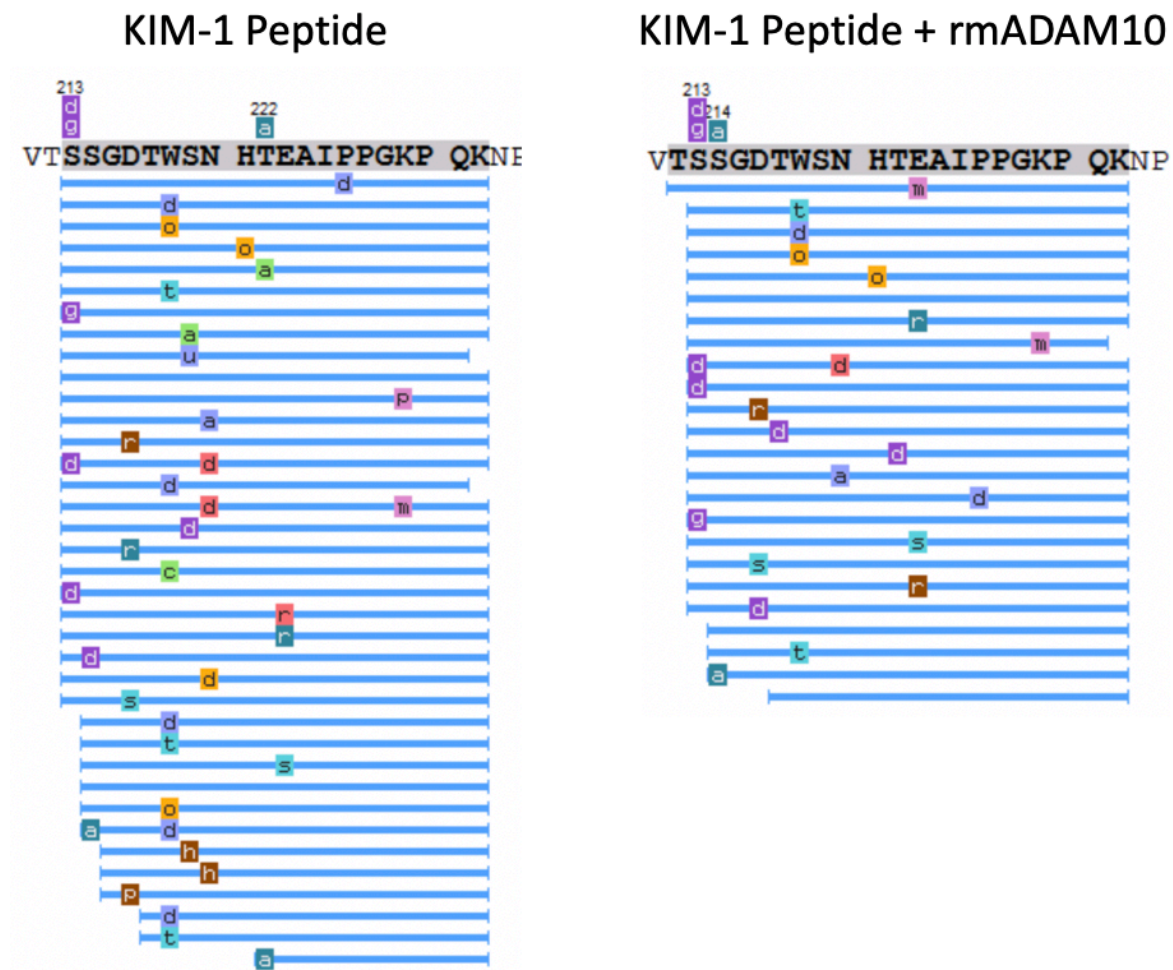
**Figure 24. Synthetic KIM-1 peptide cleavage with rmADAM10.**

KIM-1 synthetic peptide (10 µM) incubated with and without (negative control) rmADAM10 (0.1 µg) for 16 h at 37°C. Samples then analyzed by ESI-MS/MS for sequencing cleaved peptides (n=2).

## 3.8 ADAM10 specific inhibition reduces mKIM-1 cleavage in RENCA mouse cell line

Thus far, my studies utilized human HEK293 cells (containing human ADAM10) overexpressing mKIM-1 or mutants thereof. Next, I wanted to confirm that murine ADAM10 regulated the shedding of mKIM-1 using a murine kidney epithelia cell line expressing ADAM10. GI254023X inhibited shedding of mKIM-1 expressed in mouse renal epithelial cancer cell line in a dosage-dependent manner (Figure 25).

| RENCA Control | + | − | − | − | − | − | − | − |
|---|---|---|---|---|---|---|---|---|
| RENCA KIM-1 | − | + | + | + | + | + | + | + |
| ADAM10 Inhibitor GI254023X (µM) | 0 | 0 | 0.1 | 1 | 10 | 100 | PMA | Ionomycin |
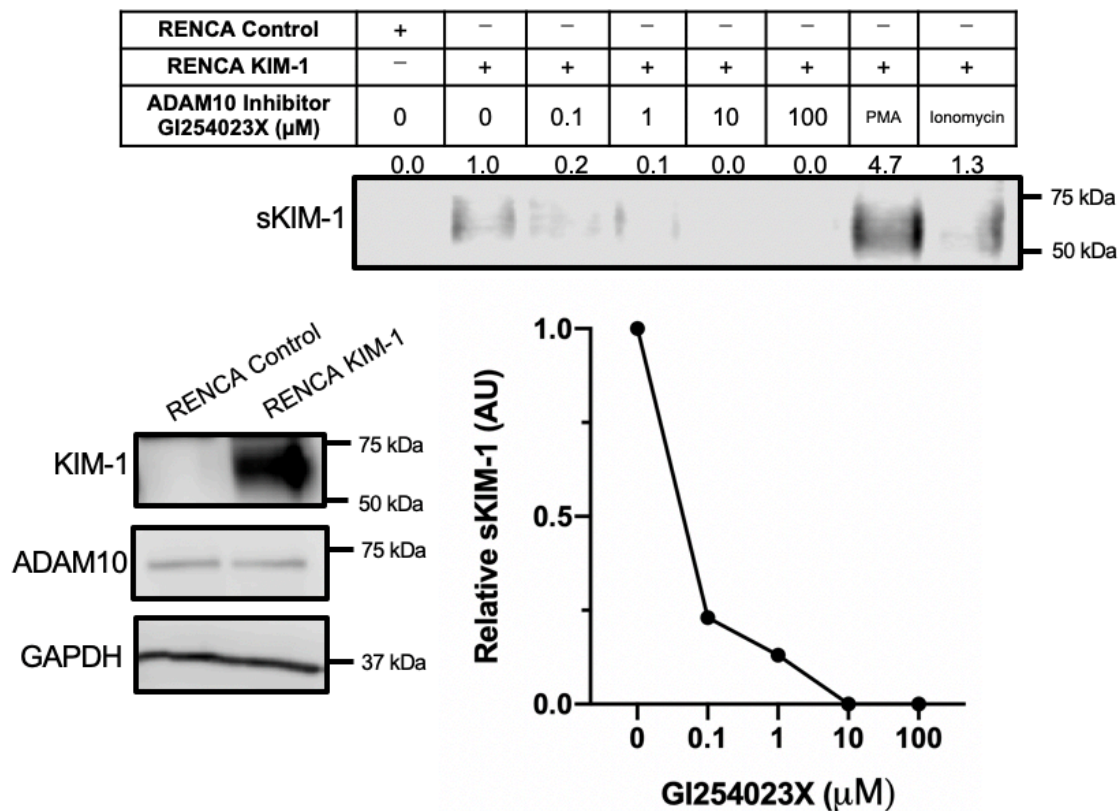


**Figure 25. GI254023X dose response on RENCA KIM-1.**

RENCA KIM-1 cells were treated with various log doses of GI254023X for 1 h in serum-free DMEM before media samples were collected for Western blot analysis (n=1). RENCA control cells were used as negative control. KIM-1 shedding was accelerated with 1 µM PMA or 500 nM ionomycin. Goat anti-KIM-1 (1:2000), mouse anti-GAPDH (1:2000), and rabbit anti-ADAM10 (1:500) antibodies were used. Densitometry values for sKIM-1 are relative to the no treatment (0 µM) control group.

## Chapter 4

# 4 Discussion

## 4.1 Major Findings

### 4.1.1 Mapping I202 as potential cleavage site on mKIM-1

In all attempts to precisely identify the cleavage site using the endogenous enzyme cleavage method, the MS sequencing results stopped at the same particular amino acid (F113), with no further downstream sequencing towards the predicted cleavage region (Figure 4, 7C, 8C, 9C) This site is unlikely to be the cleavage site for a few reasons. First, the predicted O-linked glycosylation sites of the mucin region start immediately downstream of this site, therefore it is highly likely that incomplete deglycosylation still remains a problem for sequencing this region (Figure 3). FLAG mKIM-1 sequence construct has 272 amino acids and a predicted weight of 30.04 kDa for full-length completely deglycosylated protein (Protein molecular weight – Bioinformatics.org). Full-length mKIM-1 runs much higher at ~60 kDa on western blots because of added mass from post-translational modifications on the protein (ie. glycosylations). These glycosylations can also alter protein shape and relative mass to charge ratios to cause a smeared appearance when run on gels (Figure 8A). If cleaved, the molecular weight should be smaller than 30 kDa, however the biggest shift I was able to detect was to 37 kDa from 60 kDa after TFMS deglycosylation and dialysis (Figure 8A, 9B). This could suggest incomplete deglycosylation or other post-translational modifications still present on the protein. Second, the F113 site is not within the predicted cleavage region (T194-I202). This region was mapped based on BLAST sequence alignment with the predicted cleavage region on hKIM-1, the epitope of ABE3 antibody which when bound to hKIM-1 blocks shedding (Bailly, Zhang et al. 2002). Third, it is commonly observed for enzymes like TACE and ADAM10 to cleave their substrates in the extracellular stalk region proximal to the transmembrane domain, typically within 15 amino acids (Caescu, Jeschke et al. 2009). For example, TACE-mediated cleavage of the efferocytosis receptor CD36 and Mer tyrosine kinase (MerTK) were mapped to be 12 amino acids away from the transmembrane region (Thorp, Vaisar et al. 2011, Driscoll, Vaisar et al. 2013). F113 is about 90 amino

acids away from the transmembrane region, and therefore does not fit with the typical cleavage pattern observed. Interestingly, I202 is the site on mKIM-1 that lies 12 amino acids away from the transmembrane region.

With the KIM-1 peptide cleavage method, no significant conclusions could be made, however, I202 stood out as a potential site as observed in Figure 10B. It is important to note that this synthetic peptide lacks any glycans normally observed on the endogenous protein. This may be problematic as glycosylation sites could be important for mediating the interaction between TACE/ADAM10 and KIM-1. This could be one of the reasons why I did not observe a higher concentration of peptides being cleaved at the potential cleavage site (I202). In fact, just upstream there lies an important N-linked glycosylation site (N197) which remains phylogenetically conserved from rodents to primates (Sizing, Bailly et al. 2007). This is why the first strategy involving endogenous cleavage of KIM-1 would be more reliable, and a similar cut site with this method would have increased my confidence with these results.

Although there is no definitive consensus amino acid sequence requirement for cleavage by TACE or ADAM10, some common residue properties are observed at specific positions relative to the cleavage site on various substrates (Caescu, Jeschke et al. 2009) (Figure 11). Importantly, it has been observed that just downstream of the cut site towards the C-terminus at position P1', TACE substrates are more likely to contain aliphatic hydrophobic residues such as leucine, valine, isoleucine. Alanine is the most common amino acid observed in TACE and ADAM10 substrates in the P1 position just upstream of the cut site (Caescu, Jeschke et al. 2009). The cleavage site between A201 and I202 on mKIM-1 matched with these sequence patterns making it more likely to be a potential site.

## 4.1.2    I202Q revealed potential involvement of ADAM10

The I202Q mutant was generated first based on published data of other TACE substrate cleavage sites (Caescu, Jeschke et al. 2009) to generate a mutant which was shedding defective with minimal alterations to the sequence in order to preserve other physiological functions. Q was similar in size to I but differed in polarity. Initial shedding assays with I202Q revealed an altered phenotype, where the ability to accelerate shedding via PMA, a

known potent inducer of TACE, was reduced (Figure 13). TACE was the most prominent enzyme studied with hKIM-1 cleavage and was assumed to be the major sheddase for mKIM-1 when I started my investigation (Gandhi, Yi et al. 2014). The observation that baseline shedding was still occurring alongside a defect with TACE-induced shedding suggested the possibility for a different sheddase to be involved. These results convinced me look deeper into another potential candidate metalloprotease, ADAM10, as an important sheddase involved in mKIM-1 shedding since both TACE and ADAM10 share numerous other common substrates (Edwards, Handsley et al. 2008, Kato, Hagiyama et al. 2018).

The ADAM10 specific inhibitor, GI254023X, with 100-fold more potency for ADAM10 ($IC_{50}$ = 5.3 nM) than TACE ( $IC_{50}$ = 541 nM), was used for further experimentation (Ludwig, Hundhausen et al. 2005, Hoettecke, Ludwig et al. 2010). As a hydroxamate-based inhibitor, GI254024X works by binding to the metal-ion binding active site of ADAM10 and has a higher affinity for ADAM10 than ADAM17 because of increased hydrophobic interactions (Ludwig, Hundhausen et al. 2005). Intriguingly, GI254023X blocked baseline shedding of not only I202Q mKIM-1 but also WT mKIM-1 suggesting that ADAM10 is involved with baseline shedding of mKIM-1 (Figure 14). Ionomycin, a commonly used ionophore, induces rapid $Ca^{2+}$ influx and downstream ADAM10 mediated shedding of various substrates and was also incorporated into further experiments to elucidate the role of ADAM10 (Horiuchi, Le Gall et al. 2007, Herzog, Haun et al. 2014)

Looking at the structural residue patterns near the cleavage site within the substrate, Q at position P1' is more selective of ADAM10 than TACE, and the same study showed that substitution to A at P1' position reduced selectivity and cleavage kinetics with both TACE and ADAM10 (Caescu, Jeschke et al. 2009). Therefore, the next mutation I made was I202A mKIM-1.

### 4.1.3 ADAM10 regulates both baseline and accelerated shedding

GI254023X inhibited baseline shedding as well as PMA and ionomycin accelerated shedding of WT mKIM-1 as well as the two mutants I202Q and I202A (Figure 19). This suggested that ADAM10 was involved with both baseline and accelerated shedding of

KIM-1, and perhaps the major sheddase at play. The dose response of GI254023X on HEK293 cells expressing WT mKIM-1 revealed that KIM-1 shedding could be completely abolished with higher doses of this ADAM10 specific inhibitor (Figure 18).

Potential off-target effects of drug treatment inhibition of ADAM10 with GI254023X were still possible. Therefore, ADAM10 siRNA mediated specific knockdown was used to confirm the role of ADAM10 in KIM-1 shedding. Accordingly, ADAM10 siRNA knockdown significantly reduced WT mKIM-1 shedding in HEK293 cells confirming the specific role of ADAM10 in mediating baseline KIM-1 shedding (Figure 20).

## 4.1.4    WT, I202Q and I202A mKIM-1 expression

Once the respective mutants I202Q and I202A mKIM-1 were generated and stably transfected into HEK293 cells, single high mKIM-1 protein expression colonies were selected for further testing (Figure 12 and Figure 15). When comparing total lysate mKIM-1 protein expression in the colonies selected, WT mKIM-1 had slightly lower expression than I202A, which was lower than I202Q (Figure 16A). The differences in mKIM-1 protein expression (in total lysate) levels is reflective of total KIM-1 expression anywhere in the cell, including the membrane, and could influence the levels of sKIM-1 observed in media therefore meaningful comparisons between these colonies for baseline shedding could not be made. Cell surface mKIM-1 expression profiles were similar for WT and I202A mKIM-1 with a homogenous population of high KIM-1 expression HEK293 cells (Figure 16B). I202Q, however, displayed a more heterogenous population with slightly lower and varied surface mKIM-1 expression (Figure 16B). It should be noted that the total percentage of HEK293 cells expressing KIM-1, regardless of level of expression, were comparable between WT and the two mutants (Figure 16C). The slightly lower expression levels in I202Q could potentially be the result of a disruption with trafficking the protein to the cell surface as KIM-1 undergoes dynamic endocytic recycling (Santiago, Ballesteros et al. 2007). Further testing to study endosomal trafficking would be required to elucidate the mechanisms behind this unique phenotype observed in the I202Q mutant. It is also possible that during stable integration of the gene into the genome, the WT and I202A mutants were

inserted into a region with a high expression promoter in the vicinity whereas, I202Q was inserted into a region which is transcribed less frequently. This could account for the differences that were being observed in the specific colonies that were picked for each mutation. This could be verified by studying cell surface KIM-1 expression on other stable colonies with I202Q mutant (ie. colony #10) (Figure 12).

## 4.1.5    Reduced *accelerated* shedding with I202Q and I202A

PMA and ionomycin treatment both significantly increased sKIM-1 levels of WT mKIM-1 compared to baseline levels indicating that both drugs were able to accelerate WT mKIM-1 shedding (Figure 17). However, no significant increases in sKIM-1 levels were observed after PMA or ionomycin treatment for both mutant I202Q and I202A (Figure 17). The reduced ability to accelerate shedding in these mutants is highly suggestive of the potential for I202 to be the actual mKIM-1 cleavage site.

It is likely that a single amino acid mutation at the cleavage site will not render a complete shedding defective phenotype as ADAM10 and TACE are both promiscuous enzymes and could possibly still cleave KIM-1 with minor alterations to the cleavage site. A larger deletion mutant spanning the predicted cleavage site is more likely to have a more prominent effect on shedding. For example, the shedding defective phenotype of a transmembrane efferocytosis receptor, MerTK, which is also cleaved in the ectodomain region by TACE, was generated by deleting 6 amino acids that spanned the determined cleavage site (Thorp, Vaisar et al. 2011). Moreover, the shedding defective mutant for hKIM-1 was generated with a 6 amino acid mutation in the membrane proximal region (Zhang, Humphreys et al. 2007). Therefore, it is likely that a deletion mutant (Δ199-204) spanning the predicted cleavage site I202 for mKIM-1 will result in a more noticeable shedding defective mutant.

## 4.1.6    KIM-1 shedding defect/inhibition reduces phagocytic function

It was expected that reduced shedding would increase the available full-length KIM-1 at the cell surface to act as a phagocytic receptor and therefore should increase phagocytosis levels. However, both mutants I202Q and I202A had significantly reduced phagocytic function compared to WT mKIM-1 (Figure 21). Within the mutants, I202Q showed

significantly lower phagocytic function than I202A (Figure 21). The observed phenotype of I202Q could potentially be explained by the lower cell surface expression of mKIM-1 (Figure 16B and 16C) which would mean that not as many receptors are available at the cell surface to internalize nearby apoptotic cells. The significant difference between WT and I202A however cannot be explained by differences in cell surface expression.

The presence of apoptotic cells has been shown to be a physiological inducer of hKIM-1 receptor shedding from human cell lines (Gandhi, Yi et al. 2014). We know that I202A mKIM-1 has an accelerated shedding defect after PMA or ionomycin treatment, so it remains possible that the presence of apoptotic cells in the phagocytosis assay accelerated receptor shedding of WT mKIM-1 but not I202A mKIM-1. It is intriguing to note the possible link between the accelerated receptor shedding defect and reduced phagocytic function.

Similarly, after treating HEK293 cells expressing WT mKIM-1 with GI254023X inhibitor, phagocytic function was significantly reduced (Figure 22). I observed that GI254023X treatment blocked baseline and accelerated mKIM-1 receptor shedding (Figure 19), so this again may suggest a possible link between reduced KIM-1 receptor shedding and reduced phagocytic function.

The intriguing link between reduced shedding and reduced phagocytosis is uncommon, however has been observed with triggering receptor expressed on myeloid cells 2 (TREM2). TREM2 is a phagocytic receptor expressed on myeloid immune cells and is also shed by ADAM10 (Schlepckow, Kleinberger et al. 2017). A particular missense mutation on the extracellular domain results in reduced shedding as well as reduced TREM2-dependent phagocytosis (Schlepckow, Kleinberger et al. 2017). However, this phenotype could be explained by misfolding of the protein which resulted in retention of TREM2 in the endoplasmic reticulum and subsequent low cell surface expression (Schlepckow, Kleinberger et al. 2017). With KIM-1, unlike with TREM2, reduced shedding with I202Q/A is not the result of reduced cell surface KIM-1 expression. This reduced shedding effect is being observed because ADAM10 is unable to cleave KIM-1 either because ADAM10 itself is dysfunctional (GI254023X inhibitor) or the KIM-1 mutants cause

misfolding or some other alteration which prevents the sheddase from recognizing, binding to and/or cleaving KIM-1.

It is possible that sKIM-1 or the process of KIM-1 cleavage is somehow required for efficient efferocytosis. A possible mechanism for this requirement is that sKIM-1 in the extracellular milieu decorates apoptotic cells to mark them for phagocytosis via homo- and /or heterophilic interactions with full length KIM-1 or other phagocytic receptors, respectively as observed in Figure 26.
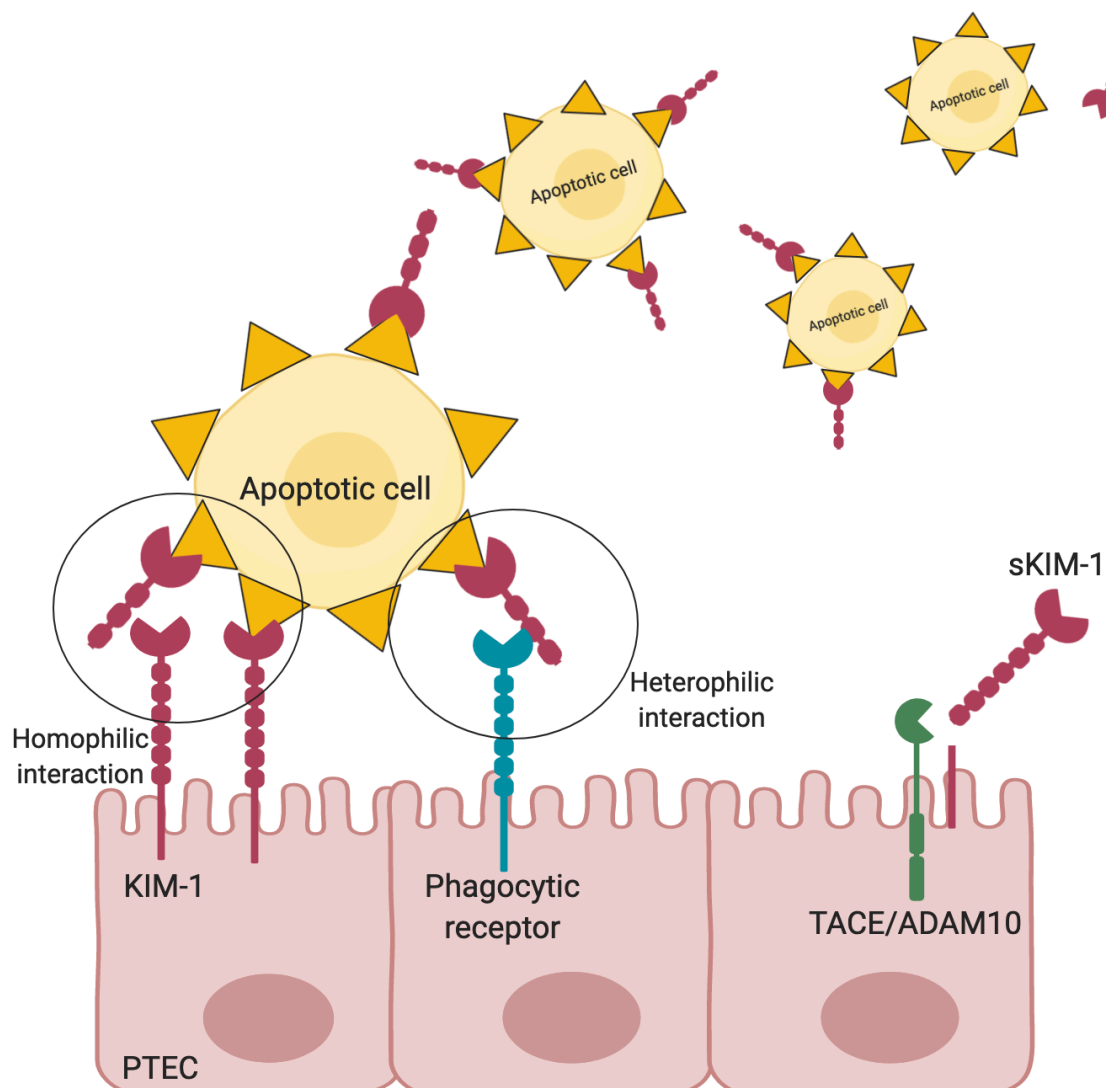
**Figure 26** Working model for possible mechanism linking KIM-1 shedding and efferocytosis. Image created using biorender.com.

Heterophilic interactions of KIM-1/TIM-1 have been identified with other cell surface proteins such as TIM-4, P-selectin and E-selectin (Meyers, Chakravarti et al. 2005, Angiari, Donnarumma et al. 2014). TIM-4 is the ligand of TIM-1, binding to its IgV domain and this interaction has been shown to mediate T-cell proliferation (Meyers, Chakravarti et al. 2005). Moreover, TIM-1 expressed on T helper 1 (Th1) and Th17 cells can bind to the adhesion receptor P-selectin, an interaction which requires both the IgV and mucin domains, or E-selectin which only requires the IgV domain (Angiari, Donnarumma et al.

2014). This interaction is important in mediating tethering and rolling of these TIM-1 expressing immune cells on vascular beds to regulate leukocyte trafficking during inflammation (Angiari, Donnarumma et al. 2014).

The shed ectodomain portion contains the phosphatidylserine binding IgV domain which allows it to bind to apoptotic cells (Gandhi, Yi et al. 2014). Based on the predicted cleavage site, sKIM-1 also contains the heavily glycosylated mucin domain (Figure 3B). Studies have shown that both the IgV domain and glycosylated mucin domain of murine sKIM-1 are capable and required for homophilic adhesion interactions with extracellular portions of full length KIM-1 receptors (Santiago, Ballesteros et al. 2007). Tubular epithelial apoptotic cells which have sloughed off into the tubular lumen may not be in close enough proximity to full length KIM-1 expressed on the apical surface of surviving epithelial cells to be phagocytosed directly. In this scenario, the biological significance of KIM-1 shedding would be to generate free sKIM-1 that can go off to bind and mark these far off apoptotic cells for homophilic interactions with sKIM-1 as well as full length KIM-1 and increase the chances of clearing it out from the tubular lumen. Previous *in vitro* studies using the shedding defective mutant for hKIM-1 ($\Delta$278-283) showed reduced phagocytic potential compared to WT hKIM-1 which is consistent with my results with mKIM-1(Gandhi, Yi et al. 2014).

It was recently shown that mice expressing KIM-1$^{\Delta mucin}$ lacking the mucin domain showed reduced KIM-1 mediated phagocytosis compared to their WT counterparts which is a phenotype that could be explained by this biological mechanism involving adhesion interactions between sKIM-1 and KIM-1 via the mucin domain (Yang, Brooks et al. 2015). Reduced KIM-1 mediated efferocytosis from the tubular lumen leads to increased pro-inflammatory cytokine production, downregulation of anti-inflammatory growth factor secretion, and an increase in activation of tissue macrophages leading to an overall proinflammatory phenotype which is initiated by AKI (Yang, Brooks et al. 2015). Kidney function and overall survival rates after AKI is also worse in these KIM-1$^{\Delta mucin}$ mice, which signifies the potential therapeutic relevance in attempting to facilitate apoptotic cell clearance by regulating KIM-1 shedding to increase concentrations of sKIM-1 in the tubular lumen (Yang, Brooks et al. 2015).

### 4.1.7   Confirming murine ADAM10 mediates shedding of mKIM-1

An important next step in this process was to confirm that murine ADAM10 mediates shedding of mKIM-1, as previous studies were conducted in HEK293 cells expressing human ADAM10. RENCA cells express mADAM10, and the dose response to GI254023X inhibitor showed reduced sKIM-1 levels in response to increasing concentrations of the ADAM10 inhibitor (Figure 25). This provides compelling evidence that ADAM10 is a major sheddase responsible for mKIM-1 shedding, whereas it has previously been shown that TACE is the major sheddase involved with hKIM-1 shedding (Gandhi, Yi et al. 2014). These species differences in shedding enzymes is not uncommon, with examples such as the transmembrane interleukin-6 receptor (IL-6R) which is shed primarily by TACE in humans and ADAM10 in mice (Garbers, Janner et al. 2011)

## 4.2   Limitations

Some of the major limitations with this project entailed biochemical obstacles that needed to be overcome for successful sequencing of the mKIM-1 cleavage site with ESI-MS/MS. The first major problem was the inability to use digestive enzymes efficiently to generate small enough peptides of sKIM-1 to be sequenced by ESI-MS/MS because of its heavily glycosylated TSP-rich mucin domain. In fact, many glycans have primary biological functions to increase the stability and half-life of proteins by protecting them against proteolysis (Russell, Oldham et al. 2009), so it was important to remove the glycans and generate clean sKIM-1 peptides for sequencing. Full length FLAG-mKIM-1 from lysates has an apparent molecular weight of about ~60 kDa as observed on western blot (Figure 17A), however the predicted molecular weight based on the 272 amino acid sequence of FLAG mKIM-1 is 30.04 kDa (Protein molecular weight – Bioinformatics.org), suggesting that about half the weight (30 kDa) could be attributed to post-translational modifications such as glycosylations, which not only add to the mass themselves but may also cause aberrant migration by altering protein shape and charge. The second major problem was the type of glycosylation. Although the majority of glycoproteins tend to have N-linked glycans (~90%) as opposed to O-linked glycans (~20%) (Apweiler, Hermjakob et al. 1999), KIM-1 consisted of mostly O-linked glycans with fewer N-linked glycans (Figure 2) (Bailly, Zhang et al. 2002). PNGase F is a common enzyme available for efficiently

removing all N-linked glycans, but a parallel enzyme for removing O-linked glycans, especially one capable of removing the complex heterogenous branches (eight possible core glycan subtypes) attached to O-glycans of a mucin domain, was not available (Van den Steen, Rudd et al. 1998, Wopereis, Lefeber et al. 2006). Therefore, preparing the sample for sequencing presented with a unique challenge. The third major problem with the heterogeneity of mucin domain glycosylations was that mass to charge (m/z) values can be altered in an unpredictable manner. Therefore, the option to use the molecular mass of a single strong peak from MS to map back to the cleavage site using the predicted mass of the FLAG mKIM-1 amino acid sequence was not available.

Other transmembrane protein substrates for TACE and /or ADAM10 have been successfully sequenced for their cleavage site, like CD36, IL-6R, MerTK and TREM2 using similar strategies (Mullberg, Oberthur et al. 1994, Thorp, Vaisar et al. 2011, Driscoll, Vaisar et al. 2013, Schlepckow, Kleinberger et al. 2017). CD36 and MerTK are heavily glycosylated proteins with N-glycans, therefore PNGase F was sufficient for complete deglycosylation before sequencing (Thorp, Vaisar et al. 2011, Driscoll, Vaisar et al. 2013). In the case of IL-6R, carboxypeptidase enzymes were used to determine which amino acid was on the C-terminal end of sIL-6R (ie. Q), then western blot analysis using various antibodies and their epitope information was used to deduce which Q was the exact cleavage site (Mullberg, Oberthur et al. 1994). TREM2 had a similar structure to KIM-1 with mucin domain glycosylations (Figure 2). Therefore an insertion was made with TEVFLAG sequence into the stalk region upstream of the predicted cleavage site, but downstream of the heavily glycosylated mucin domain (Schlepckow, Kleinberger et al. 2017). Using this approach, sTREM2 could be digested with the TEV enzyme to remove the mucin domain, and immunoprecipitated with FLAG to collect the portion of sTREM2 that was not glycosylated for cleavage site sequencing. This is an approach that can be taken for future KIM-1 sequencing attempts.

Another major limitation was the inability to normalize sKIM-1 with a loading control in the shedding assays. Since sKIM-1 is detected in media samples rather than lysates, there is no house-keeping loading control gene such as GAPDH or actin in the sample to use for normalizing sKIM-1 levels. A previous study running similar shedding assays, used a

technique involving Ponceau S staining to visualize residual albumin to serve as a loading control (Herzog, Haun et al. 2014). However, this technique did not produce any visual protein bands with the media samples I used (Appendix A3).

Species differences is a major limitation that needs to be addressed in order to confirm some of the major conclusions made with this study. HEK293 cells expressing mKIM-1 sets up a system where human sheddase enzymes (i.e. ADAM10/TACE) are made to cleave mKIM-1. HEK293 cells can be easily transfected compared to other cell lines making it an ideal candidate to use for initial studies. Repeating some of these studies in RENCA or another mouse cell line will help to confirm these findings.

Another limitation with this study was the inability to back up my findings with I202 and ADAM10 with ESI-MS/MS sequencing results for the cleavage site using KIM-1 synthetic peptide and rmADAM10. It is possible that a larger peptide (ie. >20 amino acids) was required for the enzyme to efficiently bind to nearby recognition sites. However, an interesting point to note was that the fluorescent peptide substrate (MCA-P-L-A-Q-A-V-DPA-R-S-S-S-R-NH2), used for assessment of enzymatic activity, was only 11 amino acids long and was still capable of being cleaved suggesting that length of peptide may not be such a critical factor.

## 4.3   Future Directions and Significance

From my current studies, I202 likely overlaps with the recognition site for mKIM-1 cleavage. As mentioned earlier, due to the promiscuous nature of the sheddase ADAM10, it may be necessary to generate a larger spanning deletion mutant (Δ199-204 mKIM-1) encompassing I202, to see a more noticeable effect on mKIM-1 shedding. This has been observed before with IL-6R, a common substrate for ADAM10 and ADAM17, in which point mutations at the cleavage site lead to reduced shedding, however 5 to 10 amino acid long mutations were capable of completely abolishing shedding (Mullberg, Oberthur et al. 1994). With hKIM-1, for which TACE is a major sheddase, the deletion Δ278-283 results in a shedding defective mutant (Zhang, Humphreys et al. 2007). This deletion is however in the stalk region downstream of the actual predicted cleavage site region G267 to L278 (Figure 3C) (Bailly, Zhang et al. 2002). BLAST sequence alignment of G267 to L278 on

hKIM-1 aligns with P204 to K209 on mKIM-1 so evidently deletion Δ204-209 mKIM-1 is another mutation worth attempting (Figure 3C). It should be noted that studies with IL-6R, another common substrate amongst ADAM10 and TACE, have shown that TACE mediated cleavage depends on the length of the stalk whereas ADAM10 mediated cleavage does not (Riethmueller, Ehlers et al. 2016). This could mean that the Δ278-283 mutation on hKIM-1 which shortens the stalk region could render it shedding defective because TACE is the major sheddase for hKIM-1 shedding, whereas the same phenotype may not be observed with Δ204-209 mutation on mKIM-1 which we now know is predominantly controlled by ADAM10 shedding. These species differences and functional differences between ADAM10 and TACE need to be further carefully elucidated for KIM-1 shedding.

I focused my studies on the cleavage site and shedding mechanisms of mKIM-1 as opposed to hKIM-1 with the intention of eventually being able to generate an *in vivo* mouse model expressing the shedding-defective mutant of KIM-1 (ΔShedKIM-1) and test renal response to both moderate and severe IRI. This will help to elucidate the biological significance of KIM-1 shedding in response to AKI *in vivo*.

I have hypothesized that ΔShedKIM-1 mice will exhibit more renal fibrosis (CKD phenotype) in response to severe IRI in comparison to WT. In mice, KIM-1 plays an important protective role during periods of moderate IRI. Unpublished data from our lab show that transient KIM-1 expression in WT mice during these times, correlates with lower levels of renal tissue injury in comparison to mice that lack KIM-1 expression altogether. However, with more severe levels of IRI, transient KIM-1 expressing mice show increased levels of fibrotic renal tissue in comparison to WT mice, indicating that KIM-1 may be more harmful than beneficial at this stage. Other studies have also shown that mice made to genetically overexpress KIM-1 constitutively, exhibit spontaneous triggering of renal fibrosis even in the absence of injury (Humphreys, Xu et al. 2013). Overall, this led us to conclude that KIM-1 has protective abilities, but only when it is expressed when necessary. KIM-1 ectodomain shedding can potentially be an important biological mechanism for regulating KIM-1 activity with regard to renal fibrosis. Perhaps this link between ectodomain shedding and fibrosis could be linked to phagocytic function to clear up tubular debris/cells which have sloughed off after AKI. Subsequent intraluminal casts, which form

when debris is not cleared out adequately, can result in tubular obstruction and increased intratubular pressure to exacerbate tissue damage and fibrosis (Goligorsky and DiBona 1993).

For this future study I would use the CRISPR-Cas system (Wiedenheft, Sternberg et al. 2012), to generate homozygous knockin (C57BL/6) mice expressing the shedding-defective mutant of KIM-1 (ΔShedKIM-1) and test its renal response to both moderate (35 minutes ischemia) and severe (45 minutes ischemia) IRI using established models in the laboratory (Ismail, Zhang et al. 2015). Comparisons can then be made with regards to renal function (serum creatinine), renal histology (for injury and fibrosis using Trichrome stain), markers of fibrosis such as collagen I (PCR, western blot & immunohistochemistry), and mortality (kidney failure) between WT littermates and ΔShedKIM-1 mice after 3, 7 and 28 days of reperfusion.

Furthermore, these ΔShedKIM-1 mice will be an invaluable tool for studying the role of sKIM-1, which not only gets expelled into renal tubules and urine, but also back leaks into plasma after acute and chronic AKI (Sabbisetti, Waikar et al. 2014). ΔShedKIM-1 mice in relation to their WT counterparts are predicted to have lower plasma sKIM-1 concentrations and it would be therapeutically relevant to see how this effects progression of phenotypes characteristic of ESRD and type I diabetes (Sabbisetti, Waikar et al. 2014).

# Appendices

**Appendix A 1:** R&D recombinant enzyme activity assay protocol for rmADAM10

**Assay Procedure**

- Assay Buffer: 25 mM Tris, 2.5 μM $ZnCl_2$, 0.005% (w/v) Brij-35, pH 9.0
- Recombinant Mouse ADAM10 (rmADAM10) (Catalog # 946-AD)
- Substrate: MCA-Pro-Leu-Ala-Gln-Ala-Val-DPA-Arg-Ser-Ser-Ser-Arg-$NH_2$ (Catalog # ES003)
- F16 Black Maxisorp Plate (Nunc, Catalog # 475515)
- Fluorescent Plate Reader (Model: SpectraMax Gemini EM by Molecular Devices) or equivalent

1. Dilute rmADAM10 to 2 ng/μL in Assay Buffer.
2. Dilute Substrate to 20 μM in Assay Buffer.
3. In a plate load 50 μL of 2 ng/μL rmADAM10, and start the reaction by adding 50 μL of 20 μM Substrate to wells. Include a Substrate Blank containing 50 μL Assay Buffer and 50 μL of 20 μM Substrate.
4. Read at excitation and emission wavelengths of 320 nm and 405 nm (top read), respectively, in kinetic mode for 30 minutes at 37 °C.
5. Calculate specific activity using data from 15-30 minutes:

$$\text{Specific Activity (pmol/min/μg)} = \frac{\text{Adjusted } V_{max}\text{* (RFU/min) x Conversion Factor** (pmol/RFU)}}{\text{amount of enzyme (μg)}}$$

*Adjusted for Substrate Blank
**Derived using calibration standard MCA-Pro-Leu-OH (Bachem, Catalog # M-1975).

Per Well:

- rmADAM10: 0.1 μg
- Substrate: 10 μM

# Appendix A 2: R&D recombinant enzyme activity assay protocol for rmTACE

## Assay Procedure

**Materials**
- Assay Buffer: 50 mM Tris, pH 9.0
- Recombinant Mouse TACE/ADAM17 (rmTACE) (Catalog # 2978-AD)
- Substrate: MCA-Pro-Leu-Ala-Gln-Ala-Val-DPA-Arg-Ser-Ser-Ser-Arg-NH$_2$ (Catalog # ES003), 2 mM stock in DMSO
- F16 Black Maxisorp Plate (Nunc, Catalog # 475515)
- Fluorescent Plate Reader (Model: SpectraMax Gemini EM by Molecular Devices) or equivalent

1. Dilute rmTACE to 0.2 ng/μL in Assay Buffer.
2. Dilute Substrate to 20 μM in Assay Buffer.
3. In a plate, load 50 μL of 0.2 ng/μL rmTACE to wells, and start the reaction by adding 50 μL of 20 μM Substrate. Include a Substrate Blank of 50 μL Assay Buffer and 50 μL of 20 μM Substrate.
4. Read at excitation and emission wavelengths of 320 nm and 405 nm (top read), respectively, in kinetic mode for 5 minutes.
5. Calculate specific activity:

$$\text{Specific Activity (pmol/min/μg)} = \frac{\text{Adjusted } V_{max}\text{* (RFU/min) x Conversion Factor** (pmol/RFU)}}{\text{amount of enzyme (μg)}}$$

*Adjusted for Substrate Blank
**Derived using calibration standard MCA-Pro-Leu-OH (Bachem, Catalog # M-1975).

Per Well:
- rmTACE: 0.01 μg
- Substrate: 10 μM

**Appendix A 3: Ponceau S stained transfer membrane with media samples confirmed no residual albumin bands could be detected for normalizing sKIM-1 levels.**
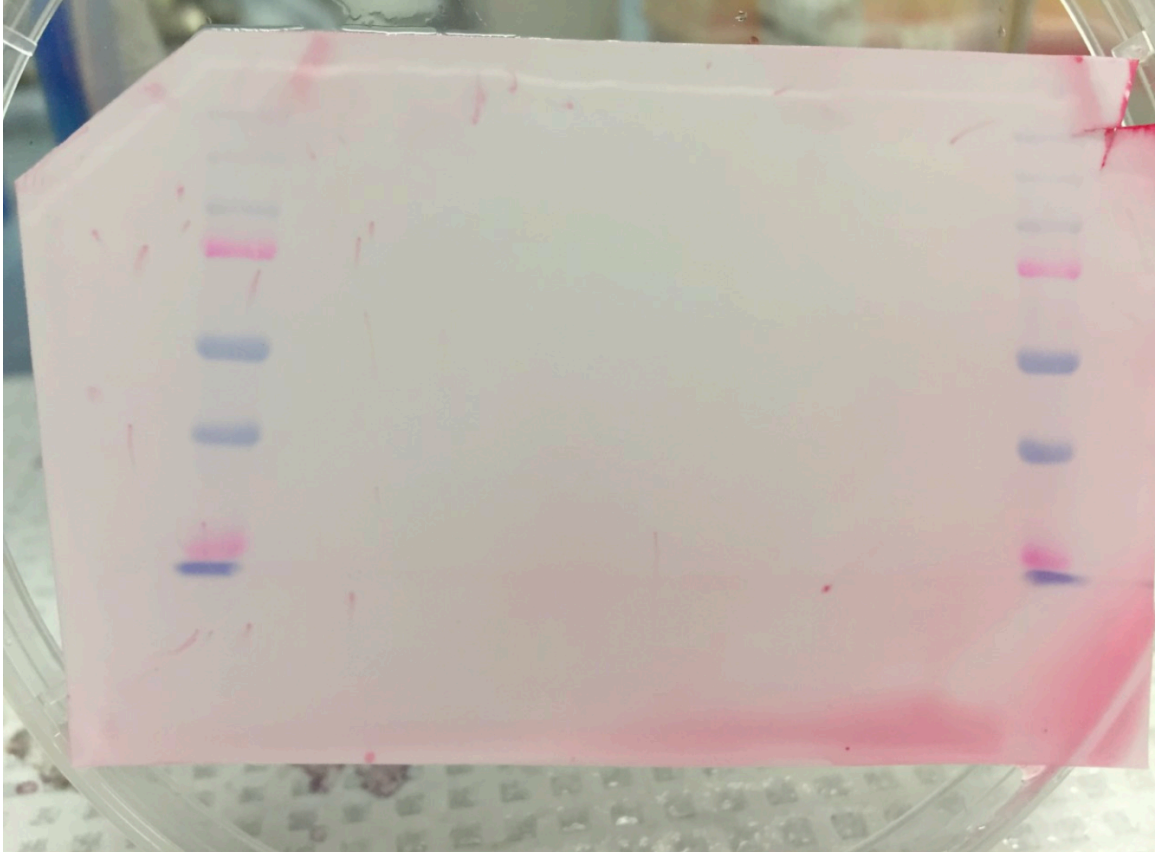
**Appendix A 4: Separation of standard peptides using Superdex Peptide 10/300 GL Column**

Column:          Superdex Peptide 10/300 GL
Sample:          1. Cytochrome c ($M_r$ 12 384) 1 mg/ml
                 2. Aprotinin ($M_r$ 6 512) 2 mg/ml
                 3. Vitamin $B_{12}$ ($M_r$ 1 355) 0.1 mg/ml
                 4. (Gly)3 ($M_r$ 189) 0.1 mg/ml
                 5. Gly ($M_r$ 75) 7.8 mg/ml
Flow rate:       0.5 ml/min, room temperature
Sample volume:   50 µl
Eluent:          0.05 M phosphate, 0.15 M NaCl, pH 7.0
System:          ÄKTAexplorer 100
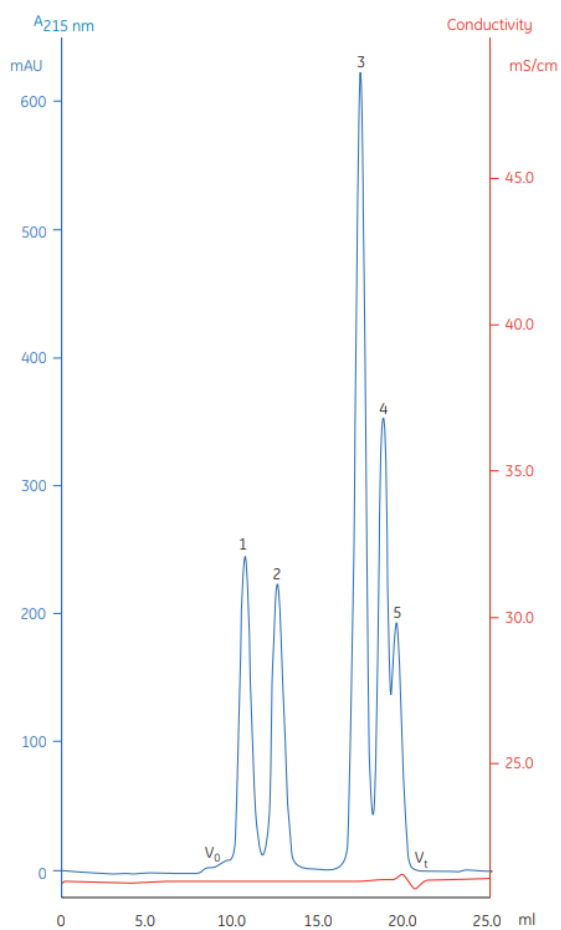


**Fig 6.** A separation of standard peptides on Superdex Peptide 10/300 GL.

https://www.gelifesciences.co.jp/catalog/pdf/18116379.pdf

**Appendix A 5:** Legend for post-translational modifications marked on ESI-MS/MS sequence results.

a Acetylation (N-term) (+42.01)
a Ammonia-loss (N) (-17.03)
a 2-amino-3-oxo-butanoic_acid (-2.02)
c Carboxymethyl (KW, X@N-term) (+58.01)
d Deamidation (NQ) (+0.98)
d Deamidation followed by a methylation (+15.00)
d Dihydroxy (+31.99)
d Dehydration (-18.01)
g Glycidamide adduct (+87.03)
h Hexose (NSY) (+162.05)
m Methylation(KR) (+14.02)
o Oxidation (HW) (+15.99)
p phosphate-ribosylation (+212.01)
P Propionamide (K, X@N-term) (+71.04)
r Replacement of 2 protons by calcium (+37.95)
r Replacement of 2 protons by iron (+53.92)
r Replacement of proton by potassium (+37.96)
s Sodium adduct (+21.98)
t Tryptophan oxidation to kynurenin (+3.99)
u Ubiquitin (+114.04)

**Appendix A 6:** Automated In-gel digestion protocol performed by Functional Proteomics Facility (FPF), Western University.

Instrument- MassPREP Station, Robotic Protein Handling System

FPF AUTOMATED PROGRAM INSTRUCTIONS

## START IN-GEL DIGESTION PROTOCOL

**FA = 2%formic acid/2% CAN**
**ACN = 100% Acetonitrile**
**ABC = 100 mM Ammonium bicarbonate**

*Coomassie de-staining (~ 20 min)*

- Heater to 40 deg C (omit)
- Remove excess liquid
- Add 50uL 100 mM ABC + 50uL 100% ACN (first coomassie de-stain)
- Pause 10 min, remove and save supernatant
- Add 50uL 100 mM ABC + 50uL 100% ACN (second coomassie de-stain)
- Pause 10 min, remove and save supernatant

*Reduction (~1 h, 15 min)*

- Add 50uL ACN (Pre-reduction dehydration)
- Pause 5 min, remove and save supernatant
- Pause 10 min, after supernatant removal (Pre-reduction evaporation)
- Add 50uL 10mM DTT (Reduction)
- Pause 30 min

*Alkylation*

- Add 50uL 55mM iodoacetamide (IAA)
- Pause 25 min

*Wash (~ 5)*

- Add 100uL 100% ACN
- Pause 5 min, remove and store supernatant

*Dehydration (~20 min)*

- Add 50uL 100 mM ABC + 50uL 100% ACN
- Pause 5 min, remove and store supernatant
- Add 50uL 100% ACN (First gel dehydration)
- Pause 5 min, remove and store supernatant
- Add 50uL 100% ACN (Second gel dehydration)
- Pause 5 min, remove and store supernatant
- Pause 5 min, after supernatant removal (ACN evaporation)

**HEATER (40 deg C) SWITCHED OFF**

**HEATER SET TO 20 deg C**

*Trypsin Addition (Overnight ~16 h + dry time)*

- Add 25uL of 3-6 ng/uL overnight (7 h, amount of trypsin is determined by the intensity of stain) (*WLS- Use 4 ng/uL trypsin in 50 mM ABC (pH 7.8 – check w pH paper)*
- Pause 30 min (Trypsin absorption)

**HEATER SET TO 40 deg C (WLS wants to omit)**

- Pause 7 h (Digestion) (*WLS wants at* 37 deg. C, 16 h)

**HEATER SET TO 20 deg C**

- Add 20uL FA (we will dry instead of FA)
- Pause 30 min

**START EXTRACTION PROTOCOL**

**FA = 2%formic acid/2% ACN**

*Extraction (~1 h 30 min)*

- Add 30 uL FA (extraction #1)
- Pause 30 min, remove and save supernatant
- Add 15 uL FA, 17 uL ACN (extraction #2)
- Pause 30 min, remove and save supernatant
- Add 16 uL FA, 19 uL ACN (extraction #3)
- Pause 30 min, remove and save supernatant

**END EXTRACTION PROTOCOL**

**Appendix A 7:** Thermo Scientific Orbitrap Elite Mass spectrometer instrument setup used for ESI-MS/MS sequencing by Biological Mass Spectrometry Laboratory at Schulich School of Medicine & Dentistry, Western University

Creator: Thermo, Orbitrap Elite
Last modified: 5/28/2019 by Thermo

MS Run Time (min): 120.00
MS Detector Settings:
Experiment Type: Nth Order Double Play
Tune Method: Current_Tune_NSI

Scan Event Details:
 1:  FTMS + p norm o(300.0-1500.0)
     CV = 0.0V
 2:  FTMS + c norm Dep MS/MS Most intense ion from (1)
     Activation Type:       HCD
     Min. Signal Required:    5000.0
     Isolation Width:       1.50
     Normalized Coll. Energy: 28.0
     Default Charge State:   2
     Activation Time:       0.100
     FT first mass mode: relative to parent mass
     FT first mass value: 0.10
     CV = 0.0V
Scan Event 2 repeated for top 6 peaks.

Lock Masses:
  Pos List Name:            445
       Source:         API Source
     Mass List:          445.120025
  Neg List Name:            N/A
       Source:         API Source
     Mass List:         (none)

Data Dependent Settings:
    Use separate polarity settings disabled
    Parent Mass List:        (none)
    Reject Mass List:        (none)
    Neutral Loss Mass List:     (none)
    Product Mass List:        (none)
    Neutral loss in top:      3
    Product in top:         3
    Most intense if no parent masses found enabled
    Add/subtract mass not enabled
    FT master scan preview mode enabled
    Charge state screening enabled

Charge state dependent ETD time not enabled
Monoisotopic precursor selection enabled
Charge state rejection enabled
  Unassigned charge states : rejected
        Charge state 1 : rejected
        Charge state 2 : not rejected
        Charge state 3 : not rejected
        Charge states 4+ : not rejected
Chromatography mode is disabled


 Global Data Dependent Settings:
    Predict ion injection time enabled
    Use global parent and reject mass lists not enabled
    Exclude parent mass from data dependent selection not enabled
    Exclusion mass width relative to mass
    Exclusion mass width relative to low (ppm):  10.0
    Exclusion mass width relative to high (ppm): 10.0
    Parent mass width relative to mass
    Parent mass width relative to low (ppm):  10.0
    Parent mass width relative to high (ppm): 10.0
    Reject mass width relative to mass
    Reject mass width relative to low (ppm):  10.0
    Reject mass width relative to high (ppm): 10.0
    Zoom/UltraZoom scan mass width relative to mass
    Zoom/UltraZoom scan mass width relative to low (ppm):  10000.0
    Zoom/UltraZoom scan mass width relative to high (ppm): 10000.0
    FT SIM scan mass width low:        5.00
    FT SIM scan mass width high:       5.00
    Neutral Loss candidates processed by decreasing intensity
    Neutral Loss mass width by mass
    Neutral Loss mass width low:  0.50
    Neutral Loss mass width high: 0.50
    Product candidates processed by decreasing intensity
    Product mass width by mass
    Product mass width low:  0.50
    Product mass width high: 0.50
    MS mass range:  300.00-4000.00
    MSn mass range by mass
    MSn mass range:  0.00-1000000.00
    Use m/z values as masses not enabled
    Analog UV data dep. not enabled
    Dynamic exclusion enabled
        Repeat Count:        1
        Repeat Duration:     5.00
        Exclusion List Size:  500
        Exclusion Duration:   15.00
        Exclusion mass width relative to mass

Exclusion mass width relative to low (ppm):  10.0
Exclusion mass width relative to high (ppm): 10.0
Expiration:   disabled
Isotopic data dependence not enabled


LC Method:

Method
  RunTime: 120.00
  AcquityTVMMethod
    AnalyticalRightValvePosition: ValvePosition_1
    TrapRightValvePosition: ValvePosition_2
    SetColumnTemperature: 35.0
    EnableAlarmBand: false
    SetAlarmBandDegC: 5.0

  nAcquityBSMMethod
    Scale: ScaleNano_1
    ApplicationMode: ApplicationMode_2
    PumpRole: PumpType_1
    FlowSourceA: 1
    FlowSourceB: 1
    SolventNameA: Water
    SolventNameB: Acetonitrile
    SealWashPeriod: 120.0
    GradientTable
      GradientRow
        Time: Initial
        Flow: 0.300
        CompositionA: 95.0
        CompositionB: 5.0
        Curve
      GradientRow
        Time: 90.00
        Flow: 0.300
        CompositionA: 60.0
        CompositionB: 40.0
        Curve: 6
      GradientRow
        Time: 95.00
        Flow: 0.300
        CompositionA: 5.0
        CompositionB: 95.0
        Curve: 6
      GradientRow
        Time: 105.00
        Flow: 0.300

          CompositionA: 5.0
          CompositionB: 95.0
          Curve: 6
      GradientRow
          Time: 105.50
          Flow: 0.300
          CompositionA: 95.0
          CompositionB: 5.0
          Curve: 6
      GradientRow
          Time: 120.00
          Flow: 0.300
          CompositionA: 95.0
          CompositionB: 5.0
          Curve: 6
   EventTable
   ElutionCompositionA: 95.0
   ElutionCompositionB: 5.0
   LowPressureLimit: 0
   HighPressureLimit: 13000

      TrappingLowPressureLimit: 0
      TrappingHighPressureLimit: 5000
      VariableFlowFactor: 0.10
      TrappingMode: TrappingMode_2

   GradientTableTP
      GradientRow
          Time: Initial
          Flow: 5.000
          CompositionA: 99.0
          CompositionB: 1.0
          Curve
      LoadingTime: 6.00

nAcquitySMMethod
  LoopOption: LoopOptionPartial_1
  WeakWashSolvent: Water
  WeakWashVolume: 600
  StrongWashSolvent: Acetonitrile
  StrongWashVolume: 200
  SampleTemperature: 8.0
  SampleTemperatureLimit: 5
  SampleLoop: 10.0

# References

Abbate, M., J. V. Bonventre and D. Brown (1994). "The microtubule network of renal epithelial cells is disrupted by ischemia and reperfusion." Am J Physiol **267**(6 Pt 2): F971-978.

Andrassy, M., H. C. Volz, J. C. Igwe, B. Funke, S. N. Eichberger, Z. Kaya, S. Buss, F. Autschbach, S. T. Pleger, I. K. Lukic, F. Bea, S. E. Hardt, P. M. Humpert, M. E. Bianchi, H. Mairbaurl, P. P. Nawroth, A. Remppis, H. A. Katus and A. Bierhaus (2008). "High-mobility group box-1 in ischemia-reperfusion injury of the heart." Circulation **117**(25): 3216-3226.

Angiari, S., T. Donnarumma, B. Rossi, S. Dusi, E. Pietronigro, E. Zenaro, V. Della Bianca, L. Toffali, G. Piacentino, S. Budui, P. Rennert, S. Xiao, C. Laudanna, J. M. Casasnovas, V. K. Kuchroo and G. Constantin (2014). "TIM-1 glycoprotein binds the adhesion receptor P-selectin and mediates T cell trafficking during inflammation and autoimmunity." Immunity **40**(4): 542-553.

Apweiler, R., H. Hermjakob and N. Sharon (1999). "On the frequency of protein glycosylation, as deduced from analysis of the SWISS-PROT database." Biochim Biophys Acta **1473**(1): 4-8.

Arai, S., K. Kitada, T. Yamazaki, R. Takai, X. Zhang, Y. Tsugawa, R. Sugisawa, A. Matsumoto, M. Mori, Y. Yoshihara, K. Doi, N. Maehara, S. Kusunoki, A. Takahata, E. Noiri, Y. Suzuki, N. Yahagi, A. Nishiyama, L. Gunaratnam, T. Takano and T. Miyazaki (2016). "Apoptosis inhibitor of macrophage protein enhances intraluminal debris clearance and ameliorates acute kidney injury in mice." Nat Med **22**(2): 183-193.

Bagnasco, S., D. Good, R. Balaban and M. Burg (1985). "Lactate production in isolated segments of the rat nephron." Am J Physiol **248**(4 Pt 2): F522-526.

Bailly, V., Z. Zhang, W. Meier, R. Cate, M. Sanicola and J. V. Bonventre (2002). "Shedding of kidney injury molecule-1, a putative adhesion protein involved in renal regeneration." J Biol Chem **277**(42): 39739-39748.

Balasubramanian, S., S. K. Kota, V. K. Kuchroo, B. D. Humphreys and T. B. Strom (2012). "TIM family proteins promote the lysosomal degradation of the nuclear receptor NUR77." Sci Signal **5**(254): ra90.

Bazzi, M. D. and G. L. Nelsestuen (1989). "Differences in the effects of phorbol esters and diacylglycerols on protein kinase C." Biochemistry **28**(24): 9317-9323.

Bhat, J. G., M. C. Gluck, J. Lowenstein and D. S. Baldwin (1976). "Renal failure after open heart surgery." Ann Intern Med **84**(6): 677-682.

Black, R. A., C. T. Rauch, C. J. Kozlosky, J. J. Peschon, J. L. Slack, M. F. Wolfson, B. J. Castner, K. L. Stocking, P. Reddy, S. Srinivasan, N. Nelson, N. Boiani, K. A. Schooley, M. Gerhart, R. Davis, J. N. Fitzner, R. S. Johnson, R. J. Paxton, C. J. March and D. P.

Cerretti (1997). "A metalloproteinase disintegrin that releases tumour-necrosis factor-alpha from cells." Nature **385**(6618): 729-733.

Bonvalet, J. P., M. Champion, A. Courtalon, N. Farman, A. Vandewalle and F. Wanstok (1977). "Number of glomeruli in normal and hypertrophied kidneys of mice and guinea-pigs." J Physiol **269**(3): 627-641.

Bonventre, J. V. (2003). "Dedifferentiation and proliferation of surviving epithelial cells in acute renal failure." J Am Soc Nephrol **14 Suppl 1**: S55-61.

Bonventre, J. V. (2009). "Kidney injury molecule-1 (KIM-1): a urinary biomarker and much more." Nephrol Dial Transplant **24**(11): 3265-3268.

Bonventre, J. V. and L. Yang (2011). "Cellular pathophysiology of ischemic acute kidney injury." J Clin Invest **121**(11): 4210-4221.

Brooks, C. R., M. Y. Yeung, Y. S. Brooks, H. Chen, T. Ichimura, J. M. Henderson and J. V. Bonventre (2015). "KIM-1-/TIM-1-mediated phagocytosis links ATG5-/ULK1-dependent clearance of apoptotic cells to antigen presentation." EMBO J **34**(19): 2441-2464.

Caescu, C. I., G. R. Jeschke and B. E. Turk (2009). "Active-site determinants of substrate recognition by the metalloproteinases TACE and ADAM10." Biochem J **424**(1): 79-88.

Chen, C. D., S. Podvin, E. Gillespie, S. E. Leeman and C. R. Abraham (2007). "Insulin stimulates the cleavage and release of the extracellular domain of Klotho by ADAM10 and ADAM17." Proc Natl Acad Sci U S A **104**(50): 19796-19801.

Coca, S. G., A. X. Garg, H. Thiessen-Philbrook, J. L. Koyner, U. D. Patel, H. M. Krumholz, M. G. Shlipak, C. R. Parikh and T.-A. Consortium (2014). "Urinary biomarkers of AKI and mortality 3 years after cardiac surgery." J Am Soc Nephrol **25**(5): 1063-1071.

Coca, S. G., B. Yusuf, M. G. Shlipak, A. X. Garg and C. R. Parikh (2009). "Long-term risk of mortality and other adverse outcomes after acute kidney injury: a systematic review and meta-analysis." Am J Kidney Dis **53**(6): 961-973.

de Souza, A. J., J. S. Oak, R. Jordanhazy, R. H. DeKruyff, D. A. Fruman and L. P. Kane (2008). "T cell Ig and mucin domain-1-mediated T cell activation requires recruitment and activation of phosphoinositide 3-kinase." J Immunol **180**(10): 6518-6526.

Ding, Q., M. Yeung, G. Camirand, Q. Zeng, H. Akiba, H. Yagita, G. Chalasani, M. H. Sayegh, N. Najafian and D. M. Rothstein (2011). "Regulatory B cells are identified by expression of TIM-1 and can be induced through TIM-1 ligation to promote tolerance in mice." J Clin Invest **121**(9): 3645-3656.

Donohoe, J. F., M. A. Venkatachalam, D. B. Bernard and N. G. Levinsky (1978). "Tubular leakage and obstruction after renal ischemia: structural-functional correlations." Kidney Int **13**(3): 208-222.

Driscoll, W. S., T. Vaisar, J. Tang, C. L. Wilson and E. W. Raines (2013). "Macrophage ADAM17 deficiency augments CD36-dependent apoptotic cell uptake and the linked anti-inflammatory phenotype." Circ Res **113**(1): 52-61.

E, O. h. and B. D. Humphreys (2017). "Fibrotic Changes Mediating Acute Kidney Injury to Chronic Kidney Disease Transition." Nephron **137**(4): 264-267.

Edwards, D. R., M. M. Handsley and C. J. Pennington (2008). "The ADAM metalloproteinases." Mol Aspects Med **29**(5): 258-289.

Freeman, G. J., J. M. Casasnovas, D. T. Umetsu and R. H. DeKruyff (2010). "TIM genes: a family of cell surface phosphatidylserine receptors that regulate innate and adaptive immunity." Immunol Rev **235**(1): 172-189.

Gandhi, R., J. Yi, J. Ha, H. Shi, O. Ismail, S. Nathoo, J. V. Bonventre, X. Zhang and L. Gunaratnam (2014). "Accelerated receptor shedding inhibits kidney injury molecule-1 (KIM-1)-mediated efferocytosis." Am J Physiol Renal Physiol **307**(2): F205-221.

Garbers, C., N. Janner, A. Chalaris, M. L. Moss, D. M. Floss, D. Meyer, F. Koch-Nolte, S. Rose-John and J. Scheller (2011). "Species specificity of ADAM10 and ADAM17 proteins in interleukin-6 (IL-6) trans-signaling and novel role of ADAM10 in inducible IL-6 receptor shedding." J Biol Chem **286**(17): 14804-14811.

Gerich, J. E. (2010). "Role of the kidney in normal glucose homeostasis and in the hyperglycaemia of diabetes mellitus: therapeutic implications." Diabet Med **27**(2): 136-142.

Ghaderian, S. B. and S. S. Beladi-Mousavi (2014). "The role of diabetes mellitus and hypertension in chronic kidney disease." J Renal Inj Prev **3**(4): 109-110.

Goligorsky, M. S. and G. F. DiBona (1993). "Pathogenetic role of Arg-Gly-Asp-recognizing integrins in acute renal failure. off." Proc Natl Acad Sci U S A **90**(12): 5700-5704.

Govorkova, E. A., G. Murti, B. Meignier, C. de Taisne and R. G. Webster (1996). "African green monkey kidney (Vero) cells provide an alternative host cell system for influenza A and B viruses." J Virol **70**(8): 5519-5524.

Guo, L., T. Takino, Y. Endo, T. Domoto and H. Sato (2012). "Shedding of kidney injury molecule-1 by membrane-type 1 matrix metalloproteinase." J Biochem **152**(5): 425-432.

Gupta, R. J., E.; Brunak, S. (2004). "Prediction of N-glycosylation sites in human proteins.", from http://www.cbs.dtu.dk/services/NetNGlyc/.

Hahn, D., A. Pischitzis, S. Roesmann, M. K. Hansen, B. Leuenberger, U. Luginbuehl and E. E. Sterchi (2003). "Phorbol 12-myristate 13-acetate-induced ectodomain shedding and phosphorylation of the human meprinbeta metalloprotease." J Biol Chem **278**(44): 42829-42839.

Han, W. K., A. Alinani, C. L. Wu, D. Michaelson, M. Loda, F. J. McGovern, R. Thadhani and J. V. Bonventre (2005). "Human kidney injury molecule-1 is a tissue and urinary tumor marker of renal cell carcinoma." J Am Soc Nephrol **16**(4): 1126-1134.

Han, W. K., V. Bailly, R. Abichandani, R. Thadhani and J. V. Bonventre (2002). "Kidney Injury Molecule-1 (KIM-1): a novel biomarker for human renal proximal tubule injury." Kidney Int **62**(1): 237-244.

Herzog, C., R. S. Haun, A. Ludwig, S. V. Shah and G. P. Kaushal (2014). "ADAM10 is the major sheddase responsible for the release of membrane-associated meprin A." J Biol Chem **289**(19): 13308-13322.

Hoettecke, N., A. Ludwig, S. Foro and B. Schmidt (2010). "Improved synthesis of ADAM10 inhibitor GI254023X." Neurodegener Dis **7**(4): 232-238.

Horiuchi, K., S. Le Gall, M. Schulte, T. Yamaguchi, K. Reiss, G. Murphy, Y. Toyama, D. Hartmann, P. Saftig and C. P. Blobel (2007). "Substrate selectivity of epidermal growth factor-receptor ligand sheddases and their regulation by phorbol esters and calcium influx." Mol Biol Cell **18**(1): 176-188.

Humphreys, B. D., S. L. Lin, A. Kobayashi, T. E. Hudson, B. T. Nowlin, J. V. Bonventre, M. T. Valerius, A. P. McMahon and J. S. Duffield (2010). "Fate tracing reveals the pericyte and not epithelial origin of myofibroblasts in kidney fibrosis." Am J Pathol **176**(1): 85-97.

Humphreys, B. D., F. Xu, V. Sabbisetti, I. Grgic, S. Movahedi Naini, N. Wang, G. Chen, S. Xiao, D. Patel, J. M. Henderson, T. Ichimura, S. Mou, S. Soeung, A. P. McMahon, V. K. Kuchroo and J. V. Bonventre (2013). "Chronic epithelial kidney injury molecule-1 expression causes murine kidney fibrosis." J Clin Invest **123**(9): 4023-4035.

Humphreys, B. D., F. Xu, V. Sabbisetti, I. Grgic, S. M. Naini, N. Wang, G. Chen, S. Xiao, D. Patel, J. M. Henderson, T. Ichimura, S. Mou, S. Soeung, A. P. McMahon, V. K. Kuchroo and J. V. Bonventre (2013). "Chronic epithelial kidney injury molecule-1 expression causes murine kidney fibrosis." J Clin Invest **123**(9): 4023-4035.

Hundhausen, C., D. Misztela, T. A. Berkhout, N. Broadway, P. Saftig, K. Reiss, D. Hartmann, F. Fahrenholz, R. Postina, V. Matthews, K. J. Kallen, S. Rose-John and A. Ludwig (2003). "The disintegrin-like metalloproteinase ADAM10 is involved in constitutive cleavage of CX3CL1 (fractalkine) and regulates CX3CL1-mediated cell-cell adhesion." Blood **102**(4): 1186-1195.

Ichimura, T., E. J. Asseldonk, B. D. Humphreys, L. Gunaratnam, J. S. Duffield and J. V. Bonventre (2008). "Kidney injury molecule-1 is a phosphatidylserine receptor that confers a phagocytic phenotype on epithelial cells." J Clin Invest 118(5): 1657-1668.

Ichimura, T., J. V. Bonventre, V. Bailly, H. Wei, C. A. Hession, R. L. Cate and M. Sanicola (1998). "Kidney injury molecule-1 (KIM-1), a putative epithelial cell adhesion molecule containing a novel immunoglobulin domain, is up-regulated in renal cells after injury." J Biol Chem 273(7): 4135-4142.

Ichimura, T., C. C. Hung, S. A. Yang, J. L. Stevens and J. V. Bonventre (2004). "Kidney injury molecule-1: a tissue and urinary biomarker for nephrotoxicant-induced renal injury." Am J Physiol Renal Physiol 286(3): F552-563.

Ismail, O., X. Zhang, J. V. Bonventre and L. Gunaratnam (2015). "G protein, 12 (Galpha12) is a negative regulator of kidney injury molecule-1-mediated efferocytosis." Am J Physiol Renal Physiol: ajprenal 00169 02015.

Ismail, O. Z., S. Sriranganathan, X. Zhang, J. V. Bonventre, A. S. Zervos and L. Gunaratnam (2018). "Tctex-1, a novel interaction partner of Kidney Injury Molecule-1, is required for efferocytosis." J Cell Physiol 233(10): 6877-6895.

Ismail, O. Z., X. Zhang, J. V. Bonventre and L. Gunaratnam (2016). "G protein alpha12 (Galpha12) is a negative regulator of kidney injury molecule-1-mediated efferocytosis." Am J Physiol Renal Physiol 310(7): F607-F620.

Ismail, O. Z., X. Zhang, J. Wei, A. Haig, B. M. Denker, R. S. Suri, A. Sener and L. Gunaratnam (2015). "Kidney injury molecule-1 protects against Galpha12 activation and tissue damage in renal ischemia-reperfusion injury." Am J Pathol 185(5): 1207-1215.

Kato, T., M. Hagiyama and A. Ito (2018). "Renal ADAM10 and 17: Their Physiological and Medical Meanings." Front Cell Dev Biol 6: 153.

Kaushal, G. P., A. G. Basnakian and S. V. Shah (2004). "Apoptotic pathways in ischemic acute renal failure." Kidney Int 66(2): 500-506.

Kirkin, V., N. Cahuzac, F. Guardiola-Serrano, S. Huault, K. Luckerath, E. Friedmann, N. Novac, W. S. Wels, B. Martoglio, A. O. Hueber and M. Zornig (2007). "The Fas ligand intracellular domain is released by ADAM10 and SPPL2a cleavage in T-cells." Cell Death Differ 14(9): 1678-1687.

Kozasa, T., N. Hajicek, C. R. Chow and N. Suzuki (2011). "Signalling mechanisms of RhoGTPase regulation by the heterotrimeric G proteins G12 and G13." J Biochem 150(4): 357-369.

Kramann, R., J. Wongboonsin, M. Chang-Panesso, F. G. Machado and B. D. Humphreys (2017). "Gli1(+) Pericyte Loss Induces Capillary Rarefaction and Proximal Tubular Injury." J Am Soc Nephrol 28(3): 776-784.

Krogh, A., B. Larsson, G. von Heijne and E. L. Sonnhammer (2001). "Predicting transmembrane protein topology with a hidden Markov model: application to complete genomes." J Mol Biol **305**(3): 567-580.

Kuchroo, V. K., D. T. Umetsu, R. H. DeKruyff and G. J. Freeman (2003). "The TIM gene family: emerging roles in immunity and disease." Nat Rev Immunol **3**(6): 454-462.

Kuehn, E. W., K. M. Park, S. Somlo and J. V. Bonventre (2002). "Kidney injury molecule-1 expression in murine polycystic kidney disease." Am J Physiol Renal Physiol **283**(6): F1326-1336.

Lee, J. Y., O. Z. Ismail, X. Zhang, A. Haig, D. Lian and L. Gunaratnam (2018). "Donor kidney injury molecule-1 promotes graft recovery by regulating systemic necroinflammation." Am J Transplant **18**(8): 2021-2028.

Lei, P., T. Bai and Y. Sun (2019). "Mechanisms of Ferroptosis and Relations With Regulated Cell Death: A Review." Front Physiol **10**: 139.

Lieberthal, W. and S. K. Nigam (1998). "Acute renal failure. I. Relative importance of proximal vs. distal tubular injury." Am J Physiol **275**(5): F623-631.

Lim, A. I., L. Y. Chan, K. N. Lai, S. C. Tang, C. W. Chow, M. F. Lam and J. C. Leung (2012). "Distinct role of matrix metalloproteinase-3 in kidney injury molecule-1 shedding by kidney proximal tubular epithelial cells." Int J Biochem Cell Biol **44**(6): 1040-1050.

Linkermann, A., R. Skouta, N. Himmerkus, S. R. Mulay, C. Dewitz, F. De Zen, A. Prokai, G. Zuchtriegel, F. Krombach, P. S. Welz, R. Weinlich, T. Vanden Berghe, P. Vandenabeele, M. Pasparakis, M. Bleich, J. M. Weinberg, C. A. Reichel, J. H. Brasen, U. Kunzendorf, H. J. Anders, B. R. Stockwell, D. R. Green and S. Krautwald (2014). "Synchronized renal tubular cell death involves ferroptosis." Proc Natl Acad Sci U S A **111**(47): 16836-16841.

Lorenzen, I., J. Lokau, Y. Korpys, M. Oldefest, C. M. Flynn, U. Kunzel, C. Garbers, M. Freeman, J. Grotzinger and S. Dusterhoft (2016). "Control of ADAM17 activity by regulation of its cellular localisation." Sci Rep **6**: 35067.

Lote, C. J. (2012). Principles of Renal Physiology(Fifth Edition).

Ludwig, A., C. Hundhausen, M. H. Lambert, N. Broadway, R. C. Andrews, D. M. Bickett, M. A. Leesnitzer and J. D. Becherer (2005). "Metalloproteinase inhibitors for the disintegrin-like metalloproteinases ADAM10 and ADAM17 that differentially block constitutive and phorbol ester-inducible shedding of cell surface molecules." Comb Chem High Throughput Screen **8**(2): 161-171.

Meyers, J. H., S. Chakravarti, D. Schlesinger, Z. Illes, H. Waldner, S. E. Umetsu, J. Kenny, X. X. Zheng, D. T. Umetsu, R. H. DeKruyff, T. B. Strom and V. K. Kuchroo (2005). "TIM-4 is the ligand for TIM-1, and the TIM-1-TIM-4 interaction regulates T cell proliferation." Nat Immunol **6**(5): 455-464.

Molitoris, B. A., R. Dahl and A. Geerdes (1992). "Cytoskeleton disruption and apical redistribution of proximal tubule Na(+)-K(+)-ATPase during ischemia." Am J Physiol **263**(3 Pt 2): F488-495.

Mullberg, J., W. Oberthur, F. Lottspeich, E. Mehl, E. Dittrich, L. Graeve, P. C. Heinrich and S. Rose-John (1994). "The soluble human IL-6 receptor. Mutational characterization of the proteolytic cleavage site." J Immunol **152**(10): 4958-4968.

Myers, B. D., F. Chui, M. Hilberman and A. S. Michaels (1979). "Transtubular leakage of glomerular filtrate in human acute renal failure." Am J Physiol **237**(4): F319-325.

Nakayama, M., H. Akiba, K. Takeda, Y. Kojima, M. Hashiguchi, M. Azuma, H. Yagita and K. Okumura (2009). "Tim-3 mediates phagocytosis of apoptotic cells and cross-presentation." Blood **113**(16): 3821-3830.

Nowak, N., J. Skupien, M. A. Niewczas, M. Yamanouchi, M. Major, S. Croall, A. Smiles, J. H. Warram, J. V. Bonventre and A. S. Krolewski (2016). "Increased plasma kidney injury molecule-1 suggests early progressive renal decline in non-proteinuric patients with type 1 diabetes." Kidney Int **89**(2): 459-467.

Nozaki, Y., D. J. Nikolic-Paterson, S. L. Snelgrove, H. Akiba, H. Yagita, S. R. Holdsworth and A. R. Kitching (2012). "Endogenous Tim-1 (Kim-1) promotes T-cell responses and cell-mediated injury in experimental crescentic glomerulonephritis." Kidney Int **81**(9): 844-855.

Nyengaard, J. R. and T. F. Bendtsen (1992). "Glomerular number and size in relation to age, kidney weight, and body surface in normal man." Anat Rec **232**(2): 194-201.

Okada, H., T. M. Danoff, R. Kalluri and E. G. Neilson (1997). "Early role of Fsp1 in epithelial-mesenchymal transformation." Am J Physiol **273**(4 Pt 2): F563-574.

Olof, P., A. Hellberg, O. Kallskog and M. Wolgast (1991). "Red cell trapping and postischemic renal blood flow. Differences between the cortex, outer and inner medulla." Kidney Int **40**(4): 625-631.

Pan, D. and G. M. Rubin (1997). "Kuzbanian controls proteolytic processing of Notch and mediates lateral inhibition during Drosophila and vertebrate neurogenesis." Cell **90**(2): 271-280.

Patel, R., J. K. McKenzie and E. G. McQueen (1964). "Tamm-Horsfall Urinary Mucoprotein and Tubular Obstruction by Casts in Acute Renal Failure." Lancet **1**(7331): 457-461.

Perazella, M. A. (2014). "Diagnosing drug-induced AIN in the hospitalized patient: a challenge for the clinician." Clin Nephrol **81**(6): 381-388.

Perez-Rojas, J., J. A. Blanco, C. Cruz, J. Trujillo, V. S. Vaidya, N. Uribe, J. V. Bonventre, G. Gamba and N. A. Bobadilla (2007). "Mineralocorticoid receptor blockade

confers renoprotection in preexisting chronic cyclosporine nephrotoxicity." <u>Am J Physiol Renal Physiol</u> **292**(1): F131-139.

Peschon, J. J., J. L. Slack, P. Reddy, K. L. Stocking, S. W. Sunnarborg, D. C. Lee, W. E. Russell, B. J. Castner, R. S. Johnson, J. N. Fitzner, R. W. Boyce, N. Nelson, C. J. Kozlosky, M. F. Wolfson, C. T. Rauch, D. P. Cerretti, R. J. Paxton, C. J. March and R. A. Black (1998). "An essential role for ectodomain shedding in mammalian development." <u>Science</u> **282**(5392): 1281-1284.

Racusen, L. C. (1998). "Epithelial cell shedding in acute renal injury." <u>Clin Exp Pharmacol Physiol</u> **25**(3-4): 273-275.

Racusen, L. C., B. A. Fivush, Y. L. Li, I. Slatnik and K. Solez (1991). "Dissociation of tubular cell detachment and tubular cell death in clinical and experimental "acute tubular necrosis"." <u>Lab Invest</u> **64**(4): 546-556.

Rangel-Frausto, M. S., D. Pittet, M. Costigan, T. Hwang, C. S. Davis and R. P. Wenzel (1995). "The natural history of the systemic inflammatory response syndrome (SIRS). A prospective study." <u>JAMA</u> **273**(2): 117-123.

Ridley, A. J. (2001). "Rho family proteins: coordinating cell responses." <u>Trends Cell Biol</u> **11**(12): 471-477.

Riethmueller, S., J. C. Ehlers, J. Lokau, S. Dusterhoft, K. Knittler, G. Dombrowsky, J. Grotzinger, B. Rabe, S. Rose-John and C. Garbers (2016). "Cleavage Site Localization Differentially Controls Interleukin-6 Receptor Proteolysis by ADAM10 and ADAM17." <u>Sci Rep</u> **6**: 25550.

Russell, D., N. J. Oldham and B. G. Davis (2009). "Site-selective chemical protein glycosylation protects from autolysis and proteolytic degradation." <u>Carbohydr Res</u> **344**(12): 1508-1514.

Sabbisetti, V. S., S. S. Waikar, D. J. Antoine, A. Smiles, C. Wang, A. Ravisankar, K. Ito, S. Sharma, S. Ramadesikan, M. Lee, R. Briskin, P. L. De Jager, T. T. Ngo, M. Radlinski, J. W. Dear, K. B. Park, R. Betensky, A. S. Krolewski and J. V. Bonventre (2014). "Blood kidney injury molecule-1 is a biomarker of acute and chronic kidney injury and predicts progression to ESRD in type I diabetes." <u>J Am Soc Nephrol</u> **25**(10): 2177-2186.

Sahin, U., G. Weskamp, K. Kelly, H. M. Zhou, S. Higashiyama, J. Peschon, D. Hartmann, P. Saftig and C. P. Blobel (2004). "Distinct roles for ADAM10 and ADAM17 in ectodomain shedding of six EGFR ligands." <u>J Cell Biol</u> **164**(5): 769-779.

Santiago, C., A. Ballesteros, L. Martinez-Munoz, M. Mellado, G. G. Kaplan, G. J. Freeman and J. M. Casasnovas (2007). "Structures of T cell immunoglobulin mucin protein 4 show a metal-Ion-dependent ligand binding site where phosphatidylserine binds." <u>Immunity</u> **27**(6): 941-951.

Santiago, C., A. Ballesteros, C. Tami, L. Martinez-Munoz, G. G. Kaplan and J. M. Casasnovas (2007). "Structures of T Cell immunoglobulin mucin receptors 1 and 2 reveal mechanisms for regulation of immune responses by the TIM receptor family." Immunity **26**(3): 299-310.

Savill, J., I. Dransfield, C. Gregory and C. Haslett (2002). "A blast from the past: clearance of apoptotic cells regulates immune responses." Nat Rev Immunol **2**(12): 965-975.

Scheller, J., A. Chalaris, C. Garbers and S. Rose-John (2011). "ADAM17: a molecular switch to control inflammation and tissue regeneration." Trends Immunol **32**(8): 380-387.

Schlepckow, K., G. Kleinberger, A. Fukumori, R. Feederle, S. F. Lichtenthaler, H. Steiner and C. Haass (2017). "An Alzheimer-associated TREM2 variant occurs at the ADAM cleavage site and affects shedding and phagocytic function." EMBO Mol Med **9**(10): 1356-1365.

Schumacher, N., D. Meyer, A. Mauermann, J. von der Heyde, J. Wolf, J. Schwarz, K. Knittler, G. Murphy, M. Michalek, C. Garbers, J. W. Bartsch, S. Guo, B. Schacher, P. Eickholz, A. Chalaris, S. Rose-John and B. Rabe (2015). "Shedding of Endogenous Interleukin-6 Receptor (IL-6R) Is Governed by A Disintegrin and Metalloproteinase (ADAM) Proteases while a Full-length IL-6R Isoform Localizes to Circulating Microvesicles." J Biol Chem **290**(43): 26059-26071.

Schweigert, O., C. Dewitz, K. Moller-Hackbarth, A. Trad, C. Garbers, S. Rose-John and J. Scheller (2014). "Soluble T cell immunoglobulin and mucin domain (TIM)-1 and -4 generated by A Disintegrin And Metalloprotease (ADAM)-10 and -17 bind to phosphatidylserine." Biochim Biophys Acta **1843**(2): 275-287.

Sizing, I. D., V. Bailly, P. McCoon, W. Chang, S. Rao, L. Pablo, R. Rennard, M. Walsh, Z. Li, M. Zafari, M. Dobles, L. Tarilonte, S. Miklasz, G. Majeau, K. Godbout, M. L. Scott and P. D. Rennert (2007). "Epitope-dependent effect of anti-murine TIM-1 monoclonal antibodies on T cell activity and lung immune responses." J Immunol **178**(4): 2249-2261.

Steentoft, C., S. Y. Vakhrushev, H. J. Joshi, Y. Kong, M. B. Vester-Christensen, K. T. Schjoldager, K. Lavrsen, S. Dabelsteen, N. B. Pedersen, L. Marcos-Silva, R. Gupta, E. P. Bennett, U. Mandel, S. Brunak, H. H. Wandall, S. B. Levery and H. Clausen (2013). "Precision mapping of the human O-GalNAc glycoproteome through SimpleCell technology." EMBO J **32**(10): 1478-1488.

Susantitaphong, P., D. N. Cruz, J. Cerda, M. Abulfaraj, F. Alqahtani, I. Koulouridis, B. L. Jaber and N. Acute Kidney Injury Advisory Group of the American Society of (2013). "World incidence of AKI: a meta-analysis." Clin J Am Soc Nephrol **8**(9): 1482-1493.

Sutton, T. A. (2009). "Alteration of microvascular permeability in acute kidney injury." Microvasc Res **77**(1): 4-7.

Thadhani, R., M. Pascual and J. V. Bonventre (1996). "Acute renal failure." N Engl J Med **334**(22): 1448-1460.

Thorp, E., T. Vaisar, M. Subramanian, L. Mautner, C. Blobel and I. Tabas (2011). "Shedding of the Mer tyrosine kinase receptor is mediated by ADAM17 protein through a pathway involving reactive oxygen species, protein kinase Cdelta, and p38 mitogen-activated protein kinase (MAPK)." J Biol Chem **286**(38): 33335-33344.

Umetsu, S. E., W. L. Lee, J. J. McIntire, L. Downey, B. Sanjanwala, O. Akbari, G. J. Berry, H. Nagumo, G. J. Freeman, D. T. Umetsu and R. H. DeKruyff (2005). "TIM-1 induces T cell activation and inhibits the development of peripheral tolerance." Nat Immunol **6**(5): 447-454.

Vaidya, V. S., J. S. Ozer, F. Dieterle, F. B. Collings, V. Ramirez, S. Troth, N. Muniappa, D. Thudium, D. Gerhold, D. J. Holder, N. A. Bobadilla, E. Marrer, E. Perentes, A. Cordier, J. Vonderscher, G. Maurer, P. L. Goering, F. D. Sistare and J. V. Bonventre (2010). "Kidney injury molecule-1 outperforms traditional biomarkers of kidney injury in preclinical biomarker qualification studies." Nat Biotechnol **28**(5): 478-485.

Van den Steen, P., P. M. Rudd, R. A. Dwek and G. Opdenakker (1998). "Concepts and principles of O-linked glycosylation." Crit Rev Biochem Mol Biol **33**(3): 151-208.

van Timmeren, M. M., S. J. Bakker, V. S. Vaidya, V. Bailly, T. A. Schuurs, J. Damman, C. A. Stegeman, J. V. Bonventre and H. van Goor (2006). "Tubular kidney injury molecule-1 in protein-overload nephropathy." Am J Physiol Renal Physiol **291**(2): F456-464.

van Timmeren, M. M., M. C. van den Heuvel, V. Bailly, S. J. Bakker, H. van Goor and C. A. Stegeman (2007). "Tubular kidney injury molecule-1 (KIM-1) in human renal disease." J Pathol **212**(2): 209-217.

Venkatachalam, M. A., D. B. Bernard, J. F. Donohoe and N. G. Levinsky (1978). "Ischemic damage and repair in the rat proximal tubule: differences among the S1, S2, and S3 segments." Kidney Int **14**(1): 31-49.

Wahlberg, J., L. Karlberg and A. E. Persson (1984). "Total and regional renal blood flow during complete unilateral ureteral obstruction." Acta Physiol Scand **121**(2): 111-118.

Waikar, S. S., K. D. Liu and G. M. Chertow (2008). "Diagnosis, epidemiology and outcomes of acute kidney injury." Clin J Am Soc Nephrol **3**(3): 844-861.

Wald, R., R. R. Quinn, J. Luo and et al. (2009). "Chronic dialysis and death among survivors of acute kidney injury requiring dialysis." JAMA **302**(11): 1179-1185.

Wald, R., R. R. Quinn, J. Luo, P. Li, D. C. Scales, M. M. Mamdani, J. G. Ray and G. University of Toronto Acute Kidney Injury Research (2009). "Chronic dialysis and death among survivors of acute kidney injury requiring dialysis." JAMA **302**(11): 1179-1185.

Wang, X. and M. R. Garrett (2017). "Nephron number, hypertension, and CKD: physiological and genetic insight from humans and animal models." Physiol Genomics **49**(3): 180-192.

Wiedenheft, B., S. H. Sternberg and J. A. Doudna (2012). "RNA-guided genetic silencing systems in bacteria and archaea." Nature **482**(7385): 331-338.

Wilson, D. M., D. R. Turner, J. S. Cameron, C. S. Ogg, C. B. Brown and C. Chantler (1976). "Value of renal biopsy in acute intrinsic renal failure." Br Med J **2**(6033): 459-461.

Wopereis, S., D. J. Lefeber, E. Morava and R. A. Wevers (2006). "Mechanisms in protein O-glycan biosynthesis and clinical and molecular aspects of protein O-glycan biosynthesis defects: a review." Clin Chem **52**(4): 574-600.

Wu, H., G. Chen, K. R. Wyburn, J. Yin, P. Bertolino, J. M. Eris, S. I. Alexander, A. F. Sharland and S. J. Chadban (2007). "TLR4 activation mediates kidney ischemia/reperfusion injury." J Clin Invest **117**(10): 2847-2859.

Yamanishi, Y., J. Kitaura, K. Izawa, A. Kaitani, Y. Komeno, M. Nakamura, S. Yamazaki, Y. Enomoto, T. Oki, H. Akiba, T. Abe, T. Komori, Y. Morikawa, H. Kiyonari, T. Takai, K. Okumura and T. Kitamura (2010). "TIM1 is an endogenous ligand for LMIR5/CD300b: LMIR5 deficiency ameliorates mouse kidney ischemia/reperfusion injury." J Exp Med **207**(7): 1501-1511.

Yamazaki, T., R. Sugisawa, E. Hiramoto, R. Takai, A. Matsumoto, Y. Senda, K. Nakashima, P. S. Nelson, J. M. Lucas, A. Morgan, Z. Li, K. I. Yamamura, S. Arai and T. Miyazaki (2016). "A proteolytic modification of AIM promotes its renal excretion." Sci Rep **6**: 38762.

Yang, L., C. R. Brooks, S. Xiao, V. Sabbisetti, M. Y. Yeung, L. L. Hsiao, T. Ichimura, V. Kuchroo and J. V. Bonventre (2015). "KIM-1-mediated phagocytosis reduces acute injury to the kidney." J Clin Invest **125**(4): 1620-1636.

Yang, L., G. Xing, L. Wang, Y. Wu, S. Li, G. Xu, Q. He, J. Chen, M. Chen, X. Liu, Z. Zhu, L. Yang, X. Lian, F. Ding, Y. Li, H. Wang, J. Wang, R. Wang, C. Mei, J. Xu, R. Li, J. Cao, L. Zhang, Y. Wang, J. Xu, B. Bao, B. Liu, H. Chen, S. Li, Y. Zha, Q. Luo, D. Chen, Y. Shen, Y. Liao, Z. Zhang, X. Wang, K. Zhang, L. Liu, P. Mao, C. Guo, J. Li, Z. Wang, S. Bai, S. Shi, Y. Wang, J. Wang, Z. Liu, F. Wang, D. Huang, S. Wang, S. Ge, Q. Shen, P. Zhang, L. Wu, M. Pan, X. Zou, P. Zhu, J. Zhao, M. Zhou, L. Yang, W. Hu, J. Wang, B. Liu, T. Zhang, J. Han, T. Wen, M. Zhao, H. Wang and I. A. b. C. Consortiums (2015). "Acute kidney injury in China: a cross-sectional survey." Lancet **386**(10002): 1465-1471.

Ympa, Y. P., Y. Sakr, K. Reinhart and J. L. Vincent (2005). "Has mortality from acute renal failure decreased? A systematic review of the literature." Am J Med **118**(8): 827-832.

Zhang, Z. and C. X. Cai (2016). "Kidney injury molecule-1 (KIM-1) mediates renal epithelial cell repair via ERK MAPK signaling pathway." Mol Cell Biochem **416**(1-2): 109-116.

Zhang, Z., B. D. Humphreys and J. V. Bonventre (2007). "Shedding of the urinary biomarker kidney injury molecule-1 (KIM-1) is regulated by MAP kinases and juxtamembrane region." J Am Soc Nephrol **18**(10): 2704-2714.

Zhang, Z. X., K. Shek, S. Wang, X. Huang, A. Lau, Z. Yin, H. Sun, W. Liu, B. Garcia, S. Rittling and A. M. Jevnikar (2010). "Osteopontin expressed in tubular epithelial cells regulates NK cell-mediated kidney ischemia reperfusion injury." J Immunol **185**(2): 967-973.

Zuk, A., J. V. Bonventre, D. Brown and K. S. Matlin (1998). "Polarity, integrin, and extracellular matrix dynamics in the postischemic rat kidney." Am J Physiol **275**(3): C711-731.

Zuk, A., J. V. Bonventre and K. S. Matlin (2001). "Expression of fibronectin splice variants in the postischemic rat kidney." Am J Physiol Renal Physiol **280**(6): F1037-1053.

# Curriculum Vitae

**Name:**            Saranga Sriranganathan

**Post-secondary**    B.M.Sc. in Medical Sciences
**Education and**      Honours Specialization in Physiology and Pharmacology
**Degrees:**          University of Western Ontario
London, Ontario, Canada
2013-2017

M.Sc. in Physiology and Pharmacology
The University of Western Ontario
London, Ontario, Canada
2017-2019

**Honours and**      Graduate Teaching Assistant Award of Excellence
**Awards:**          2017-2018

Internal Research Fund Studentship Award Fall 2017
London Health Research Institute
2017-2018

**Related Work**     Graduate Teaching Assistant
**Experience**       Human Physiology 2130
The University of Western Ontario
London, Ontario, Canada
2017-2019

**Publications:**

Ola Z. Ismail, **Saranga Sriranganathan**, Xizhong Zhang, Joseph V. Bonventre, Antonis S. Zervos, Lakshman Gunaratnam. (2018). *Tctex-1, a novel interaction partner of Kidney Injury Molecule-1, is required for efferocytosis*. Journal of Cellular Physiology. DOI Number: 10.1002/jcp.26578.